

GEOMETRIC DISCRETIZATION OF LAGRANGIAN MECHANICS AND FIELD THEORIES

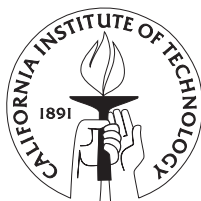
Thesis by

Ari Stern

In Partial Fulfullment of the Requirements

for the Degree of

Doctor of Philosophy



California Institute of Technology

Pasadena, California

2009

(Defended December 5, 2008)

© 2009 Ari Stern
All rights reserved

Acknowledgments

This work would never have been possible without the support of many people, to whom I am sincerely grateful. I have been lucky to have at Caltech not one, but two incredible advisors and mentors, Jerrold E. Marsden and Mathieu Desbrun, who have always been generous with their time, knowledge, and advice. It has been a true honor to learn from them, and to have the opportunity to work alongside them. I would also like to thank Nawaf Bou-Rabee, Marco Castrillón López, Roger Donaldson, Eitan Grinspun, Eva Kanso, Melvin Leok, Michael Ortiz, Houman Owhadi, Peter Schröder, Yiyi Tong, and Joris Vankerschaver for valuable conversations and insightful comments that helped me in the development of this work. I also owe much to my undergraduate mentor at Columbia University, Michael Thaddeus, whose infectious enthusiasm for mathematics inspired my own, and to all the people who have taught me (both formally and informally) over the years. In addition, I would like to express my thanks to the Gordon and Betty Moore Foundation, whose long-term fellowship support during my first four years at Caltech enabled me to spend my time searching for answers in my studies and research, rather than searching for a source of funding.

Last, and certainly not least, I am profoundly grateful to my family and friends for always supporting and encouraging me, in my studies and in everything else. Most of all, I would like to thank my wife, Erika, whose love, support, and patience (even when her husband's mind occasionally sails off into math-land in the middle of dinner) have been beyond measure.

I would also like to acknowledge those who provided helpful input for specific parts of this thesis. For the work presented in Chapter 2, I would first and foremost like to acknowledge Eitan Grinspun, who has been my collaborator in developing

variational implicit-explicit integrators. In addition, I would like to thank Will Fong and Adrian Lew for helpful conversations about the stability of AVI methods, Houman Owhadi for suggesting that we examine the Fermi–Pastor–Ulam problem, Dion O’Neale for advice regarding the simulation plots, Teng Zhang for pointing out a bug in an earlier version of the MATLAB code, and Reinout Quispel for his valuable suggestions and feedback. I especially wish to acknowledge Marlis Hochbruck, Arieh Iserles, and Christian Lubich for suggesting that we try to understand the variational IMEX scheme as a modified impulse method; this perspective led us directly to the results in Section 2.2.5.

The work on computational electromagnetics, presented in Chapter 3, was developed in collaboration with Yiyi Tong, Mathieu Desbrun, and Jerrold E. Marsden. We would like to thank several people for their inspiration and suggestions. First of all, Alain Bossavit for suggesting many years ago that we take the present DEC approach to computational electromagnetism, and for his excellent lectures at Caltech on the subject. Second, Michael Ortiz and Eva Kanso for their ongoing interactions on related topics and suggestions. We also thank Doug Arnold, Uri Ascher, Robert Kotiuga, Melvin Leok, Adrian Lew, and Matt West for their feedback and encouragement. In addition, the 3-D AVI simulations were programmed and implemented by Patrick Xia, as part of a Summer Undergraduate Research Fellowship (for which I was a co-advisor).

Finally, the work on discrete gauge theory and general relativity presented in Chapter 4 (much of which is still ongoing) owes a great deal to the help and advice of several people, particularly John Baez, Jim Hartle, Michael Holst, Lee Lindblom, Kip Thorne, Joris Vankerschaver, and Ruth Williams.

Abstract

This thesis presents a unified framework for geometric discretization of highly oscillatory mechanics and classical field theories, based on Lagrangian variational principles and discrete differential forms. For highly oscillatory problems in mechanics, we present a variational approach to two families of geometric numerical integrators: implicit-explicit (IMEX) and trigonometric methods. Next, we show how discrete differential forms in spacetime can be used to derive a structure-preserving discretization of Maxwell's equations, with applications to computational electromagnetics. Finally, we sketch out some future directions in discrete gauge theory, providing foundations based on fiber bundles and Lie groupoids, as well as discussing applications to discrete Riemannian geometry and numerical general relativity.

Contents

Acknowledgments	iii
Abstract	v
Contents	vii
1 Introduction	1
1.1 Overview	1
1.2 Lagrangian Mechanics and Variational Integrators	2
1.3 Differential Forms, PDEs, and Discretization	10
1.4 Summary of Contributions	27
2 Variational Integrators for Highly Oscillatory Problems in Mechanics	29
2.1 Introduction	29
2.2 A Variational Implicit-Explicit Method	34
2.3 Variational Trigonometric Integrators	47
3 Computational Electromagnetics	53
3.1 Introduction	53
3.2 Maxwell's Equations	58
3.3 Discrete Forms in Computational Electromagnetics	63
3.4 Implementing Maxwell's Equations with DEC	67
3.5 Theoretical Results	82
3.6 Conclusion	87

4 Future Directions: Foundations for Discrete Gauge Theory and General Relativity	91
4.1 Fiber Bundles and Gauge Theory	91
4.2 Lie Groupoids and Bundle Connections	94
4.3 Discrete Riemannian Geometry with Frame Bundles	98
Bibliography	103

Chapter One

Introduction

1.1 OVERVIEW

In recent years, two important techniques for geometric numerical discretization have been developed. In computational electromagnetics, spatial discretization has been improved by the use of mixed finite elements and discrete differential forms. Simultaneously, the dynamical systems and mechanics communities have developed structure-preserving time integrators, notably variational integrators that are constructed from a Lagrangian action principle.

In this thesis, we present several contributions to time discretization for highly oscillatory mechanical systems, and to *spacetime* discretization for classical field theories, both from a common Lagrangian variational perspective. The resulting numerical methods have several geometrically desirable properties, including multisymplecticity, conservation of momentum maps via a discrete version of Noether's theorem, preservation of differential structure and gauge symmetries, lack of spurious modes, and excellent long-time energy conservation behavior. Many traditional numerical integrators (such as Runge–Kutta and node-based finite element methods) may fail to preserve one or more of these properties, particularly when simulating dynamical systems with important differential-geometric symmetries and structures—as is the case, in particular, with discrete field theories such as computational electromagnetics and numerical relativity. Like finite element methods, however, the geometric methods presented here can be readily applied to unstructured meshes (such as simplicial complexes), with little restriction of mesh topology or geometry.

The main idea for constructing these methods, drawing from recent work on variational integrators for mechanics, is the following: *rather than discretizing*

the equations of motion directly, first discretize the Lagrangian action functional of the system, and then derive the discrete equations of motion from a variational principle. That is, when the continuous system satisfies Euler–Lagrange equations for a particular action, then a variational integrator will consist of discrete Euler–Lagrange equations associated to some discrete action. In previous work, this action integral has been discretized using a numerical quadrature rule on a mesh of support nodes, e.g., using nodal finite elements of a certain order. While this approach was quite successful for certain problems, such as integrating ODEs in mechanics or PDEs in elastodynamics, it was less successful in its application to other field theories, especially electromagnetics. This thesis departs from previous efforts in discretizing field theories by *treating the Lagrangian itself as a discrete differential form.*

1.2 LAGRANGIAN MECHANICS AND VARIATIONAL INTEGRATORS

In this section, we provide a brief review of some of the key concepts and techniques from continuous-time Lagrangian mechanics. In addition, we show how *variational integrators* can be used to develop numerical time-discretization methods that preserve this Lagrangian structure. For a more comprehensive review of these topics, the reader may refer to Marsden and Ratiu (1999) and Marsden and West (2001).

1.2.1 Continuous-Time Lagrangian Mechanics.

The Lagrangian and the Action Integral. To define a mechanical system, we let Q be a smooth manifold, called the configuration space, and let TQ be its tangent bundle, called the phase space. The *Lagrangian* is a function $L: TQ \rightarrow \mathbb{R}$. For a path $q: [0, T] \rightarrow Q$, with initial time 0 and final time T , define the *action functional*

$$S[q] = \int_0^T L(q(t), \dot{q}(t)) dt.$$

Here, the “dot” notation $\dot{q}(t) = \frac{d}{dt} q(t)$ denotes an ordinary derivative with respect to time. For notational brevity, we will often suppress the time parameter (t) where it is implicitly clear, for example, writing $L(q, \dot{q})$.

Hamilton's Principle and the Euler–Lagrange Equations. Suppose we wish to find the trajectory $q(t)$ whose values at the initial and final time are given to be $q(0) = q_0$ and $q(T) = q_T$. *Hamilton's principle of stationary action* says that this trajectory must satisfy $\delta S[q] = \mathbf{d}S[q] \cdot \delta q = 0$, where δq is any variation of the path that preserves the initial- and final-time conditions, i.e., $\delta q(0) = \delta q(T) = 0$. The variation of the action can then be written as

$$\begin{aligned}\mathbf{d}S[q] \cdot \delta q &= \int_0^T \left[\frac{\partial L}{\partial q}(q, \dot{q}) \cdot \delta q + \frac{\partial L}{\partial \dot{q}}(q, \dot{q}) \cdot \delta \dot{q} \right] dt \\ &= \int_0^T \left[\frac{\partial L}{\partial q}(q, \dot{q}) - \frac{d}{dt} \frac{\partial L}{\partial \dot{q}}(q, \dot{q}) \right] \cdot \delta q dt \\ &= 0,\end{aligned}$$

where in the second step we have integrated by parts, noting that the boundary terms disappear since δq vanishes at the endpoints. Since δq is an arbitrary variation, the trajectory q satisfies Hamilton's principle if and only if it solves the *Euler–Lagrange equations*,

$$\frac{\partial L}{\partial q}(q, \dot{q}) - \frac{d}{dt} \frac{\partial L}{\partial \dot{q}}(q, \dot{q}) = 0,$$

which is a second-order system of ordinary differential equations in q .

Example 1.2.1. For a system with constant mass matrix M and a potential $V: Q \rightarrow \mathbb{R}$, the Lagrangian is given by the difference between kinetic and potential energy, $L(q, \dot{q}) = \frac{1}{2} \dot{q}^T M \dot{q} - V(q)$. The Euler–Lagrange equations are therefore $-\nabla V(q) - \frac{d}{dt}(M\dot{q}) = 0$, or equivalently $M\ddot{q} = -\nabla V(q)$. This coincides with the familiar $F = Ma$ expression of Newton's second law for a conservative force.

Remark. This Lagrangian variational structure is closely related to the “weak formulation” of a problem, often encountered in the analysis of differential equations, and commonly used as a framework to develop variational numerical methods (e.g., by solving a variational problem on a space of finite elements). Suppose we define $\mathcal{C}(Q)$ to be the space of C^2 paths $q: [0, T] \rightarrow Q$ satisfying the boundary conditions, so that variations δq live in the tangent space $T_q \mathcal{C}(Q)$. In this language, Hamilton's principle specifies the following weak problem:

Find $q \in \mathcal{C}(Q)$ such that for all $\delta q \in T_q \mathcal{C}(Q)$, we have $\mathbf{d}S[q] \cdot \delta q = 0$.

It should be noted that this is developed as a variational problem from first principles; by contrast, it is common practice to “reverse engineer” a variational problem by, for example, integrating the desired differential equation against a test function and then performing integration by parts.

Euler–Lagrange Flows are Symplectic. Let us define the one-parameter flow map $F_t: TQ \rightarrow TQ$, taking $(q_0, \dot{q}_0) \mapsto (q(t), \dot{q}(t))$, where q is the solution to the Euler–Lagrange equations with initial conditions $(q(0), \dot{q}(0)) = (q_0, \dot{q}_0)$. It is then possible to define a *restricted action functional* $S_{TQ}: TQ \rightarrow \mathbb{R}$, using the flow map to pull the Lagrangian back to the space of initial conditions

$$S_{TQ}(q_0, \dot{q}_0) = \int_0^T F_t^* L(q_0, \dot{q}_0) dt = \int_0^T L(q, \dot{q}) dt.$$

Now, let us vary with respect to the initial conditions, along variations δq_0 and $\delta \dot{q}_0$

$$\begin{aligned} dS_{TQ}(q_0, \dot{q}_0) \cdot (\delta q_0, \delta \dot{q}_0) &= \int_0^T \left[\frac{\partial L}{\partial q}(q, \dot{q}) \cdot \delta q + \frac{\partial L}{\partial \dot{q}}(q, \dot{q}) \cdot \delta \dot{q} \right] dt \\ &= \int_0^T \left[\frac{\partial L}{\partial q}(q, \dot{q}) - \frac{d}{dt} \frac{\partial L}{\partial \dot{q}}(q, \dot{q}) \right] \cdot \delta q dt + \left[\frac{\partial L}{\partial \dot{q}}(q, \dot{q}) \cdot \delta q \right]_0^T \\ &= \left[\frac{\partial L}{\partial \dot{q}}(q, \dot{q}) \cdot \delta q \right]_0^T. \end{aligned}$$

Note that, because these variations do not have the fixed-endpoint property as before, we pick up a boundary term when integrating by parts in step 2. Moreover, the nonboundary term vanishes in step 3, since q is a solution of the Euler–Lagrange equations.

Now, let us define the *canonical 1-form* $\theta_L \in \Omega^1(TQ)$ such that $\theta_L \cdot \delta q = \frac{\partial L}{\partial \dot{q}} \cdot \delta q$, or in coordinates, $\theta_L = \frac{\partial L}{\partial \dot{q}^i} dq^i$. Then the previous equation can be rewritten simply as $dS_{TQ} = F_T^* \theta_L - \theta_L$. Taking the exterior derivative of both sides and noting that $ddS_{TQ} = 0$, we get

$$F_T^*(d\theta_L) = d\theta_L.$$

Therefore, defining the *symplectic 2-form* $\omega_L = -d\theta_L = dq^i \wedge d\frac{\partial L}{\partial \dot{q}^i}$, it follows that the Euler–Lagrange flow map preserves ω_L and hence is a symplectic flow.

Remark. Symplecticity is typically discussed in the context of Hamiltonian flows on T^*Q , where one defines the canonical 1-form $\theta_H = p_i dq^i$ and symplectic 2-form

$\omega_H = -d\theta_H = dq^i \wedge dp_i$. This is equivalent to the Lagrangian formulation with respect to the Legendre transformation $TQ \rightarrow T^*Q$, which takes $(q, \dot{q}) \mapsto (q, p) = \left(q, \frac{\partial L}{\partial \dot{q}}(q, \dot{q})\right)$.

Noether's Theorem and Momentum Maps. Suppose that a Lie group G with Lie algebra \mathfrak{g} acts on Q , and that the Lagrangian is invariant with respect to this G -action. Then, if we take some element $\xi \in \mathfrak{g}$ with infinitesimal generator $\xi_{TQ} \in TQ$, this invariance says that

$$dS_{TQ}(q_0, \dot{q}_0) \cdot \xi_{TQ} = 0.$$

However, we have previously shown that $dS_{TQ} = F_T^*\theta_L - \theta_L$, so it follows that

$$F_T^*(\theta_L \cdot \xi_{TQ}) = \theta_L \cdot \xi_{TQ},$$

and so the quantity $\theta_L \cdot \xi_{TQ}$ is conserved by the Euler–Lagrange flow. Therefore, we can define a conserved *momentum map* $J: TQ \rightarrow \mathfrak{g}^*$, given by $\langle J(q, \dot{q}), \xi \rangle = \theta_L(q, \dot{q}) \cdot \xi_{TQ}$. This fundamental result is known as *Noether's theorem*.

The Hamilton–Pontryagin Variational Principle. Another variational approach to Lagrangian mechanics—which has the added appeal of intrinsically combining the Hamiltonian point of view on T^*Q and the Lagrangian perspective on TQ —is the so-called *Hamilton–Pontryagin principle*, whose variational structure was studied by Yoshimura and Marsden (2006). Rather than extremizing the action over paths q on Q , one defines an extended action functional on paths $(q, v, p) \in TQ \oplus T^*Q$, consisting of position as well as velocity and momentum; this bundle is called the *Pontryagin bundle*. The Hamilton–Pontryagin action is given by

$$S[q, v, p] = \int_0^T [L(q, v) + \langle p, \dot{q} - v \rangle] dt,$$

where $\langle \cdot, \cdot \rangle$ is the pairing between covectors and vectors. The idea is to treat position q and velocity v as independent variables, and then to use the momentum p as a Lagrange multiplier to (weakly) enforce the constraint $v = \dot{q}$.

If we take variations of this action, assuming as before that q satisfies boundary conditions, so that $\delta q = 0$ at the endpoints, we get

$$\begin{aligned} \mathbf{d}S[q, v, p] \cdot (\delta q, \delta v, \delta p) &= \int_0^T \left[\left\langle \frac{\partial L}{\partial q}(q, v), \delta q \right\rangle + \left\langle \frac{\partial L}{\partial v}(q, v), \delta v \right\rangle \right. \\ &\quad \left. + \langle \delta p, \dot{q} - v \rangle + \langle p, \delta \dot{q} - \delta v \rangle \right] \\ &= \int_0^T \left[\left\langle \frac{\partial L}{\partial q}(q, v) - \dot{p}, \delta q \right\rangle + \left\langle \frac{\partial L}{\partial v}(q, v) - p, \delta v \right\rangle + \langle \delta p, \dot{q} - v \rangle \right]. \end{aligned}$$

Setting this equal to zero, one obtains the *implicit Euler–Lagrange equations*

$$\dot{p} = \frac{\partial L}{\partial q}(q, v), \quad p = \frac{\partial L}{\partial v}(q, v), \quad \dot{q} = v.$$

Thus, in addition to the Euler–Lagrange equations and the constraint $\dot{q} = v$, one also obtains the Legendre transform as part of the equations, an automatic consequence of the Hamilton–Pontryagin variational principle.

1.2.2 Discrete Mechanics and Variational Integrators.

The Discrete Lagrangian and the Action Sum. Suppose that we wish to discretize a mechanical system, whose continuous Lagrangian is $L: TQ \rightarrow \mathbb{R}$, on the time interval $[0, T]$. First, we partition the time interval by a finite number of points $0 = t_0 < \dots < t_N = T$; likewise, the path $q: [0, T] \rightarrow Q$ is replaced by a sequence of configurations q_0, \dots, q_N , where $q_n \approx q(t_n)$. Then the *discrete Lagrangian* is a function $L_h: Q \times Q \rightarrow \mathbb{R}$, so that $L_h(q_n, q_{n+1}) \approx \int_{t_n}^{t_{n+1}} L(q, \dot{q}) dt$, e.g., using a particular quadrature rule. The continuous action functional is therefore approximated by the *discrete action sum*

$$S_h(q_0, \dots, q_N) = \sum_{n=0}^{N-1} L_h(q_n, q_{n+1}) \approx \int_0^T L(q, \dot{q}) dt.$$

The Discrete Hamilton’s Principle and Euler–Lagrange Equations. We say that a discrete trajectory satisfies Hamilton’s stationary action principle if $\delta S_h(q_0, \dots, q_N) = 0$; again we require the endpoints to be fixed, so $\delta q_0 = \delta q_N = 0$. The variation of the discrete action is therefore

$$\delta S_h(q_0, \dots, q_N) = \sum_{n=0}^{N-1} [D_1 L_h(q_n, q_{n+1}) \cdot \delta q_n + D_2 L_h(q_n, q_{n+1}) \cdot \delta q_{n+1}],$$

where $D_1 L_h$ and $D_2 L_h$ denote the partial derivatives of L_h with respect to the first and second arguments. Performing “summation by parts” and using the fact that the variation at the endpoints is fixed, we get

$$\delta S_h(q_0, \dots, q_N) = \sum_{n=1}^{N-1} [D_1 L_h(q_n, q_{n+1}) + D_2 L_h(q_{n-1}, q_n)] \cdot \delta q_n = 0.$$

Therefore, since the variations δq_n are arbitrary, Hamilton’s principle is equivalent to the *Discrete Euler–Lagrange (DEL) equations*

$$D_1 L_h(q_n, q_{n+1}) + D_2 L_h(q_{n-1}, q_n) = 0, \quad n = 1, \dots, N-1.$$

This defines a discrete update rule taking $(q_{n-1}, q_n) \mapsto (q_n, q_{n+1})$, which can be thought of as the flow map of the DEL equations.

This specifies a numerical method, called a *variational integrator*, for approximating solutions to the Euler–Lagrange equations.

Example 1.2.2. Consider a mechanical system with the Lagrangian $L: TQ \rightarrow \mathbb{R}$, where Q is a vector space, and suppose we wish to discretize this system at the times $t_0 < \dots < t_N$, with uniform time step size $h = t_{n+1} - t_n$ for $n = 0, \dots, N-1$. Then, using the second-order trapezoidal quadrature rule, we obtain the discrete Lagrangian

$$L_h^{\text{trap}}(q_n, q_{n+1}) = \frac{1}{2} \left[L\left(q_n, \frac{q_{n+1} - q_n}{h}\right) + L\left(q_{n+1}, \frac{q_{n+1} - q_n}{h}\right) \right].$$

This results in the DEL equations

$$\begin{aligned} \frac{1}{2} \left[\frac{\partial L}{\partial q} \left(q_n, \frac{q_{n+1} - q_n}{h} \right) + \frac{\partial L}{\partial q} \left(q_n, \frac{q_n - q_{n-1}}{h} \right) \right] &= \frac{1}{2h} \left[\frac{\partial L}{\partial \dot{q}} \left(q_n, \frac{q_{n+1} - q_n}{h} \right) \right. \\ &\quad \left. + \frac{\partial L}{\partial \dot{q}} \left(q_{n+1}, \frac{q_{n+1} - q_n}{h} \right) - \frac{\partial L}{\partial \dot{q}} \left(q_n, \frac{q_n - q_{n-1}}{h} \right) - \frac{\partial L}{\partial \dot{q}} \left(q_{n-1}, \frac{q_n - q_{n-1}}{h} \right) \right], \end{aligned}$$

which can be seen as an approximation of the continuous Euler–Lagrange equations.

In particular, if the Lagrangian is of the form $L(q, \dot{q}) = \frac{1}{2} \dot{q}^T M \dot{q} - V(q)$, for a constant mass matrix M and potential function $V: Q \rightarrow \mathbb{R}$, then the discrete Lagrangian becomes

$$L_h(q_n, q_{n+1}) = \frac{h}{2} \left(\frac{q_{n+1} - q_n}{h} \right)^T M \left(\frac{q_{n+1} - q_n}{h} \right) - \frac{h}{2} [V(q_n) + V(q_{n+1})],$$

and the DEL equations can be written

$$M \frac{q_{n+1} - 2q_n + q_{n-1}}{h^2} = -\nabla V(q_n).$$

This is equivalent to the Störmer/Verlet method, which is a second-order symplectic integrator.

Initial and Final Conditions in Phase Space. This formulation of variational integrators presents one immediate difficulty. To solve an initial value problem, for example, we must specify the first two positions (q_0, q_1) , and compute up to the final two positions (q_{N-1}, q_N) . However, this is not how most problems are posed; rather, we usually wish to specify the initial position and velocity $(q_0, \dot{q}_0) \in TQ$ and solve for the final conditions $(q_N, \dot{q}_N) \in TQ$. In addition, the symplectic form is defined on TQ (or T^*Q), so to speak about the symplecticity of a numerical method, we will also have to understand the relationship between flows in $Q \times Q$ and flows in the phase space TQ .

To do this, suppose we add two additional time steps very close to the initial and final times, $t_{-\varepsilon} = t_0 - \varepsilon$ and $t_{N+\varepsilon} = t_N + \varepsilon$. Then, taking fixed-endpoint variations of q_n , we have $\delta q_{-\varepsilon} = \delta q_{N+\varepsilon} = 0$, while δq_0 and δq_N can now be nonzero. Therefore, in addition to the usual DEL equations for $k = 1, \dots, N-1$, we get two new equations

$$\begin{aligned} D_1 L_h(q_0, q_1) + D_2 L_h(q_{-\varepsilon}, q_0) &= 0 \\ D_1 L_h(q_N, q_{N+\varepsilon}) + D_2 L_h(q_{N-1}, q_N) &= 0. \end{aligned}$$

Now, let us look at the limiting behavior of these equations as $\varepsilon \rightarrow 0$. Supposing $L_h(q_{-\varepsilon}, q_0) \approx \varepsilon L(q_{-\varepsilon}, \frac{q_0 - q_{-\varepsilon}}{\varepsilon})$, i.e., the discrete Lagrangian approximates the action integral to at least first-order accuracy, we then have

$$D_2 L_h(q_{-\varepsilon}, q_0) \approx \frac{\partial L}{\partial \dot{q}}\left(q_{-\varepsilon}, \frac{q_0 - q_{-\varepsilon}}{\varepsilon}\right) \rightarrow \frac{\partial L}{\partial \dot{q}}(q_0, \dot{q}_0).$$

Likewise, at the final time step we have the limit

$$D_1 L_h(q_N, q_{N+\varepsilon}) \rightarrow -\frac{\partial L}{\partial \dot{q}}(q_N, \dot{q}_N).$$

Therefore, we can define a transformation between initial conditions (q_0, \dot{q}_0) and (q_0, q_1) so as to satisfy

$$D_1 L_h(q_0, q_1) + \frac{\partial L}{\partial \dot{q}}(q_0, \dot{q}_0) = 0.$$

Similarly, we have another transformation for the final conditions, defined by the equation

$$-\frac{\partial L}{\partial \dot{q}}(q_N, \dot{q}_N) + D_2 L_h(q_{N-1}, q_N) = 0.$$

Pulling back by the continuous form of the Legendre transform, $p = \frac{\partial L}{\partial \dot{q}}(q, \dot{q})$, we can write these conditions as

$$\begin{aligned} D_1 L_h(q_0, q_1) + p_0 &= 0 \\ -p_N + D_2 L_h(q_{N-1}, q_N) &= 0, \end{aligned}$$

which agrees with the *discrete Legendre transform* (see Marsden and West, 2001). This shows that the discrete Legendre transform, far from being an arbitrary map between T^*Q and $Q \times Q$, can be defined in terms of the original variational principle by using a limiting argument. Later, we will extend this argument to understand the initial, final, and boundary values of discrete field theories, as well as their multisymplectic structure.

Variational Integrators are Symplectic. Now that we have shown how to define initial and final conditions on TQ for variational integrators, we can define a *discrete flow map* $F_h: TQ \rightarrow TQ$, taking $(q_0, \dot{q}_0) \mapsto (q_1, \dot{q}_1)$, which corresponds to one time step of the DEL equations. (For multiple time steps, F_h can be applied repeatedly by composition.) Then, as in the continuous case, we have a restricted action, which is simply

$$S_{h,TQ}(q_0, \dot{q}_0) = L_h(q_0, q_1).$$

Taking variations of this restricted action with respect to the initial conditions, we get

$$\begin{aligned} \delta S_{h,TQ}(q_0, \dot{q}_0) &= D_1 L_h(q_0, q_1) \cdot \delta q_0 + D_2 L_h(q_0, q_1) \cdot \delta q_1 \\ &= -\frac{\partial L}{\partial \dot{q}}(q_0, \dot{q}_0) \cdot \delta q_0 + \frac{\partial L}{\partial \dot{q}}(q_1, \dot{q}_1) \cdot \delta q_1. \end{aligned}$$

In terms of the canonical 1-form θ_L , defined as before, this expression can be written as

$$dS_{h,TQ} = F_h^* \theta_L - \theta_L.$$

Finally, taking the exterior derivative of both sides and recalling the definition of the symplectic 2-form $\omega_L = -d\theta_L$, then the identity $dd = 0$ implies

$$F_h^* \omega_L = \omega_L,$$

and hence the discrete flow map is symplectic. This is, of course, also true when taking N time steps for any $N \in \mathbb{N}$, since the composition $\overbrace{F_h \circ \cdots \circ F_h}^N$ of symplectic maps is also symplectic.

Discrete Noether's Theorem: Variational Integrators Preserve Momentum Maps. As in the continuous case, consider the momentum map $J: TQ \rightarrow \mathfrak{g}^*$ defined by $\langle J(q, \dot{q}), \xi \rangle = \theta_L(q, \dot{q}) \cdot \xi_{TQ}$, where again, the Lagrangian is invariant with respect to the Lie group G , ξ is an arbitrary element of its Lie algebra \mathfrak{g} , and ξ_{TQ} is the infinitesimal generator of ξ . Then

$$0 = dS_{h,TQ} \cdot \xi_{TQ} = F_h^*(\theta_L \cdot \xi_{TQ}) - \theta_L \cdot \xi_{TQ},$$

and hence

$$F_h^*(\theta_L \cdot \xi_{TQ}) = \theta_L \cdot \xi_{TQ}.$$

Therefore, the flow of the DEL equations conserves the quantity $\theta_L \cdot \xi_{TQ}$, and so the momentum map J is invariant with respect to this flow.

1.3 DIFFERENTIAL FORMS, PDES, AND DISCRETIZATION

As we have seen, variational integrators provide a geometric framework for time discretization. While this is sufficient for the ODEs of classical mechanics, the PDEs of classical field theory require a unified approach to discretizing both time and space. Differential forms provide a useful foundation for doing this. In addition to being covariant (which is useful in itself for field theories on smooth manifolds), they are also readily discretized using the chains and cochains of algebraic topology, which preserve important topological structures and invariants from homology and cohomology theory.

1.3.1 Elliptic and Hyperbolic PDEs on Smooth Manifolds. First, we will outline how some common elliptic and hyperbolic PDEs can be written in terms of differential forms on smooth manifolds. In particular, we will focus on the Laplace–Beltrami operator, and its application to Laplace’s and Poisson’s equations, as well as the wave equation. Later, in Chapter 3, we will apply this same general approach to Maxwell’s equations for electromagnetism.

The Laplace–Beltrami Operator. We will first quickly recall the basic operators of exterior calculus, in order to define the Laplace–Beltrami operator on differential forms. (For a more exhaustive review of exterior calculus, see Abraham, Marsden, and Ratiu, 1988, Chapter 7).

Let X be a smooth, orientable $(n+m)$ -dimensional pseudo-Riemannian manifold, with metric signature (n, m) . Let $\Omega^k(X)$ denote the space of differential k -forms on X , where $d: \Omega^k(X) \rightarrow \Omega^{k+1}(X)$ is the exterior derivative and $*: \Omega^k(X) \rightarrow \Omega^{n+m-k}(X)$ is the Hodge star associated to the metric on X . Next, we define the codifferential operator $\delta: \Omega^{k+1}(X) \rightarrow \Omega^k(X)$ to be

$$\delta = (-1)^{(n+m)k+1+m} * d * .$$

Finally, we define the *Laplace–Beltrami operator*, applied to scalar functions on X , to be $\delta d: \Omega^0(X) \rightarrow \Omega^0(X)$. One can also apply the Laplace–Beltrami operator to k -forms for general k ; another generalization is the *Laplace–de Rham operator* $(\delta d + d\delta): \Omega^k(X) \rightarrow \Omega^k(X)$, which reduces to Laplace–Beltrami when $k = 0$.

Laplace–Beltrami as an Elliptic Operator. Suppose that X is an n -dimensional Riemannian manifold, and let $u \in \Omega^0(X)$ be a scalar function on X . If $X = \mathbb{R}^n$ with the Euclidean metric, then the Laplace–Beltrami operator δd is precisely the usual Laplacian Δ , up to a sign. To see this, observe that in standard coordinates

$$*d*du = *d*(\partial_i u dx^i) = *d(\partial^i u d^{n-1}x_i) = *(\partial_i \partial^i u d^n x) = \partial_i \partial^i u = \Delta u,$$

where this expression uses the Einstein index notation for summing over i .

More generally, suppose that X has the Riemannian metric g . Then in local coordinates, we have $g = g_{ij} dx^i \otimes dx^j$, and

$$\begin{aligned} *d*du &= *d*(\partial_i u dx^i) \\ &= *d\left(\sqrt{|g|}\partial^i u d^{n-1}x_i\right) \\ &= *\left[\partial_i\left(\sqrt{|g|}\partial^i u\right)d^n x\right] \\ &= \frac{1}{\sqrt{|g|}}\partial_i\left(\sqrt{|g|}\partial^i u\right). \end{aligned}$$

Here, following the usual conventions of tensor calculus, $|g|$ denotes the (absolute) determinant of the matrix (g_{ij}) and $\partial^i = g^{ij}\partial_j$, where (g^{ij}) is the inverse matrix of (g_{ij}) . Therefore, a general elliptic operator—traditionally written as $\nabla \cdot a \nabla$ for some function a —can be expressed as the Laplace–Beltrami operator for a suitable metric. This includes the possibility for the metric to be inhomogeneous and/or anisotropic, relative to a certain coordinate parametrization.

Laplace's and Poisson's Equations. One of the most fundamental elliptic PDEs is *Poisson's equation*

$$\Delta u = f,$$

which is called *Laplace's equation* in the special case $f = 0$. We can use the Laplace–Beltrami operator to translate this problem in terms of differential forms on a Riemannian manifold X .

Given some scalar function $f \in \Omega^0(X)$, we wish to find another scalar function $u \in \Omega^0(X)$ such that

$$\delta du = f.$$

This is the second-order formulation of Poisson's equation. One can also introduce an auxiliary field $v \in \Omega^1(X)$, and then rewrite this as a first-order system of equations

$$du = v, \quad \delta v = f.$$

Alternatively, this can be written, following the approach to multisymplectic field theory outlined in Bridges (2006), as

$$\begin{pmatrix} 0 & \delta \\ d & 0 \end{pmatrix} \begin{pmatrix} u \\ v \end{pmatrix} = \begin{pmatrix} f \\ v \end{pmatrix}.$$

Here, the matrix $J_\partial = \begin{pmatrix} 0 & \delta \\ d & 0 \end{pmatrix}$ provides a generalization of the operator $J \frac{d}{dt}$ in Hamiltonian mechanics, where $J = \begin{pmatrix} 0 & -I \\ I & 0 \end{pmatrix}$ is the usual symplectic matrix.

Now, suppose that u is simply a scalar potential for the 1-form $v = du$, and we only care about solving for the values of v . In this case, we can eliminate the explicit dependence on u by observing that $dv = ddu = 0$, and therefore we can simply solve the system

$$dv = 0, \quad \delta v = f.$$

This is equivalent to finding a vector field $v^\sharp \in \mathfrak{X}(X)$, which is curl-free and has divergence f . If, later, one needs to reconstruct u from a solution for v , then this can be done (at least locally) by using the Poincaré lemma.

Laplace–Beltrami as a Hyperbolic Operator. Suppose now that X is an $(n+1)$ -dimensional Lorentzian manifold, i.e., a pseudo-Riemannian manifold with metric signature $(n, 1)$. In this case, since the metric is positive-definite in n dimensions and negative-definite in 1 dimension, the Laplace–Beltrami operator δd becomes a *hyperbolic operator*. In particular, the negative term arises when taking the first Hodge star, in order to raise the index $\partial^i = g^{ij}\partial_j$.

Consider the simple $(1+1)$ -dimensional example of $X = \mathbb{R}^{1,1}$, where in coordinates the metric is given by

$$g = dx \otimes dx - dt \otimes dt.$$

Then, if $u \in \Omega^0(X)$, we have

$$\begin{aligned} *d*d u &= *d*(u_x dx + u_t dt) \\ &= *d(u_x dt + u_t dx) \\ &= *(u_{xx} dx \wedge dt + u_{tt} dt \wedge dx) \\ &= u_{xx} - u_{tt} \\ &= \square u, \end{aligned}$$

where \square denotes the *d'Alembertian wave operator*. Therefore, the Laplace–Beltrami operator δd generalizes the d'Alembertian \square on a Lorentzian manifold, much as it generalizes the Laplacian Δ on a Riemannian manifold. In particular, the wave speed can be specified by choosing the appropriate Lorentzian metric g .

The Wave and Transport Equations. The *wave equation* is the hyperbolic PDE

$$\square u = 0.$$

In $\mathbb{R}^{1,1}$, it is common in the PDE literature to “factor” the wave operator as

$$\square u = \left(\frac{\partial^2}{\partial x^2} - \frac{\partial^2}{\partial t^2} \right) u = \left(\frac{\partial}{\partial x} - \frac{\partial}{\partial t} \right) \left(\frac{\partial}{\partial x} + \frac{\partial}{\partial t} \right) u,$$

so by substituting $v = \left(\frac{\partial}{\partial x} + \frac{\partial}{\partial t} \right) u$, one can simply study the first-order equation

$$v_t = v_x,$$

which is also called the *transport equation*.

On a general Lorentzian manifold, the wave equation is simply written as

$$\delta du = 0,$$

which is formally identical to Laplace's equation. Again, the wave speed is determined by the metric, which manifests in the Hodge star operator. Just as before, we can rewrite this as the first-order system

$$du = v, \quad \delta v = 0,$$

or simply in terms of $v \in \Omega^1(X)$ as

$$dv = 0, \quad \delta v = 0.$$

This latter formulation can be seen as a more *geometric* version of the transport equation. Furthermore, because the “factorization” $\square = \delta \circ d$ works for any n , not just $n = 1$, this can be seen as a coordinate-free generalization of transport and conservation laws for any number of spatial dimensions.

1.3.2 Lagrangian Variational Principles and Multisymplectic Geometry. Just as the ODEs of classical mechanics can be described by a Lagrangian variational structure, so too can the PDEs of classical field theory. Because the Lagrangian is defined as a quantity to be integrated (via the action integral), it is natural to develop a generalization of this structure in terms of differential forms. To do this, we will replace the Lagrangian function L by a *Lagrangian density* $\mathcal{L} \in \Omega^{n+m}(X)$, so that the action integral is given by $S = \int \mathcal{L}$. Ordinary Lagrangian mechanics is a special case: given a time interval $X = [0, T]$ and a Lagrangian function $L: TQ \rightarrow \mathbb{R}$, the corresponding Lagrangian density is $\mathcal{L} = L dt$. Furthermore, this variational structure leads to a generalization of symplectic geometry, called *multisymplectic geometry*, which reduces to ordinary symplecticity in the one-dimensional case of mechanics.

In the above summary, we have glossed over one fundamental question—What is the appropriate generalization of the tangent bundle TQ and cotangent bundle T^*Q to fields over the higher-dimensional manifold X ?—to which several possible answers have been given. One approach (as in Marsden, Patrick, and Shkoller, 1998; Marsden, Pekarsky, Shkoller, and West, 2001; and Gotay and Marsden, 2008) is to view fields over X as sections of some fiber bundle $B \rightarrow X$, with fiber Y , and then to consider the first *jet bundle* $J^1 B$ and its dual $(J^1 B)^*$ as the appropriate analogs of the tangent and cotangent bundles. (Informally, the jet bundle consists of Y -valued functions and their Jacobians.) One drawback of this approach, however, is that it is more general than required for fields of differential forms: one often cares only about the *antisymmetric part* of the Jacobian (i.e., the exterior derivative) rather than all of its components individually. We will follow an approach that hews more closely to that of Bridges (2006), who uses the so-called *total exterior algebra bundle*, consisting of differential forms over X , rather than the jet bundle. However, our approach will diverge from Bridges' in several ways, particularly in the generalization of the Hamilton–Pontryagin variational principle, and the associated Legendre–Hodge transform (which generalizes the Legendre transform from mechanics).

In this section, we will develop this theory relatively quickly, primarily by example, examining its application to the scalar PDEs introduced in the previous section. Later chapters will expand this treatment to more sophisticated field theories, in-

cluding electromagnetics and nonabelian gauge theories, such as general relativity. Note that we will avoid the δ notation for taking variations, reserving the use of this symbol for the codifferential. (As done earlier without comment, we use a bold \mathbf{d} to indicate a *functional* exterior derivative, which can be evaluated along a variation, in order to distinguish it from the usual exterior derivative d for forms on X .)

Hamilton's Principle and Euler–Lagrange Equations. As before, let X be an orientable pseudo-Riemannian manifold, with $u \in \Omega^0(X)$ a scalar field, and consider the Lagrangian density

$$\mathcal{L}(u, du) = -\frac{1}{2}du \wedge *du.$$

This expression is closely related to the \mathbb{L}^2 inner product $(\cdot, \cdot) : \Omega^k(X) \times \Omega^k(X) \rightarrow \mathbb{R}$ on differential k -forms, which is defined by

$$(\alpha, \beta) = \int_X \alpha \wedge * \beta.$$

An important property of this inner product is that the codifferential δ is dual to the exterior derivative d (hence its name), corresponding to integration by parts, assuming that the boundary terms vanish. Specifically, let $\alpha \in \Omega^k(X)$, $\beta \in \Omega^{k+1}(X)$, and then by the Leibniz rule,

$$d(\alpha \wedge * \beta) = d\alpha \wedge * \beta - \alpha \wedge * d\beta.$$

Integrating over X and applying Stokes' theorem,

$$\int_{\partial X} \alpha \wedge * \beta = (d\alpha, \beta) - (\alpha, \delta\beta),$$

so when the left-hand side vanishes, we have $(d\alpha, \beta) = (\alpha, \delta\beta)$.

Therefore, the action associated to the Lagrangian density \mathcal{L} is

$$S[u] = \int_X \mathcal{L} = -\frac{1}{2} (du, du).$$

Let $\tilde{u} \in \Omega^0(X)$ be a variation of u preserving boundary conditions, so that $\tilde{u}|_{\partial X} = 0$. Then the variation of the action along \tilde{u} is

$$\mathbf{d}S[u] \cdot \tilde{u} = -(d\tilde{u}, du) = -(\tilde{u}, \delta du).$$

Setting this variation equal to zero, we get the Euler–Lagrange equation

$$\delta \mathrm{d}u = 0,$$

which coincides with Laplace's equation or the wave equation, respectively, when X is Riemannian or Lorentzian.

More generally, a nonhomogeneous linear system, such as Poisson's equation, is obtained by adding a term to the Lagrangian density

$$\mathcal{L} = -\frac{1}{2} \mathrm{d}u \wedge * \mathrm{d}u + u \wedge *f,$$

for some $f \in \Omega^0(X)$, where f does not depend on u . If f does depend on u (i.e., the system is nonlinear) then one must take a slightly different approach: keeping the Lagrangian density as before, $\mathcal{L} = -\frac{1}{2} \mathrm{d}u \wedge * \mathrm{d}u$, one can use the modified variational principle

$$\mathbf{d}S[u] \cdot \tilde{u} + (\tilde{u}, f) = 0,$$

which generalizes the Lagrange–d'Alembert principle from mechanics.

A Generalized Hamilton–Pontryagin Principle for Fields. Following a similar approach to the Hamilton–Pontryagin principle, we define two auxiliary fields $v \in \Omega^1(X)$, $w \in \Omega^{n+m-1}(X)$, using w as a Lagrange multiplier to weakly enforce the constraint $v = \mathrm{d}u$. To do this, we define the extended action

$$S[u, v, w] = \int_X [\mathcal{L}(u, v) + (v - \mathrm{d}u) \wedge w].$$

For example, take the Lagrangian density corresponding to Poisson's equation,

$$\mathcal{L}(u, v) = -\frac{1}{2} v \wedge *v + u \wedge *f.$$

Now, suppose that \tilde{u} , \tilde{v} , \tilde{w} are variations that vanish on the boundary ∂X . Then the variation of the extended action is

$$\begin{aligned} \mathbf{d}S[u, v, w] \cdot (\tilde{u}, \tilde{v}, \tilde{w}) &= \int_X [-\tilde{v} \wedge *v + \tilde{u} \wedge *f + (\tilde{v} - \mathrm{d}\tilde{u}) \wedge w + (v - \mathrm{d}u) \wedge \tilde{w}] \\ &= \int_X [\tilde{u} \wedge (*f + \mathrm{d}w) - \tilde{v} \wedge (*v - w) + (v - \mathrm{d}u) \wedge \tilde{w}]. \end{aligned}$$

Setting this equal to zero, we get the implicit Euler–Lagrange equations

$$\mathrm{d}w = -*f, \quad w = *v, \quad \mathrm{d}u = v.$$

This formulation effectively separates the *topological* content of the equations (the first and third equations, which only involve exterior derivatives of the fields) from their *geometric* content (the second equation, which uses the metric to establish duality between w and v).

The second equation is analogous to the Legendre transform in mechanics; Bridges (2006) refers to a closely related generalization as the *Legendre–Hodge transform*. In this case, the transform is defined simply by the Hodge star operator between a 1-form and its dual. In fact, we will see later that this transform plays a crucial role in electromagnetics, where it corresponds to the constitutive laws for Maxwell’s equations.

Multisymplectic Geometry. Returning to Hamilton’s action principle, suppose now that we restrict u to the space of Euler–Lagrange solutions, while taking a variation η that no longer vanishes the boundary ∂X . In this case, if we vary the restricted action along η , we get only the boundary integral term

$$\mathbf{d}S[u] \cdot \eta = \int_{\partial X} \eta \wedge * \mathrm{d}u.$$

If we vary this yet again, along another variation v , this becomes

$$\mathbf{d}\mathbf{d}S[u] \cdot \eta \cdot v = \int_{\partial X} \frac{1}{2} (\eta \wedge * \mathrm{d}v - v \wedge * \mathrm{d}\eta).$$

The left-hand side vanishes, since $\mathbf{d}\mathbf{d} \equiv 0$, resulting in the identity

$$\int_{\partial X} (\eta \wedge * \mathrm{d}v - v \wedge * \mathrm{d}\eta) = 0$$

for all η and v . We can verify this directly, as follows. Since η and v are variations taken in the space of Euler–Lagrange solutions, then we must have $\delta \mathrm{d}\eta = \delta \mathrm{d}v = 0$. Now, applying Stokes’ theorem to the left-hand side above, and using this fact about

η and ν , we get

$$\begin{aligned} \int_{\partial X} (\eta \wedge *d\nu - \nu \wedge *d\eta) &= \int_X (d\eta \wedge *d\nu - \eta \wedge *\delta d\nu - d\nu \wedge *d\eta + \nu \wedge *\delta d\eta) \\ &= \int_X (d\eta \wedge *d\nu - d\nu \wedge *d\eta) \\ &= (d\eta, d\nu) - (d\nu, d\eta) \\ &= 0, \end{aligned}$$

since the inner product (\cdot, \cdot) is symmetric.

Let us now rephrase these statements in the language of multisymplectic geometry. Take the canonical Cartan 1-form, associated to the Lagrangian density \mathcal{L} , to be $\theta_{\mathcal{L}} = du \wedge *du$, so that varying the restricted action gives

$$\mathbf{d}S[u] \cdot \eta = \int_{\partial X} \theta_{\mathcal{L}} \cdot \eta.$$

Then the multisymplectic 2-form is $\omega_{\mathcal{L}} = -\mathbf{d}\theta_{\mathcal{L}} = du \wedge d*du$, and thus

$$\mathbf{d}\mathbf{d}S[u] \cdot \eta \cdot \nu = \int_{\partial X} \omega_{\mathcal{L}} \cdot \eta \cdot \nu = 0.$$

This last equation is called the *multisymplectic form formula*. Returning to the special case of mechanics, where $X = [0, T] \Rightarrow \partial X = \{0, T\}$, this reduces to the statement that the (multi)symplectic 2-form is equal at the two endpoints.

Note that, with respect to the Legendre–Hodge transform $(u, du, *du) \mapsto (u, v, w)$, we have $\omega_{\mathcal{L}} = du \wedge dw$. This formally agrees with the canonical symplectic 2-form $\omega_L = dq \wedge dp$ for the case of Lagrangian mechanics.

1.3.3 Discrete Differential Forms and Operators. In this section, we show how to define differential forms and operators on a discrete mesh, in preparation for using this framework for computational modeling of classical fields. By construction, the calculus of discrete differential forms automatically preserves a number of important geometric structures, including Stokes' theorem, integration by parts (with a proper treatment of boundaries), the de Rham complex, Poincaré duality, Poincaré's lemma, and Hodge theory. Therefore, this provides a suitable foundation for the coordinate-free discretization of geometric field theories. In subsequent chapters, we will also use these discrete differential forms as the space of fields on which we will define discrete Lagrangian variational principles.

The particular “flavor” of discrete differential forms and operators we will be using is known as *discrete exterior calculus*, or *DEC* for short; see Hirani (2003) and Leok (2004). (For related efforts in this direction, see also Harrison, 2005; and Arnold, Falk, and Winther, 2006.) Guided by Cartan’s exterior calculus of differential forms on smooth manifolds, DEC is a discrete calculus developed, *ab initio*, on discrete manifolds, so as to maintain the covariant nature of the quantities involved. This computational tool is based on the notion of discrete chains and cochains, used as basic building blocks for compatible discretizations of important geometric structures such as the de Rham complex (Desbrun, Kanso, and Tong, 2005). The chain and cochain representations are not only attractive from a computational perspective due to their conceptual simplicity and elegance; as we will see, they also originate from a theoretical framework defined by Whitney (1957), who introduced the Whitney and de Rham maps that establish an isomorphism between simplicial cochains and Lipschitz differential forms.

Mesh and Dual Mesh. DEC is concerned with problems in which the smooth n -dimensional manifold X is replaced by a discrete mesh—precisely, by a cell complex that is manifold, admits a metric, and is orientable. The simplest example of such a mesh is a finite simplicial complex, such as a triangulation of a 2-D surface. We will generally denote the complex by K , and a cell in the complex by σ .

Given a mesh K , one can construct a *dual mesh* $*K$, where each k -cell σ corresponds to a dual $(n - k)$ -cell $*\sigma$. ($*K$ is “dual” to K in the sense of a graph dual.) One way to do this is as follows: place a dual vertex at the circumcenter of each n -simplex, then connect two dual vertices by an edge wherever the corresponding n -simplices share an $(n - 1)$ -simplex, and so on. This is called the *circumcentric dual*, and it has the important property that primal and dual cells are automatically orthogonal to one another, which is advantageous when defining an inner product (as we will see later in this section). For example, the circumcentric dual of a Delaunay triangulation, with the Euclidean metric, is its corresponding Voronoi diagram (see Figure 1.1). For more on the dual relationship between Delaunay triangulations and Voronoi diagrams, a standard reference is O’Rourke (1998). A similar construction of the circumcenter can be carried out for higher-dimensional Euclidean simplicial complexes, as well as for simplicial meshes in Minkowski

space. Note that, in both the Euclidean and Lorentzian cases, the circumcenter may actually lie *outside* the simplex if it has a very bad aspect ratio, underscoring the importance of mesh quality for good numerical results.

There are alternative ways to define the dual mesh—for example, placing dual vertices at the barycenter rather than the circumcenter—but we will use the circumcentric dual unless otherwise noted. Note that a refined definition of the dual mesh, where dual cells at the boundary are restricted to K , will be discussed in Chapter 3 to allow proper enforcement of boundary conditions in computational electromagnetics.

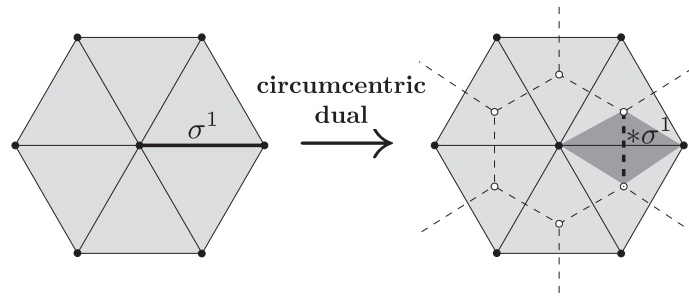


Figure 1.1: Given a 2-D simplicial mesh (left), we can construct its circumcentric dual mesh, called the Voronoi diagram of the primal mesh (right). In bold, we show one particular primal edge σ^1 (left) and its corresponding dual edge $*\sigma^1$ (right); the convex hull of these cells $\text{CH}(\sigma^1, *\sigma^1)$ is shaded dark grey.

Discrete Differential Forms. The fundamental objects of DEC are discrete differential forms. A discrete k -form α^k assigns a real number to each oriented k -dimensional cell σ^k in the mesh K . (The superscripts k are not actually required by the notation, but they are often useful as reminders of what order of form or cell we are dealing with.) This value is denoted by $\langle \alpha^k, \sigma^k \rangle$, and can be thought of as the value of α^k “integrated over” the element σ^k , i.e.,

$$\langle \alpha, \sigma \rangle \equiv \int_{\sigma} \alpha.$$

For example, 0-forms assign values to vertices, 1-forms assign values to edges, etc. We can extend this to integrate over discrete paths by linearity: simply add the form’s values on each cell in the path, taking care to flip the sign if the path is

oriented opposite the cell. Formally, these “paths” of k -dimensional elements are called *chains*, and discrete differential forms are *cochains*, where $\langle \cdot, \cdot \rangle$ is the pairing between cochains and chains.

Differential forms can be defined either on the mesh K or on its dual $*K$. We will refer to these as *primal forms* and *dual forms*, respectively. Note that there is a natural correspondence between primal k -forms and dual $(n - k)$ -forms, since each primal k -cell has a dual $(n - k)$ -cell. This is an important property that will be used below to define the discrete Hodge star operator.

Exterior Derivative. The discrete exterior derivative d is constructed to satisfy Stokes’ theorem, which in the continuous sense is written

$$\int_{\sigma} d\alpha = \int_{\partial\sigma} \alpha.$$

Therefore, if α is a discrete differential k -form, then the $(k + 1)$ -form $d\alpha$ is defined on any $(k + 1)$ -chain σ by

$$\langle d\alpha, \sigma \rangle = \langle \alpha, \partial\sigma \rangle,$$

where $\partial\sigma$ is the k -chain boundary of σ . For this reason, d is often called the *coboundary* operator in cohomology theory.

Diagonal Hodge Star. The discrete Hodge star transforms k -forms on the primal mesh into $(n - k)$ -forms on the dual mesh, and vice-versa. In our setup, we will use the so-called diagonal (or mass-lumped) approximation of the Hodge star (Bossavit, 1998) because of its simplicity, but note that higher-order accurate versions can be substituted. Given a discrete form α , its *Hodge star* $*\alpha$ is defined by the relation

$$\frac{1}{|*\sigma|} \langle *\alpha, *\sigma \rangle = \kappa(\sigma) \frac{1}{|\sigma|} \langle \alpha, \sigma \rangle,$$

where $|\sigma|$ and $|*\sigma|$ are the volumes of these elements, and κ is the causality operator, which equals $+1$ when σ is spacelike and -1 otherwise. (For more information on alternative discrete Hodge operators, the reader may refer to, e.g., Arnold et al., 2006; Auchmann and Kurz, 2006; Tarhasaari, Kettunen, and Bossavit, 1999; and Wang, Weiwei, Tong, Desbrun, and Schröder, 2006.)

Inner Product. Define the \mathbb{L}^2 *inner product* (\cdot, \cdot) between two primal k -forms to be

$$\begin{aligned} (\alpha, \beta) &= \sum_{\sigma^k} \kappa(\sigma) \binom{n}{k} \frac{|\text{CH}(\sigma, * \sigma)|}{|\sigma|^2} \langle \alpha, \sigma \rangle \langle \beta, \sigma \rangle \\ &= \sum_{\sigma^k} \kappa(\sigma) \frac{|* \sigma|}{|\sigma|} \langle \alpha, \sigma \rangle \langle \beta, \sigma \rangle \end{aligned}$$

where the sum is taken over all k -dimensional elements σ , and $\text{CH}(\sigma, * \sigma)$ is the n -dimensional convex hull of $\sigma \cup * \sigma$ (see Figure 1.1). The final equality holds as a result of using the circumcentric dual, since σ and $* \sigma$ are orthogonal to one another, and hence $|\text{CH}(\sigma, * \sigma)| = \binom{n}{k}^{-1} |\sigma| |* \sigma|$. (Indeed, this is one of the advantages of using the circumcentric dual, since one only needs to store volume information about the primal and dual cells themselves, and not about these primal-dual convex hulls.) This inner product can be expressed in terms of $\alpha \wedge * \beta$, as in the continuous case, for a particular choice of the discrete primal-dual wedge product; see Desbrun, Hirani, and Marsden (2003).

Note that since we have already defined a discrete version of the operators d and $*$, we immediately have a discrete codifferential δ , with the same formal expression as given previously. See Figure 1.2 for a visual diagram of primal and dual discrete forms, along with the corresponding operators $d, *, \delta$, for the case where K is a 3-D tetrahedral mesh.

Implementing DEC. DEC can be implemented simply and efficiently using linear algebra. A k -form α can be stored as a vector, where its entries are the values of α on each k -cell of the mesh. That is, given a list of k -cells σ_i^k , the entries of the vector are $\alpha_i = \langle \alpha, \sigma_i^k \rangle$. The exterior derivative d , taking k -forms to $(k+1)$ -forms, is then represented as a matrix: in fact, it is precisely the *incidence matrix* between k -cells and $(k+1)$ -cells in the mesh, with sparse entries ± 1 . The Hodge star taking primal k -forms to dual $(n-k)$ -forms becomes a square matrix, and in the case of the diagonal Hodge star, it is the diagonal matrix with entries $\kappa(\sigma_i^k) \frac{|* \sigma_i^k|}{|\sigma_i^k|}$. The discrete inner product is then simply the Hodge star matrix taken as a quadratic form.

Because of this straightforward isomorphism between DEC and linear algebra, problems posed in the language of DEC can take advantage of existing numerical

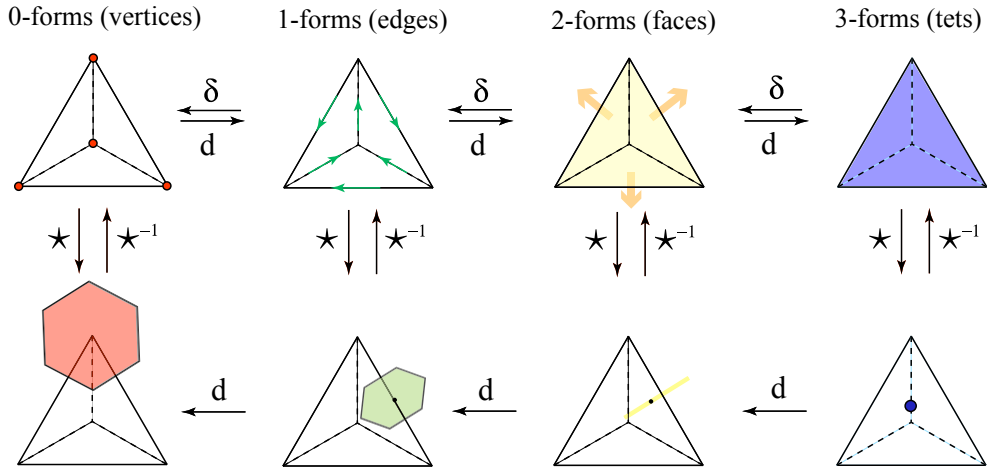


Figure 1.2: This figure is an illustration of discrete differential forms and operators on a 3-D simplicial mesh. In the top row, we see how a discrete k -form lives on k -cells of the primal mesh, for $k = 0, 1, 2, 3$; the bottom row shows the location of the corresponding dual $(n - k)$ -forms on the dual mesh. The differential operators d and δ map “horizontally” between k and $(k + 1)$ forms, while the Hodge star $*$ and its inverse $*^{-1}$ map “vertically” between primal and dual forms.

linear algebra codes. As an illustration, see Figure 1.3, in which spherical harmonics have been computed by constructing the discrete Laplace–Beltrami matrix for a triangulated sphere, and then using a standard numerical eigensolver to compute the eigenvectors of this matrix. For more details on programming and implementation, refer to Elcott and Schröder (2005).

Algebraic Foundations of Discrete Differential Forms. The above ideas can be formalized by introducing the following definitions from homological algebra (for reference see, e.g., Weibel, 1994; and Bott and Tu, 1982).

Definition 1.3.1. A *chain complex* C_\bullet consists of a sequence of abelian groups C_k , connected by homomorphisms $\partial_k: C_k \rightarrow C_{k-1}$ satisfying $\partial_k \circ \partial_{k+1} = 0$. This can be represented by the diagram

$$\cdots \rightarrow C_{k+1} \xrightarrow{\partial_{k+1}} C_k \xrightarrow{\partial_k} C_{k-1} \rightarrow \cdots,$$

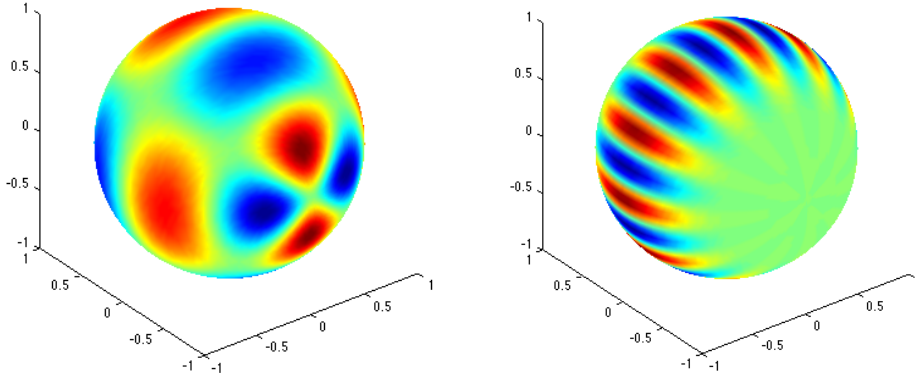


Figure 1.3: A visualization of spherical harmonics. These images show two eigenvectors of the discrete Laplace–Beltrami matrix for a triangulated 2-sphere.

where the composition of any two consecutive arrows is zero. These homomorphisms ∂_k are called *boundary maps*.

Definition 1.3.2. A *cochain complex* C^\bullet consists of a sequence of abelian groups C^k , connected by homomorphisms $d^k: C^k \rightarrow C^{k+1}$ satisfying $d^k \circ d^{k-1} = 0$. This can be represented by the diagram

$$\cdots \rightarrow C^{k-1} \xrightarrow{d^{k-1}} C^k \xrightarrow{d^k} C^{k+1} \rightarrow \cdots,$$

where the composition of any two consecutive arrows is zero. These homomorphisms d^k are called *coboundary maps*.

Remark. Chain and cochain complexes have an even more general definition, where the spaces C_k and C^k are taken to be R -modules for some ring R . For our purposes, however, we will only be encountering the case where $R = \mathbb{Z}$ is the ring of integers. A \mathbb{Z} -module is simply an abelian group, where integer multiplication corresponds to repeated addition in the group.

One of the most important examples of a cochain complex is the *de Rham complex* of differential forms on a manifold X , written as $\Omega^\bullet(X)$. In this case, the coboundary map $d^k: \Omega^k(X) \rightarrow \Omega^{k+1}(X)$ is given by the exterior derivative, which takes k -forms to $(k+1)$ -forms. In fact, our earlier, heuristic definition of discrete

k -forms as “one degree of freedom per oriented k -cell” is far from arbitrary. Rather, it allows us to construct a cochain complex of discrete differential forms on a mesh, whose geometric structure is closely tied to that of the de Rham complex.

Suppose for example that K is an oriented simplicial complex, where an *oriented k -simplex* is an equivalence class of ordered k -tuples of vertices $(v_{i_0}, \dots, v_{i_k})$, modulo even permutations. There are two equivalence classes for each set of vertices, corresponding to even and odd permutations, which we write as $\pm [v_{i_0}, \dots, v_{i_k}]$ for $i_0 < \dots < i_k$. (For example, $[v_0, v_1]$ is the directed edge from $v_0 \rightarrow v_1$, while $-[v_0, v_1]$ is the opposite-directed edge $v_0 \leftarrow v_1$.) A k -simplex also has $k+1$ incident faces of dimension $k-1$, which are obtained by omitting one of the vertices. We use the notation $[v_{i_0}, \dots, \widehat{v_{i_j}}, \dots, v_{i_k}]$ to denote the face which omits the j th vertex, v_{i_j} .

Definition 1.3.3. Given a simplicial complex K , the *simplicial chain complex* $C_\bullet(K)$ is defined as follows. The space of *simplicial k -chains* $C_k(K)$ is the free abelian group generated by the oriented k -simplices of K (i.e., formal linear combinations of k -simplices with integer weights). The *simplicial boundary maps* $\partial_k: C_k(K) \rightarrow C_{k-1}(K)$ are given by

$$\partial_k([v_{i_0}, \dots, v_{i_k}]) = \sum_{j=0}^k (-1)^j [v_{i_0}, \dots, \widehat{v_{i_j}}, \dots, v_{i_k}].$$

Note that, since the groups $C_k(K)$ are free, it suffices to define the boundary maps on the basis elements in this way.

It is easy to see that this forms a chain complex, i.e., that $\partial_k \circ \partial_{k+1} = 0$. Notice that in the expression $(\partial_k \circ \partial_{k+1})([v_{i_0}, \dots, v_{i_{k+1}}])$, the term $[v_{i_0}, \dots, \widehat{v_{i_j}}, \dots, \widehat{v_{i_{j'}}}, \dots, v_{i_{k+1}}]$ appears twice for each $0 \leq j < j' \leq k+1$, once with + sign and once with - sign, and so all the terms cancel.

Definition 1.3.4. Let K be an oriented simplicial complex with chain complex $C_\bullet(K)$. Then we can define the *simplicial cochain complex* $C^\bullet(K)$ as follows. The space of *simplicial k -cochains* is $C^k(K) = \text{Hom}(C_k(K), \mathbb{R})$, which is the abelian group of homomorphisms from $C_k(K)$ into \mathbb{R} . There is a natural pairing $\langle \cdot, \cdot \rangle: C^k(K) \times C_k(K) \rightarrow \mathbb{R}$ given by $\langle \alpha, c \rangle = \alpha(c)$. The *simplicial coboundary operator* $d^k: C^k(K) \rightarrow C^{k+1}(K)$ can then be defined as the dual of $\partial_{k+1}: C_{k+1}(K) \rightarrow C_k(K)$ with respect to the pairing. That is, we define it such that $\langle d\alpha, c \rangle = \langle \alpha, \partial c \rangle$.

These simplicial k -cochains are precisely the discrete k -forms introduced previously, while the coboundary maps d^k give the discrete exterior derivative. Furthermore, we can generalize the above definition to a complex of *A-valued discrete forms*, for any abelian group A , by taking $C^k(K; A) = \text{Hom}(C_k(K), A)$.

1.4 SUMMARY OF CONTRIBUTIONS

In Chapter 2, we discuss the application of variational integrators to highly oscillatory mechanical systems. This consists of two primary contributions. First, we introduce a new variational implicit-explicit (IMEX) integrator—which achieves superior numerical stability to explicit multiple-time-stepping methods, yet at a lower computational cost than fully implicit time integrators—and demonstrate its behavior by performing several numerical experiments, including an application to the Fermi–Pasta–Ulam problem. After this, we show how another class of integrators for highly oscillatory problems, the so-called trigonometric integrators, can be understood as variational integrators by use of a specially tailored quadrature approximation for the discrete Lagrangian.

In Chapter 3, we show how Maxwell’s equations can be discretized using discrete differential forms in spacetime. By treating the electromagnetic Lagrangian density as a differential form, these methods are able to combine the techniques of variational integrators for time discretization, along with those of discrete differential forms and conforming finite elements for spatial discretization. Moreover, we use this foundation to construct an asynchronous variational integrator (AVI) for Maxwell’s equations, which allows for improved efficiency by taking different time step sizes at different locations in space.

Finally, in Chapter 4, we lay the foundations for future work in discretizing noncommutative gauge theories, for which the existing abelian framework of discrete differential forms is insufficient. Drawing on the mathematical tools of fiber bundles and Lie groupoids, we provide some initial results toward understanding discretization of connection 1-forms and curvature 2-forms, showing particularly how discrete Riemannian geometry and general relativity may be modeled in terms of orthonormal frame bundles.

Chapter Two

Variational Integrators for Highly Oscillatory Problems in Mechanics

2.1 INTRODUCTION

2.1.1 Problem Background. Many systems in Lagrangian mechanics have components acting on different time scales, posing a challenge for traditional numerical integrators. Examples include:

1. *Elasticity*: Several spatial elements of varying stiffness, resulting from irregular meshes and/or inhomogeneous materials (Lew, Marsden, Ortiz, and West, 2003).
2. *Planetary Dynamics*: N -body problem with nonlinear gravitational forces, arising from pairwise inverse-square potentials. Multiple time scales result from the different distances between the bodies (Farr and Bertschinger, 2007).
3. *Highly Oscillatory Problems*: Potential energy can be split into a “fast” linear oscillatory component and a “slow” nonlinear component. These problems are widely encountered in modeling molecular dynamics (Leimkuhler, Reich, and Skeel, 1996), but have also been used to model other diverse applications, for example, in computer animation (Etzmuß, Eberhardt, and Hauth, 2000; Boxerman and Ascher, 2004).

Because these systems each satisfy a Lagrangian variational principle, they lend themselves readily to *variational integrators*: a class of geometric numerical integrators designed for simulating Lagrangian mechanical systems. By construction, variational integrators preserve a discrete version of this Lagrangian variational struc-

ture; consequently, they are automatically symplectic and momentum-conserving, with good long-time energy behavior (Marsden and West, 2001).

Explicit Methods, Multiple Time Stepping, and Resonance Instability. The Störmer/Verlet (or leapfrog) method is one of the canonical examples of a geometric (and variational) numerical integrator (see Hairer, Lubich, and Wanner, 2003). Yet, it and other simple, explicit time stepping methods do not perform well for problems with multiple time scales. The maximum stable time step for these methods is dictated by the stiffest mode of the underlying system; therefore, the fastest force dictates the number of evaluations that must be taken for *all* forces, despite the fact that the slow-scale forces may be (and often are) much more expensive to evaluate.

To reduce the number of costly function evaluations associated to the slow force, several explicit variational integrators use *multiple time stepping*, whereby different time step sizes are used to advance the fast and slow degrees of freedom. These include substepping methods, such as Verlet-I/r-RESPA and mollified impulse, where for each slow time step, an integer number of fast substeps are taken (Izaguirre, Ma, Matthey, Willcock, Slabach, Moore, and Viamontes, 2002). More recently, asynchronous variational integrators (AVIs) have been developed, removing the restriction for fast and slow time steps to be integer (or even rational) multiples of one another (Lew et al., 2003). Multiple-time-stepping methods can be more efficient than single-time-stepping explicit methods, like Störmer/Verlet, since one can fully resolve the fast oscillations while taking many fewer evaluations of the slow forces. This is especially advantageous for highly oscillatory problems, where the slow forces are nonlinear and hence more computationally expensive to evaluate.

One drawback of multiple-time-stepping methods, however, is that they can exhibit *linear resonance instability*. This phenomenon occurs when the slow impulses are nearly synchronized, in phase, with the the fast oscillations. These impulses artificially drive the system at a resonant frequency, causing the energy (and hence the numerical error) to increase without bound. The problem of numerical resonance is well known for substepping methods (Biesiadecki and Skeel, 1993), and has also recently been shown for AVIs as well—in fact, the subset of fast and slow time step size pairs leading to resonance instability is *dense* in the space of all possible

parameters (Fong, Darve, and Lew, 2007). Resonance instability can therefore be difficult to avoid, particularly in highly oscillatory systems with many degrees of freedom, as in molecular dynamics applications.

Implicit Methods for Single Time Stepping with Longer Step Sizes. Because multiple-time-stepping methods have these resonance problems, a number of single-time-stepping methods have been developed specifically for highly oscillatory problems. As noted earlier, single-time-stepping methods cannot fully resolve the fast oscillations without serious losses in efficiency. Therefore, the goal of these methods is to take long time steps, *without* actually resolving the fast oscillations, while still accurately capturing the macroscopic behavior that emerges from the coupling between fast and slow scales. The challenge is to design methods that allow for these longer time steps, without destroying either numerical stability or geometric structure.

One obvious candidate integrator is the implicit midpoint method, which is (linearly) unconditionally stable, as well as variational (hence symplectic) and symmetric. Unfortunately, the stability of the method comes at a cost: because the integrator is implicit in the slow (nonlinear) force, a nonlinear system of equations must be solved at every time step. Therefore, just like the fully resolved Störmer/Verlet method, this means that the implicit midpoint method requires an excessive number of function evaluations.

Implicit-Explicit Integration. For highly oscillatory problems, *implicit-explicit* (IMEX) integrators have been proposed as a potentially attractive alternative to either explicit, multiple-time-stepping methods or implicit, single-time-stepping methods. Rather than using separate fast and slow time step sizes, IMEX methods combine implicit integration (e.g., backward Euler) for the fast force with explicit integration (e.g., forward Euler) for the slow force. Because the fast force is linear, this semi-implicit approach requires only a linear solve for the implicit portion, as opposed to the expensive nonlinear solve that would be required for a fully implicit integrator, like the implicit midpoint method.

IMEX methods were developed by Crouzeix (1980), and have continued to progress, including the introduction of IMEX Runge–Kutta schemes for PDEs

by Ascher, Ruuth, and Spiteri (1997). However, in all of these methods, the splitting is done at the level of the Euler–Lagrange differential equations, rather than at the variational level of the Lagrangian. Consequently, a wide variety of IMEX schemes have been created, both geometric and non-geometric, but in general they cannot guarantee properties such as symplecticity, momentum conservation, or good long-time energy behavior, which are known for variational integrators. As an example of an IMEX integrator that is not “geometric” in the usual sense, consider the LI and LIN methods of Zhang and Schlick (1993), which combine the backward Euler method with explicit Langevin dynamics for molecular systems. Because the use of backwards Euler introduces artificial numerical dissipation, these methods use Langevin dynamics (i.e., stochastic forcing) to inject the missing energy back into the system.

Chapter Overview. In Section 2.2, we develop IMEX numerical integration from a Lagrangian, variational point of view. We do this by splitting the fast and slow potentials at the level of the Lagrangian action integral, rather than with respect to the differential equations or the Hamiltonian. From this viewpoint, implicit-explicit integration is an automatic consequence of discretizing the action integral using two distinct quadrature rules for the slow and fast potentials. The resulting discrete Euler–Lagrange equations coincide with a semi-implicit algorithm that was originally introduced by Zhang and Skeel (1997) as a “cheaper” alternative to the implicit midpoint method; Ascher and Reich (1999b) also studied a variant of this method for certain problems in molecular dynamics, replacing the implicit midpoint step by the energy-conserving (but non-symplectic) Simo–Gonzales method.

We also show that this variational IMEX method is free of resonance instabilities; the proof of this fact is naturally developed at the level of the Lagrangian, and does not require an examination of the associated Euler–Lagrange equations. We then compare the resonance-free behavior of variational IMEX to the multiple-time-stepping method r-RESPA in a numerical simulation of coupled slow and fast oscillators. Next, we evaluate the stability of the variational IMEX method, for large time steps, in a computation of slow energy exchange in the Fermi–Pasta–Ulam problem. Finally, we prove that the variational IMEX method accurately preserves this slow energy exchange behavior (as observed in the numerical experiments) by

showing that it corresponds to a modified impulse method.

After this, in Section 2.3, we briefly show how variational integrators can be used to model another popular class of methods for highly-oscillatory problems, called *trigonometric integrators*.

2.1.2 A Brief Review of Variational Integrators. The idea of variational integrators was studied by Suris (1990) and Moser and Veselov (1991), among others, and a general theory was developed over the subsequent decade (see Marsden and West, 2001, for a comprehensive survey).

Suppose we have a mechanical system on a configuration manifold Q , specified by a Lagrangian $L: TQ \rightarrow \mathbb{R}$. Given a set of discrete time points $t_0 < \dots < t_N$ with uniform step size h , we wish to compute a numerical approximation $q_n \approx q(t_n)$, $n = 0, \dots, N$, to the continuous trajectory $q(t)$. To construct a variational integrator for this problem, we define a *discrete Lagrangian* $L_h: Q \times Q \rightarrow \mathbb{R}$, replacing tangent vectors by pairs of consecutive configuration points, so that with respect to some numerical quadrature rule we have

$$L_h(q_n, q_{n+1}) \approx \int_{t_n}^{t_{n+1}} L(q, \dot{q}) dt.$$

Then the action integral over the whole time interval is approximated by the *discrete action sum*

$$S_h[q] = \sum_{n=0}^{N-1} L_h(q_n, q_{n+1}) \approx \int_{t_0}^{t_N} L(q, \dot{q}) dt.$$

If we apply Hamilton's principle to this action sum, so that $\delta S_h[q] = 0$ when variations are taken over paths with fixed endpoints, then this yields the *discrete Euler–Lagrange equations*

$$D_1 L_h(q_n, q_{n+1}) + D_2 L_h(q_{n-1}, q_n) = 0, \quad n = 1, \dots, N-1,$$

where D_1 and D_2 denote partial differentiation in the first and second arguments, respectively. This defines a two-step numerical method on $Q \times Q$, mapping $(q_{n-1}, q_n) \mapsto (q_n, q_{n+1})$. The equivalent one-step method on the cotangent bundle T^*Q , mapping $(q_n, p_n) \mapsto (q_{n+1}, p_{n+1})$, is defined by the *discrete Legendre transform*

$$p_n = -D_1 L_h(q_n, q_{n+1}), \quad p_{n+1} = D_2 L_h(q_n, q_{n+1}),$$

where the first equation updates q , and the second updates p .

Examples. Consider a Lagrangian of the form $L(q, \dot{q}) = \frac{1}{2}\dot{q}^T M \dot{q} - V(q)$, where $Q = \mathbb{R}^d$, M is a constant $d \times d$ mass matrix, and $V: Q \rightarrow \mathbb{R}$ is a potential. If we use trapezoidal quadrature to approximate the contribution of V to the action integral, we get

$$L_h^{\text{trap}}(q_n, q_{n+1}) = \frac{h}{2} \left(\frac{q_{n+1} - q_n}{h} \right)^T M \left(\frac{q_{n+1} - q_n}{h} \right) - h \frac{V(q_n) + V(q_{n+1})}{2},$$

which we call the *trapezoidal discrete Lagrangian*. It is straightforward to see that the discrete Euler–Lagrange equations for L_h^{trap} correspond to the explicit Störmer/Verlet method. Alternatively, if we use midpoint quadrature to approximate the integral of the potential, this yields the *midpoint discrete Lagrangian*,

$$L_h^{\text{mid}}(q_n, q_{n+1}) = \frac{h}{2} \left(\frac{q_{n+1} - q_n}{h} \right)^T M \left(\frac{q_{n+1} - q_n}{h} \right) - h V \left(\frac{q_n + q_{n+1}}{2} \right),$$

for which the resulting integrator is the implicit midpoint method.

2.2 A VARIATIONAL IMPLICIT-EXPLICIT METHOD

In this section, we show how to develop a variational integrator that combines aspects of the Störmer/Verlet and implicit midpoint methods mentioned above. The main idea is that, given a splitting of the potential energy into fast and slow components, we define the discrete Lagrangian by applying the midpoint quadrature rule to the fast potential and the trapezoidal quadrature rule to the slow potential. The resulting variational integrator is implicit in the fast force and explicit in the slow force. After this, we focus on the specific case of highly oscillatory problems, where the fast potential is quadratic (corresponding to a linear fast force). In this case, we show that the IMEX integrator can be understood as Störmer/Verlet with a modified mass matrix.

2.2.1 The IMEX Discrete Lagrangian and Equations of Motion. Suppose that we have a Lagrangian of the form $L(q, \dot{q}) = \frac{1}{2}\dot{q}^T M \dot{q} - U(q) - W(q)$, where U is a slow potential and W is a fast potential, for the configuration space $Q = \mathbb{R}^d$. Then define the *IMEX discrete Lagrangian*

$$L_h^{\text{IMEX}}(q_n, q_{n+1}) = \frac{h}{2} \left(\frac{q_{n+1} - q_n}{h} \right)^T M \left(\frac{q_{n+1} - q_n}{h} \right) - h \frac{U(q_n) + U(q_{n+1})}{2} - h W \left(\frac{q_n + q_{n+1}}{2} \right),$$

using (explicit) trapezoidal approximation for the slow potential and (implicit) midpoint approximation for the fast potential. The discrete Euler–Lagrange equations give the two-step variational integrator on $Q \times Q$

$$q_{n+1} - 2q_n + q_{n-1} = -h^2 M^{-1} \left[\nabla U(q_n) + \frac{1}{2} \nabla W\left(\frac{q_{n-1} + q_n}{2}\right) + \frac{1}{2} \nabla W\left(\frac{q_n + q_{n+1}}{2}\right) \right],$$

and the corresponding discrete Legendre transform is given by

$$\begin{aligned} p_n &= M\left(\frac{q_{n+1} - q_n}{h}\right) + \frac{h}{2} \nabla U(q_n) + \frac{h}{2} \nabla W\left(\frac{q_n + q_{n+1}}{2}\right), \\ p_{n+1} &= M\left(\frac{q_{n+1} - q_n}{h}\right) - \frac{h}{2} \nabla U(q_{n+1}) - \frac{h}{2} \nabla W\left(\frac{q_n + q_{n+1}}{2}\right). \end{aligned}$$

To see how this translates into an algorithm for a one-step integrator on T^*Q , it is helpful to introduce the intermediate stages

$$p_n^+ = p_n - \frac{h}{2} \nabla U(q_n), \quad p_{n+1}^- = p_{n+1} + \frac{h}{2} \nabla U(q_{n+1}).$$

Substituting these into the previous expression and rearranging yields the algorithm

$$\begin{aligned} \textbf{Step 1:} \quad p_n^+ &= p_n - \frac{h}{2} \nabla U(q_n), \\ \textbf{Step 2:} \quad \begin{cases} q_{n+1} = q_n + hM^{-1}\left(\frac{p_n^+ + p_{n+1}^-}{2}\right), \\ p_{n+1}^- = p_n^+ - h\nabla W\left(\frac{q_n + q_{n+1}}{2}\right), \end{cases} \\ \textbf{Step 3:} \quad p_{n+1} &= p_{n+1}^- - \frac{h}{2} \nabla U(q_{n+1}), \end{aligned}$$

where Step 2 corresponds to a step of the implicit midpoint method.

This can be summarized, in the style of impulse methods, as:

1. **kick:** explicit kick from U advances $(q_n, p_n) \mapsto (q_n, p_n^+)$,
2. **oscillate:** implicit midpoint method with W advances $(q_n, p_n^+) \mapsto (q_{n+1}, p_{n+1}^-)$,
3. **kick:** explicit kick from U advances $(q_{n+1}, p_{n+1}^-) \mapsto (q_{n+1}, p_{n+1})$.

In particular, notice that this reduces to the Störmer/Verlet method when $\nabla W \equiv 0$ and to the implicit midpoint method when $\nabla U \equiv 0$. Also, if the momentum p_n does not actually need to be recorded at the full time step (i.e., collocated with the position q_n), then Step 3 can be combined with Step 1 of the next iteration to create a staggered “leapfrog” method.

Interpretation as a Hamiltonian Splitting Method. This algorithm on T^*Q can also be interpreted as a fast-slow splitting method (McLachlan and Quispel, 2002; Hairer, Lubich, and Wanner, 2006, II.5 and VIII.4.1) for the separable Hamiltonian $H = T + U + W$, where T is the kinetic energy, as follows. Let $\Phi_h^{T+W} : T^*Q \rightarrow T^*Q$ denote the numerical flow of the implicit midpoint method with time step size h , applied to the fast portion of the Hamiltonian $T + W$, and let $\varphi_h^U : T^*Q \rightarrow T^*Q$ be the exact Hamiltonian flow for the slow potential U (i.e., constant acceleration without displacement). Then the variational IMEX method has the flow map $\Psi_h : T^*Q \rightarrow T^*Q$, which can be written as the following composition of exact and numerical flows:

$$\Psi_h = \varphi_{h/2}^U \circ \Phi_h^{T+W} \circ \varphi_{h/2}^U.$$

This formulation highlights the fact that variational IMEX is symmetric (since it is a symmetric composition of symmetric methods) as well as symplectic (since it can be written as a composition of symplectic maps).

2.2.2 Application to Highly Oscillatory Problems. For highly oscillatory problems on $Q = \mathbb{R}^d$, we start by taking a quadratic fast potential

$$W(q) = \frac{1}{2} q^T \Omega^2 q, \quad \Omega \in \mathbb{R}^{d \times d} \text{ symmetric and positive semidefinite.}$$

A prototypical Ω is given by the block-diagonal matrix $\Omega = \begin{pmatrix} 0 & 0 \\ 0 & \omega I \end{pmatrix}$, where some of the degrees of freedom are subjected to an oscillatory force with constant fast frequency $\omega \gg 1$. We also denote the slow force $g(q) = -\nabla U(q)$ and assume, without loss of generality, that the constant mass matrix is given by $M = I$. Therefore, the nonlinear system we wish to approximate numerically is

$$\ddot{q} + \Omega^2 q = g(q).$$

This is the conventional setup for highly oscillatory problems, used by Hairer et al. (2006, XIII) and others.

Applying the IMEX method to this example, we get the discrete Lagrangian

$$\begin{aligned} L_h^{\text{IMEX}}(q_n, q_{n+1}) &= \frac{h}{2} \left(\frac{q_{n+1} - q_n}{h} \right)^T \left(\frac{q_{n+1} - q_n}{h} \right) \\ &\quad - h \frac{U(q_n) + U(q_{n+1})}{2} - h \left(\frac{q_n + q_{n+1}}{2} \right)^T \Omega^2 \left(\frac{q_n + q_{n+1}}{2} \right), \end{aligned}$$

and so the two-step IMEX scheme is given by the discrete Euler–Lagrange equations

$$q_{n+1} - 2q_n + q_{n-1} + \frac{h^2}{4}\Omega^2(q_{n+1} + 2q_n + q_{n-1}) = h^2 g(q_n).$$

Combining terms, we can rewrite this as

$$\left[I + \frac{h^2}{4}\Omega^2 \right] (q_{n+1} - 2q_n + q_{n-1}) + h^2\Omega^2 q_n = h^2 g(q_n),$$

which is equivalent to Störmer/Verlet with a modified mass matrix $I + (h\Omega/2)^2$. This equivalence can similarly be shown to hold for the one-step formulation of the IMEX scheme on T^*Q —that is, the two methods also produce the same p_n , as well as the same q_n .

In fact, this correspondence between IMEX and a modified Störmer/Verlet method is true not just in the discrete Euler–Lagrange equations, but in the discrete Lagrangian itself. This follows immediately from the following proposition.

Proposition 2.2.1. *Suppose we have a Lagrangian $L(q, \dot{q}) = \frac{1}{2}\dot{q}^T M \dot{q} - \frac{1}{2}q^T \Omega^2 q$ and its corresponding midpoint discrete Lagrangian L_h^{mid} . Next, define the modified Lagrangian $\tilde{L}(q, \dot{q}) = \frac{1}{2}\dot{q}^T \tilde{M} \dot{q} - \frac{1}{2}q^T \Omega^2 q$, having the same quadratic potential but a different mass matrix \tilde{M} , and take its trapezoidal discrete Lagrangian $\tilde{L}_h^{\text{trap}}$. Then $L_h^{\text{mid}} \equiv \tilde{L}_h^{\text{trap}}$ when $\tilde{M} = M + (h\Omega/2)^2$.*

Proof. The midpoint discrete Lagrangian is given by

$$L_h^{\text{mid}}(q_n, q_{n+1}) = \frac{h}{2} \left(\frac{q_{n+1} - q_n}{h} \right)^T M \left(\frac{q_{n+1} - q_n}{h} \right) - \frac{h}{2} \left(\frac{q_n + q_{n+1}}{2} \right)^T \Omega^2 \left(\frac{q_n + q_{n+1}}{2} \right).$$

Now, notice that we can rearrange the terms

$$\begin{aligned} - \left(\frac{q_n + q_{n+1}}{2} \right)^T \Omega^2 \left(\frac{q_n + q_{n+1}}{2} \right) &= \left(\frac{q_{n+1} - q_n}{2} \right)^T \Omega^2 \left(\frac{q_{n+1} - q_n}{2} \right) - \frac{1}{2} q_n^T \Omega^2 q_n - \frac{1}{2} q_{n+1}^T \Omega^2 q_{n+1} \\ &= \left(\frac{q_{n+1} - q_n}{h} \right)^T \left(\frac{h\Omega}{2} \right)^2 \left(\frac{q_{n+1} - q_n}{h} \right) - \frac{1}{2} q_n^T \Omega^2 q_n - \frac{1}{2} q_{n+1}^T \Omega^2 q_{n+1}. \end{aligned}$$

Therefore the discrete Lagrangian can be written in the trapezoidal form

$$L_h^{\text{mid}}(q_n, q_{n+1}) = \frac{h}{2} \left(\frac{q_{n+1} - q_n}{h} \right)^T \left[M + \left(\frac{h\Omega}{2} \right)^2 \right] \left(\frac{q_{n+1} - q_n}{h} \right) - \frac{h}{2} \left(\frac{1}{2} q_n^T \Omega^2 q_n + \frac{1}{2} q_{n+1}^T \Omega^2 q_{n+1} \right),$$

which is precisely $\tilde{L}_h^{\text{trap}}(q_n, q_{n+1})$ when $\tilde{M} = M + (h\Omega/2)^2$. \square

Corollary 2.2.2. Consider a highly oscillatory system with an arbitrary slow potential U , quadratic fast potential $W(q) = \frac{1}{2}q^T\Omega^2q$, and constant mass matrix $M = I$, so that the Lagrangian L and IMEX discrete Lagrangian L_h^{IMEX} are defined as above. Next, take the modified Lagrangian \tilde{L} with the same potentials but different mass matrix \tilde{M} . Then $L_h^{\text{IMEX}} \equiv \tilde{L}_h^{\text{trap}}$ when $\tilde{M} = I + (h\Omega/2)^2$.

2.2.3 Analysis of Linear Resonance Stability. To study the linear resonance stability of this IMEX integrator, we consider a model problem where U and W both correspond to linear oscillators. Let $U(q) = \frac{1}{2}q^T q$ and $W(q) = \frac{1}{2}q^T\Omega^2q$, where $\Omega = \omega I$ for some $\omega \gg 1$, and again let the mass matrix $M = I$. Although this is something of a “toy problem”—obviously, one could simply combine U and W into a single quadratic potential $\frac{1}{2}(1 + \omega^2)q^T q$ —it is illustrative for studying the numerical resonance of multiple-time-stepping methods, since the system has no external forcing terms and hence no real *physical* resonance.

To prove that the IMEX method does not exhibit linear resonance instability, we show that the stability condition only requires that the time step be stable for the explicit slow force, and is independent of the fast frequency ω . The idea of the proof is to use the results from Section 2.2.2, showing that the IMEX method is equivalent to Störmer/Verlet with a modified mass matrix, and then to apply the well-known stability criteria for Störmer/Verlet.

In particular, for a harmonic oscillator with unit mass and frequency ν , the Störmer/Verlet method is linearly stable if and only if $|h\nu| \leq 2$, as can be shown by a straightforward calculation of the eigenvalues of the propagation matrix (Hairer et al., 2006, p. 23). For a system with constant mass m , this condition generalizes to $h^2\nu^2 \leq 4m$.

Theorem 2.2.3. *The IMEX method is linearly stable, for the system described above, if and only if $h \leq 2$ (i.e., if and only if h is a stable time step size for the slow oscillator alone).*

Proof. As proved in the previous section, the IMEX method for this system is equivalent to Störmer/Verlet with the modified mass matrix $I + (h\Omega/2)^2$. Now, this modified oscillatory system has constant mass $m = 1 + (h\omega/2)^2$ and frequency

$\nu = \sqrt{1 + \omega^2}$. Therefore, the necessary and sufficient condition for linear stability is

$$h^2(1 + \omega^2) \leq 4 \left(1 + \frac{h^2}{4} \omega^2\right),$$

and since the $h^2\omega^2$ terms cancel on both sides, this is equivalent to $h^2 \leq 4$, or $h \leq 2$. \square

This shows that, in contrast to multiple-time-stepping methods, the IMEX method does not exhibit linear resonance instability. It should be noted that *non-linear* instability is known to be possible for the implicit midpoint method, although even that can be avoided with a time step size restriction that is considerably weaker than that required for explicit methods (see Ascher and Reich, 1999a).

2.2.4 Numerical Experiments.

Coupled Linear Oscillators. To illustrate the numerical resonance behavior of the variational IMEX scheme, as compared with a multiple-time-stepping method, we consider the model problem from Section 2.2.3 for dimension $d = 1$ (i.e., $Q = \mathbb{R}$). Figure 2.1 shows a log plot of the maximum absolute error in total energy (i.e., the Hamiltonian) for both r-RESPA and the variational IMEX method, for a variety of frequencies ω . MATLAB simulations were performed over the time interval $[0, 1000]$, with fixed time step size $h = 0.1$, and with the normalized frequency $\omega h/\pi$ ranging over $(0, 4.5]$. Additionally, to fully resolve the fast oscillations, r-RESPA took 100 fast substeps of size $h/100 = 0.001$ for each full time step of size h .

The r-RESPA method exhibits “spikes” in the total energy error near integer values of $\omega h/\pi$, corresponding to the parameters where resonance instability develops and the numerical solution becomes unbounded. (The finite size of these spikes is due to the fact that the numerical simulation was run only for a finite interval of time. Interestingly, one also sees “negative spikes,” where the fast and slow oscillations are exactly out-of-phase and cancel one another.) It should be noted that the small substep size of r-RESPA is sufficient for stable integration of the fast force alone; it is only the introduction of the slow force that makes things unstable. By contrast, the maximum energy error for the variational IMEX method

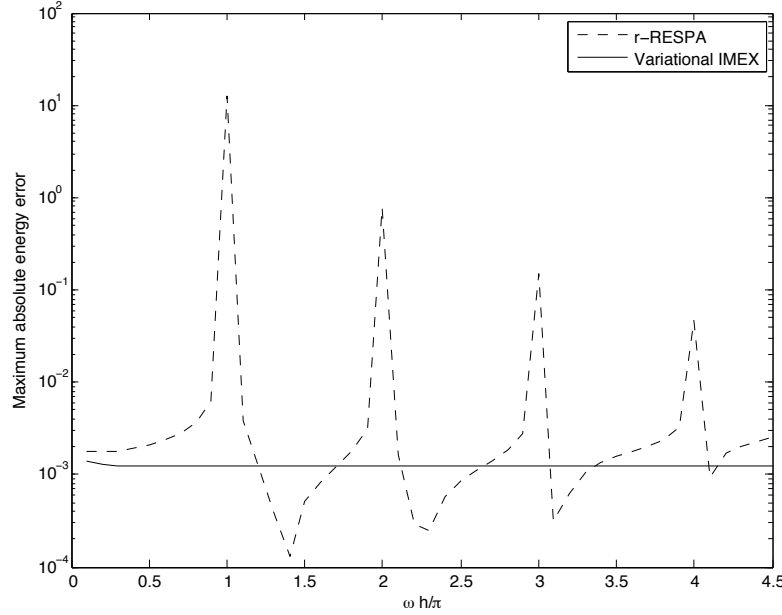


Figure 2.1: Maximum energy error of r-RESPA and variational IMEX, integrated over the time interval $[0, 1000]$ for a range of parameters ω . The r-RESPA method exhibits resonance instability near integer values of $\omega h/\pi$, while the variational IMEX method remains stable.

is nearly constant for all values of ω , showing no sign of resonance. This is fully consistent with the theoretical result obtained in Theorem 2.2.3.

The Fermi–Pasta–Ulam Problem. As an example of a nontrivial highly oscillatory problem with nonlinear slow potential, we chose the modified Fermi–Pasta–Ulam (FPU) problem considered by Hairer et al. (2006, I.5 and XIII), whose treatment we will now briefly review. The FPU problem consists of 2ℓ unit point masses, which are chained together, in series, by alternating weak nonlinear springs and stiff linear springs. The displacements of the point masses are denoted $q_1, \dots, q_{2\ell} \in \mathbb{R}$ (where the endpoints $q_0 = q_{2\ell+1} = 0$ are taken to be fixed), and their conjugate momenta are $p_i = \dot{q}_i$ for $i = 1, \dots, 2\ell$. (This particular setup is due to Galgani et al., 1992, and is a variant of the problem originally introduced by Fermi, Pasta, and Ulam, 1955.)

In these variables, the FPU system has the Hamiltonian

$$H(q, p) = \frac{1}{2} \sum_{i=1}^{\ell} (p_{2i-1}^2 + p_{2i}^2) + \frac{\omega^2}{4} \sum_{i=1}^{\ell} (q_{2i} - q_{2i-1})^2 + \sum_{i=0}^{\ell} (q_{2i+1} - q_{2i})^4,$$

which contains a quadratic potential for the ℓ stiff linear springs, each with frequency ω , and a quartic potential for the $\ell + 1$ soft nonlinear (cubic) springs. However, it is helpful to perform the coordinate transformation (following Hairer et al., 2006, p. 22)

$$\begin{aligned} x_{0,i} &= \frac{q_{2i} + q_{2i-1}}{\sqrt{2}}, & x_{1,i} &= \frac{q_{2i} - q_{2i-1}}{\sqrt{2}}, \\ y_{0,i} &= \frac{p_{2i} + p_{2i-1}}{\sqrt{2}}, & y_{1,i} &= \frac{p_{2i} - p_{2i-1}}{\sqrt{2}}, \end{aligned}$$

so that (modulo rescaling) $x_{0,i}$ corresponds to the location of the i th stiff spring's center, $x_{1,i}$ corresponds to its length, and $y_{0,i}, y_{1,i}$ are the respective conjugate momenta. Writing the Hamiltonian in these new variables, we have

$$\begin{aligned} H(x, y) = & \frac{1}{2} \sum_{i=1}^{\ell} (y_{0,i}^2 + y_{1,i}^2) + \frac{\omega^2}{2} \sum_{i=1}^{\ell} x_{1,i}^2 \\ & + \frac{1}{4} \left[(x_{0,1} - x_{1,1})^4 + \sum_{i=1}^{\ell-1} (x_{0,i+1} - x_{1,i+1} - x_{0,i} - x_{1,i})^4 + (x_{0,\ell} + x_{1,\ell})^4 \right], \end{aligned}$$

which considerably simplifies the form of the fast quadratic potential.

Following the example treated numerically by Hairer et al. (2006) and McLachlan and O'Neale (2007), we consider an instance of the FPU problem, integrated over the time interval $[0, 200]$, with parameters $\ell = 3$, $\omega = 50$, whose initial conditions are

$$x_{0,1}(0) = 1, \quad y_{0,1}(0) = 1, \quad x_{1,1}(0) = \omega^{-1}, \quad y_{1,1}(0) = 1,$$

with zero for all other initial values. This displays an interesting and complex property of the FPU problem, called *slow energy exchange*, which results from the slow nonlinear coupling between the stiff springs. If we consider only the energy in the stiff springs, written as

$$I_j(x_{1,j}, y_{1,j}) = \frac{1}{2} (y_{1,j}^2 + \omega^2 x_{1,j}^2), \quad j = 1, 2, 3,$$

then the initial conditions start with all of the energy in I_1 and none in I_2, I_3 . Over the course of the time interval, this energy is transferred in a characteristic way

from I_1 to I_3 , gradually transitioning through the middle spring I_2 . Furthermore, the total stiff energy $I = I_1 + I_2 + I_3$ remains nearly constant, i.e., is an adiabatic invariant of the system.

Figure 2.2 shows several numerical simulations of this FPU energy exchange, computed both with Störmer/Verlet and with the variational IMEX method for different choices of time step size. The first plot is a reference solution, computed using Störmer/Verlet with $h = 0.001$, fully resolving the fast oscillations. However, we see that the Störmer/Verlet solution's quality and stability degrade rapidly as we increase the step size (for $h = 0.03$, we have $h\omega = 1.5$, which is near the upper end of the stability region $|h\omega| \leq 2$). By contrast, the variational IMEX method performs extremely well for $h = 0.03\text{--}0.15$, degrading gradually as the time step size increases. Even as the numerical solution begins to undergo serious degradation for $h = 0.2\text{--}0.3$, the qualitative structure of the energy exchange behavior between I_1, I_2, I_3 is still maintained. (Compare Hairer et al., 2006, p. 24, Figure 5.3; see also McLachlan and O’Neale, 2007, who examine a wide variety of geometric integrators, particularly trigonometric integrators, for the FPU problem, with respect to both resonance stability and slow energy exchange.)

In Figure 2.3 we show the numerical behavior of the variational IMEX method, applied to this same FPU problem, on a longer time scale ($T = 4000$) and for large time steps ($h = 0.1, 0.3$). At $h = 0.1$, the IMEX simulation still displays the correct qualitative energy behavior, with respect to both the slow energy exchange and the adiabatic invariant I , and the numerical solution remains bounded. However, by $h = 0.3$, numerical stability has broken down, as oscillatory coupling in the fast modes leads to unbounded amplitude growth. This illustrates one of the drawbacks of implicit midpoint-type methods: despite the lack of linear resonances, numerical instability can still result for very large time steps due to nonlinear coupling (Ascher and Reich, 1999a,b).

This example was chosen to demonstrate that the variational IMEX method does not attain its stability merely by “smoothing out” the fast frequencies, in a way that might destroy the structure of any fast-slow nonlinear coupling. Rather, despite the fact that it does not resolve the fast frequencies, the method is still capable of capturing the complex multiscale interactions seen in the FPU problem.

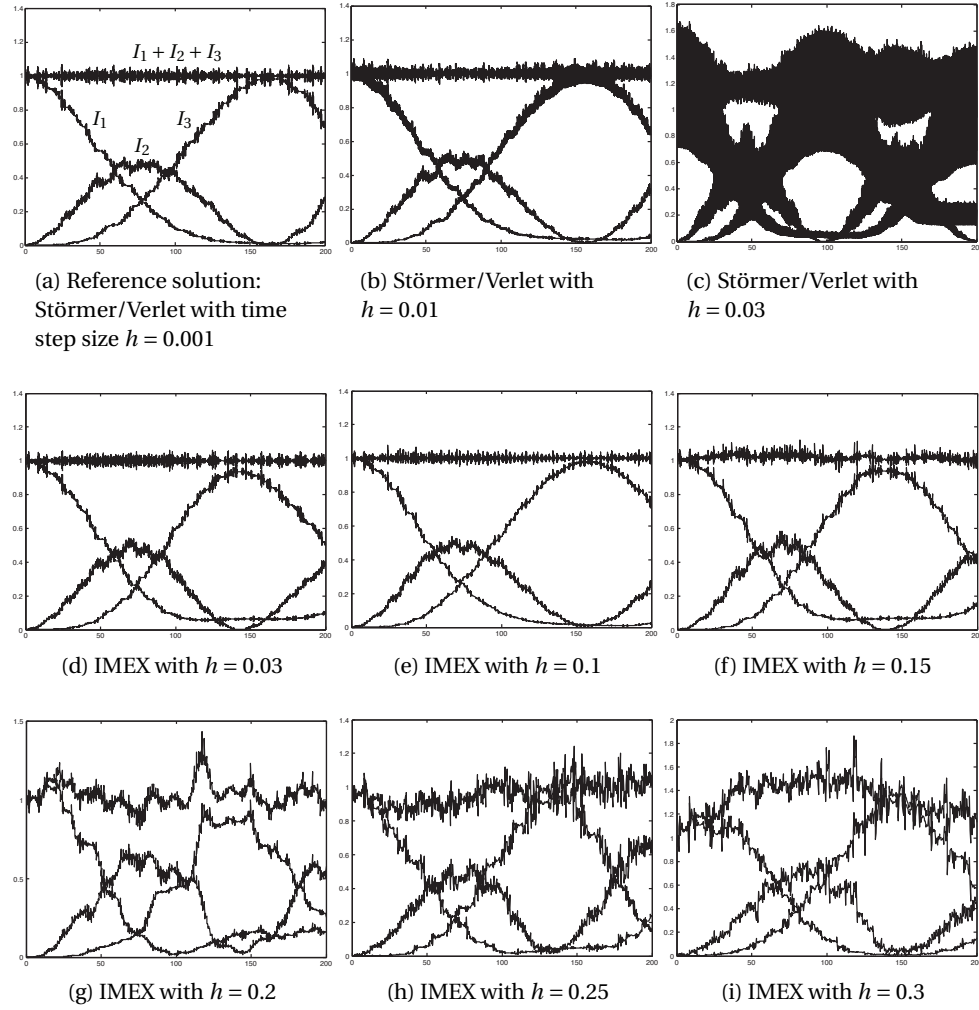


Figure 2.2: The IMEX method robustly captures slow energy exchange in the Fermi-Pasta-Ulam problem with $\omega = 50$, even for large time steps. Because the fast force is integrated implicitly, IMEX remains stable and degrades gradually as the time step size increases—unlike the fully explicit Störmer/Verlet method, which rapidly becomes unstable.

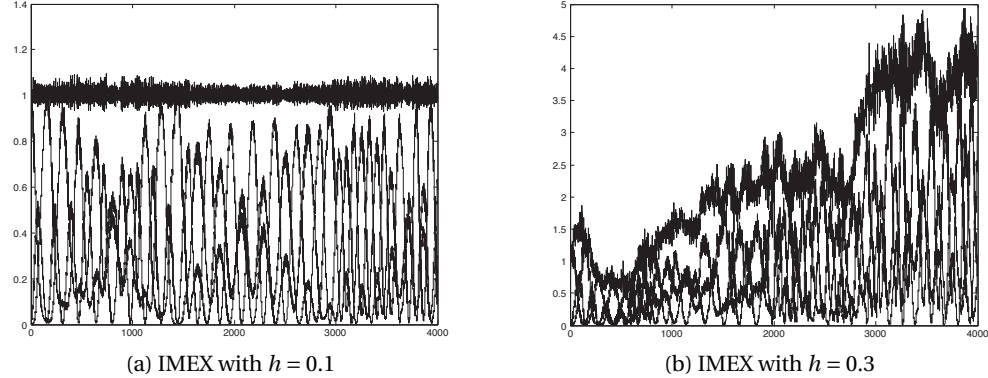


Figure 2.3: Numerical simulation of the FPU problem for $T = 4000$, which shows the behavior of the IMEX method on the ω^2 scale. For $h = 0.1$, we already have $h\omega = 5$, yet the oscillatory behavior and adiabatic invariant are qualitatively correct. By contrast, for $h = 0.3$, the method has begun to blow up; oscillatory coupling is a drawback of implicit midpoint methods for large time steps.

2.2.5 Analysis of Slow Energy Exchange in the IMEX Method. In the previous section, the numerical experiments for the Fermi–Pasta–Ulam problem seemed to suggest that the variational IMEX method preserves the slow energy exchange between the fast oscillatory modes. This is somewhat surprising, since the method does not actually resolve these fast oscillations. However, in this section, we will prove that, in fact, this method *does* accurately reproduce the slow energy exchange behavior, as long as the numerical solutions remain bounded. This is demonstrated by showing that the variational IMEX method can be understood as a *modified impulse method*; that is, the midpoint step exactly resolves the oscillations of some modified differential equation. We can then apply some of the existing theory about numerical energy exchange for impulse methods.

First, let us rewrite the fast oscillatory system as

$$\begin{pmatrix} \Omega \dot{q} \\ \dot{p} \end{pmatrix} = \begin{pmatrix} 0 & \Omega \\ -\Omega & 0 \end{pmatrix} \begin{pmatrix} \Omega q \\ p \end{pmatrix},$$

so it follows that the exact solution satisfies

$$\begin{pmatrix} \Omega q(t+h) \\ p(t+h) \end{pmatrix} = \begin{pmatrix} \cos(h\Omega) & \sin(h\Omega) \\ -\sin(h\Omega) & \cos(h\Omega) \end{pmatrix} \begin{pmatrix} \Omega q(t) \\ p(t) \end{pmatrix}.$$

Now, in these transformed coordinates, the implicit midpoint method has the expression

$$\begin{pmatrix} I & -h\Omega/2 \\ h\Omega/2 & I \end{pmatrix} \begin{pmatrix} \Omega q_{n+1} \\ p_{n+1} \end{pmatrix} = \begin{pmatrix} I & h\Omega/2 \\ -h\Omega/2 & I \end{pmatrix} \begin{pmatrix} \Omega q_n \\ p_n \end{pmatrix}.$$

Therefore, if we take the skew matrix

$$A = \begin{pmatrix} 0 & h\Omega \\ -h\Omega & 0 \end{pmatrix},$$

it follows that

$$\begin{pmatrix} \Omega q_{n+1} \\ p_{n+1} \end{pmatrix} = (I - A/2)^{-1} (I + A/2) \begin{pmatrix} \Omega q_n \\ p_n \end{pmatrix}.$$

Notice that the expression $(I - A/2)^{-1} (I + A/2) = \text{cay}(A)$ is the *Cayley transform*, which maps skew matrices to special orthogonal matrices (and can be seen as an approximation to the exponential map). Hence the stability matrix is special orthogonal, so we can write

$$\begin{pmatrix} \Omega q_{n+1} \\ p_{n+1} \end{pmatrix} = \begin{pmatrix} \cos(h\tilde{\Omega}) & \sin(h\tilde{\Omega}) \\ -\sin(h\tilde{\Omega}) & \cos(h\tilde{\Omega}) \end{pmatrix} \begin{pmatrix} \Omega q_n \\ p_n \end{pmatrix}$$

for some modified frequency $\tilde{\Omega}$. Therefore, the stability matrix for the implicit midpoint method corresponds to the *exact* flow matrix for a modified oscillatory system.

As an example, suppose we have $\Omega = \begin{pmatrix} 0 & 0 \\ 0 & \omega I \end{pmatrix}$ for some constant frequency ω . Applying the Cayley transform, it can be seen that the modified frequency $\tilde{\omega}$ satisfies

$$h\omega/2 = \tan(h\tilde{\omega}/2).$$

Squaring both sides, this becomes

$$(h\omega/2)^2 = \tan^2(h\tilde{\omega}/2) = \frac{1 - \cos(h\tilde{\omega})}{1 + \cos(h\tilde{\omega})},$$

which finally gives the solution for the modified frequency,

$$\tilde{\omega} = \frac{1}{h} \arccos \left(\frac{1 - (h\omega/2)^2}{1 + (h\omega/2)^2} \right).$$

Remark. This perspective provides another explanation as to why the variational IMEX method does not exhibit resonance: we always have $h\tilde{\omega} < \pi$. In fact, the Cayley transform does not map to a rotation by π , except in the limit as $h\omega \rightarrow \infty$. Therefore, for any finite h and ω , we will never encounter the resonance points corresponding to integer multiples of π .

However, it should be noted that this leads to another possible source of instability, if the time step size h becomes too large. Since $\tilde{\omega} < \pi/h$, the modified frequency $\tilde{\omega}$ must shrink as h grows. If $\tilde{\omega}$ is very small, this can lead to unbounded amplitude growth in the fast modes (as we saw in Figure 2.3) since it requires less energy to induce this amplification.

Since the implicit midpoint method has now been seen as the exact solution of a modified system, we can write the variational IMEX method as the following modified impulse scheme:

$$\begin{aligned}\textbf{Step 1:} \quad p_n^+ &= p_n - \frac{h}{2} \nabla U(q_n), \\ \textbf{Step 2:} \quad \begin{pmatrix} \Omega q_{n+1} \\ p_{n+1}^- \end{pmatrix} &= \begin{pmatrix} \cos(h\tilde{\Omega}) & \sin(h\tilde{\Omega}) \\ -\sin(h\tilde{\Omega}) & \cos(h\tilde{\Omega}) \end{pmatrix} \begin{pmatrix} \Omega q_n \\ p_n^+ \end{pmatrix}, \\ \textbf{Step 3:} \quad p_{n+1}^- &= p_{n+1}^- - \frac{h}{2} \nabla U(q_{n+1}).\end{aligned}$$

Suppose again that $\Omega = \begin{pmatrix} 0 & 0 \\ 0 & \omega I \end{pmatrix}$ for some constant frequency ω , and likewise $\tilde{\Omega} = \begin{pmatrix} 0 & 0 \\ 0 & \tilde{\omega} I \end{pmatrix}$. (This includes the case of the FPU problem.) We now finally have what we need to prove our main result on the slow energy exchange behavior of the variational IMEX method, following essentially the same approach as Hairer et al. (2006, XIII, especially XIII.8).

Theorem 2.2.4. *Let the variational IMEX method be applied to the problem above, and suppose the numerical solution remains bounded. Then the ordinary differential equation describing the slow energy exchange in the numerical solution is consistent with that for the exact solution; this holds up to order $\mathcal{O}(\omega^{-3})$.*

Proof. As demonstrated by Hairer et al. (2006, p. 495), the slow energy exchange behavior in the exact solution is governed by the equation

$$2i\omega \dot{z}_1 = \frac{\partial g_1}{\partial x_1}(y_0, 0) z_1 + \mathcal{O}(\omega^{-3}),$$

where the variables appearing above are coefficients in the modulated Fourier expansion of the exact solution. Furthermore, Hairer et al. establish that (bounded) numerical solutions for the *unmodified* impulse method satisfy

$$2i\omega \dot{z}_{h,1} = \frac{\partial g_1}{\partial x_1} (y_{h,0}, 0) z_{h,1} + \mathcal{O}(\omega^{-3}),$$

where the variables are now coefficients in the modulated Fourier expansion of the numerical solution. Hence, slow energy exchange for the unmodified impulse method is consistent with that for the exact solution.

For the modified impulse method, we must now replace ω with $\tilde{\omega}$ on the left hand side of the equation above. However, notice that Step 2 of the modified method advances the *original* state vector $\begin{pmatrix} \Omega q_n \\ p_n \end{pmatrix}$, rather than the modified $\begin{pmatrix} \tilde{\Omega} q_n \\ p_n \end{pmatrix}$. Changing from $\begin{pmatrix} \Omega q_n \\ p_n \end{pmatrix}$ to $\begin{pmatrix} \tilde{\Omega} q_n \\ p_n \end{pmatrix}$ introduces a scaling factor of $\tilde{\omega}/\omega$ on the right hand side. Therefore, the variational IMEX method satisfies the slow energy exchange equation

$$2i\tilde{\omega} \dot{z}_{h,1} = \frac{\tilde{\omega}}{\omega} \frac{\partial g_1}{\partial x_1} (y_{h,0}, 0) z_{h,1} + \mathcal{O}(\omega^{-4}\tilde{\omega}).$$

Finally, cancelling the $\tilde{\omega}$ factors and multiplying by ω , we once again get

$$2i\omega \dot{z}_{h,1} = \frac{\partial g_1}{\partial x_1} (y_{h,0}, 0) z_{h,1} + \mathcal{O}(\omega^{-3}),$$

which is the same as the original impulse method. This completes the proof. \square

2.3 VARIATIONAL TRIGONOMETRIC INTEGRATORS

Another popular approach to highly oscillatory problems has been that of *trigonometric integrators* (see Hairer et al., 2006, Chapter XIII). These methods are constructed to *exactly* integrate a harmonic oscillator, which corresponds to the case where the slow potential vanishes. In general, these can be written either as a two-step method on $Q \times Q$

$$q_{n+1} - 2 \cos(h\Omega) q_n + q_{n-1} = h^2 \Psi g(\Phi q_n),$$

or as a one-step method on T^*Q

$$\begin{aligned} q_1 &= \cos(h\Omega)q_0 + \Omega^{-1}\sin(h\Omega) + \frac{h^2}{2}\Psi g_0 \\ p_1 &= -\Omega\sin(h\Omega)q_0 + \cos(h\Omega)p_0 + \frac{h}{2}(\Psi_0g_0 + \Psi_1g_1), \end{aligned}$$

where these Ψ and Φ correspond to a certain choice of *filter functions* evaluated $h\Omega$.

In this section, we show how these integrators can be derived from a discrete Lagrangian variational principle, using a quadrature approximation that is specially tailored for “nearly linear” highly oscillatory systems. We begin by doing this for the simplified 1-D case where q and ω are scalars, and move on to the general case where $q \in \mathbb{R}^d$ is a vector and $\Omega \in \mathbb{R}^{d \times d}$ a matrix.

2.3.1 Scalar Case.

Exact Quadrature for Oscillatory Lagrangians. Suppose that we have a purely oscillatory system with the Lagrangian

$$L(q, \dot{q}) = \frac{1}{2}\dot{q}^2 - \frac{1}{2}\omega^2q^2.$$

We wish to construct a discrete Lagrangian that is exact for systems of this type.

Let $q(t) = a\cos(\omega t) + b\sin(\omega t)$, and define $q_0 = q(-h/2)$ and $q_1 = q(h/2)$. Then the coefficients a and b can be expressed as

$$a = \frac{q_0 + q_1}{2\cos\left(\frac{h\omega}{2}\right)}, \quad b = \frac{q_1 - q_0}{2\sin\left(\frac{h\omega}{2}\right)}.$$

Next, we compute the integral

$$\begin{aligned} \int_{-h/2}^{h/2} L(q, \dot{q}) dt &= \int_{-h/2}^{h/2} \left[\frac{1}{2}\dot{q}^2 - \frac{1}{2}\omega^2q^2 \right] dt \\ &= \frac{\omega}{2\sin(h\omega)} [\cos(h\omega)(q_0^2 + q_1^2) - 2q_0q_1] \\ &= \frac{\omega}{2\sin(h\omega)} [(q_1 - q_0)^2 - (1 - \cos(h\omega))(q_0^2 + q_1^2)] \\ &= \frac{\omega}{2\sin(h\omega)} \left[h^2 \left(\frac{q_1 - q_0}{h} \right)^2 - \frac{4}{\omega^2} \sin^2\left(\frac{h\omega}{2}\right) \left(\frac{1}{2}\omega^2q_0^2 + \frac{1}{2}\omega^2q_1^2 \right) \right] \\ &= \frac{h^2\omega}{2\sin(h\omega)} \left[\left(\frac{q_1 - q_0}{h} \right)^2 - \operatorname{sinc}^2\left(\frac{h\omega}{2}\right) \left(\frac{1}{2}\omega^2q_0^2 + \frac{1}{2}\omega^2q_1^2 \right) \right] \\ &= \frac{h}{2\operatorname{sinc}(h\omega)} \left[\left(\frac{q_1 - q_0}{h} \right)^2 - \operatorname{sinc}^2\left(\frac{h\omega}{2}\right) \left(\frac{1}{2}\omega^2q_0^2 + \frac{1}{2}\omega^2q_1^2 \right) \right] \end{aligned}$$

which begins to resemble the kinetic-minus-potential form of a discrete Lagrangian for this purely oscillatory system.

Generalization to Highly Oscillatory Problems. Inspired by this, we define the following discrete Lagrangian

$$L_h(q_0, q_1) = \frac{h}{2 \operatorname{sinc}(h\omega)} \left[\left(\frac{q_1 - q_0}{h} \right)^2 - \operatorname{sinc}^2\left(\frac{h\omega}{2}\right) [V(q_0) + V(q_1)] \right],$$

where $V(q) = \frac{1}{2}\omega^2 q^2 + U(q)$. (This is exact when the slow potential U vanishes.) To allow filtering, we define an even more general discrete Lagrangian

$$L_h(q_0, q_1) = \frac{h}{2 \operatorname{sinc}(h\omega)} \left[\left(\frac{q_1 - q_0}{h} \right)^2 - \Psi \Phi^{-1} [V(\Phi q_0) + V(\Phi q_1)] \right],$$

where $\Psi \Phi = \operatorname{sinc}^2(h\omega/2)$. The resulting one-step scheme is

$$\begin{aligned} q_1 &= \cos(h\omega) q_0 + \omega^{-1} \sin(h\omega) p_0 + \frac{h^2}{2} \Psi g_0 \\ p_1 &= -\omega \sin(h\omega) q_0 + \cos(h\omega) p_0 + \frac{h}{2} (\Psi_0 g_0 + \Psi_1 g_1), \end{aligned}$$

where $g_n = -\nabla U(\Phi q_n)$, $\Psi_1 \operatorname{sinc}(h\omega) = \Psi$, and $\Psi_0 = \cos(h\omega) \Psi_1$.

2.3.2 Vector Case. More generally, suppose that Ω^2 is a symmetric, positive semidefinite matrix, and that the fast oscillatory potential is $\frac{1}{2}q^T \Omega^2 q$. Then, similar to the previous case, we have

$$\begin{aligned} \int_{-h/2}^{h/2} L(q, \dot{q}) dt &= \frac{h}{2} \left[\left(\frac{q_1 - q_0}{h} \right)^T (\operatorname{sinc}(h\Omega))^{-1} \left(\frac{q_1 - q_0}{h} \right) \right. \\ &\quad \left. - \frac{1}{2} q_0^T \left[\Omega \operatorname{sinc}\left(\frac{h\Omega}{2}\right) \right]^2 (\operatorname{sinc}(h\Omega))^{-1} q_0 - \frac{1}{2} q_1^T \left[\Omega \operatorname{sinc}\left(\frac{h\Omega}{2}\right) \right]^2 (\operatorname{sinc}(h\Omega))^{-1} q_1 \right]. \end{aligned}$$

This suggests a discrete Lagrangian of the general form

$$L_h(q_0, q_1) = \frac{h}{2} \left(\frac{q_1 - q_0}{h} \right)^T \Psi^{-1} \Phi \left(\frac{q_1 - q_0}{h} \right) - \frac{h}{2} [V(\Phi q_0) + V(\Phi q_1)].$$

Taking the partial derivatives of this discrete Lagrangian, we have

$$\begin{aligned} p_0 &= -D_1(q_0, q_1) = \Psi^{-1} \Phi \left(\frac{q_1 - q_0}{h} \right) + \frac{h}{2} \Phi \nabla V(\Phi q_0) \\ p_1 &= D_2(q_0, q_1) = \Psi^{-1} \Phi \left(\frac{q_1 - q_0}{h} \right) - \frac{h}{2} \Phi \nabla V(\Phi q_1). \end{aligned}$$

This gives a two-step scheme of the form

$$q_{n+1} - 2q_n + q_{n-1} = -h\Psi\nabla V(\Phi q_n).$$

The associated one-step scheme is

$$\begin{aligned} q_1 &= q_0 + h\Psi\Phi^{-1}p_0 - \frac{h^2}{2}\Psi\nabla V(\Phi q_0) \\ p_1 &= \Psi^{-1}\Phi\left(\frac{q_1 - q_0}{h}\right) - \frac{h}{2}\Phi\nabla V(q_1) \\ &= p_0 - \frac{h}{2}\Phi[\nabla V(\Phi q_0) + \nabla V(\Phi q_1)]. \end{aligned}$$

Highly Oscillatory Problem. As before, we now suppose that the potential has the form $V(q) = \frac{1}{2}q^T\Omega^2q + U(q)$, and define the slow force $g(q) = -\nabla U(q)$. Then the one-step scheme becomes

$$\begin{aligned} q_1 &= q_0 + h\Psi\Phi^{-1}p_0 - \frac{h^2}{2}\Psi[\Omega^2\Phi q_0 - g_0] \\ &= \left(I - \frac{h^2}{2}\Psi\Omega^2\Phi\right)q_0 + h\Psi\Phi^{-1}p_0 + \frac{h^2}{2}\Psi g_0, \end{aligned}$$

and similarly, for the momentum,

$$\begin{aligned} p_1 &= p_0 - \frac{h}{2}\Phi[\Omega^2\Phi q_0 - g_0 + \Omega^2\Phi q_1 - g_1] \\ &= -\frac{h}{2}\Phi^2\Omega^2(q_0 + q_1) + p_0 + \frac{h}{2}\Phi(g_0 + g_1) \\ &= -\frac{h}{2}\Phi^2\Omega^2\left[\left(2I - \frac{h^2}{2}\Psi\Omega^2\Phi\right)q_0 + h\Psi\Phi^{-1}p_0 + \frac{h^2}{2}\Psi g_0\right] + p_0 + \frac{h}{2}\Phi(g_0 + g_1) \\ &= -h\Phi^2\Omega^2\left(I - \frac{h^2}{4}\Psi\Phi\Omega^2\right)q_0 + \left(I - \frac{h^2}{2}\Psi\Phi\Omega^2\right)p_0 + \frac{h}{2}\Phi\left[\left(I - \frac{h^2}{2}\Psi\Phi\Omega^2\right)g_0 + g_1\right]. \end{aligned}$$

Back to Exact Quadrature. Now, in the exact quadrature case, we had the filters

$$\Phi = \text{sinc}\left(\frac{h\Omega}{2}\right)\text{sinc}(h\Omega)^{-1/2}, \quad \Psi = \Phi \text{sinc}(h\Omega) = \text{sinc}\left(\frac{h\Omega}{2}\right)\text{sinc}(h\Omega)^{1/2}.$$

If we substitute the product $\Psi\Phi = \text{sinc}^2\left(\frac{h\Omega}{2}\right)$, we get

$$I - \frac{h^2}{4}\Psi\Phi\Omega^2 = I - \left(\frac{h\Omega}{2}\right)^2 \text{sinc}^2\left(\frac{h\Omega}{2}\right) = 1 - \sin^2\left(\frac{h\Omega}{2}\right) = \cos^2\left(\frac{h\Omega}{2}\right),$$

as well as

$$h\Phi^2\Omega^2 = \frac{h\Omega^2 \operatorname{sinc}^2\left(\frac{h\Omega}{2}\right)}{\operatorname{sinc}(h\Omega)} = \frac{4\Omega \sin^2\left(\frac{h\Omega}{2}\right)}{\sin(h\Omega)} = \frac{4\Omega \sin^2\left(\frac{h\Omega}{2}\right)}{2 \sin(h\Omega) \cos(h\Omega)} = 2\Omega \tan\left(\frac{h\Omega}{2}\right),$$

and so multiplying these together, we arrive at

$$2\Omega \tan\left(\frac{h\Omega}{2}\right) \cos^2\left(\frac{h\Omega}{2}\right) = 2\Omega \sin\left(\frac{h\Omega}{2}\right) \cos\left(\frac{h\Omega}{2}\right) = \Omega \sin(h\Omega).$$

Similarly, for the other terms

$$I - \frac{h^2}{2} \Psi \Phi \Omega^2 = 1 - 2 \sin^2\left(\frac{h\Omega}{2}\right) = \cos(h\Omega).$$

To simplify the g_0 and g_1 terms, we define

$$\Psi_1 = \Phi, \quad \Psi_0 = \Psi_1 \cos(h\Omega).$$

The final one-step algorithm, in this case, is thus

$$\begin{aligned} q_1 &= \cos(h\Omega) q_0 + \Omega^{-1} \sin(h\Omega) + \frac{h^2}{2} \Psi g_0 \\ p_1 &= -\Omega \sin(h\Omega) q_0 + \cos(h\Omega) p_0 + \frac{h}{2} (\Psi_0 g_0 + \Psi_1 g_1), \end{aligned}$$

the same form as Hairer et al. (2006).

Chapter Three

Computational Electromagnetics

In this chapter, we introduce a general family of variational, multisymplectic numerical methods for solving Maxwell's equations, using discrete differential forms in spacetime. In doing so, we demonstrate several new results, which apply both to some well-established numerical methods and to new methods introduced here. First, we show that Yee's finite-difference time-domain (FDTD) scheme, along with a number of related methods, are multisymplectic and derive from a discrete Lagrangian variational principle. Second, we generalize the Yee scheme to unstructured meshes, not just in space, but in 4-D spacetime. This relaxes the need to take uniform time steps, or even to have a preferred time coordinate at all. Finally, as an example of the type of methods that can be developed within this general framework, we introduce a new asynchronous variational integrator (AVI) for solving Maxwell's equations. These results are illustrated with some prototype simulations that show excellent energy and conservation behavior.

3.1 INTRODUCTION

The Yee scheme (also known as finite-difference time-domain, or FDTD) was introduced in Yee (1966) and remains one of the most successful numerical methods used in the field of computational electromagnetics, particularly in the area of microwave problems. Although it is not a “high-order” method, it is still preferred for many applications because it preserves important structural features of Maxwell's equations that other methods fail to capture. Among these distinguishing attributes are that the electrical charge density constraint $\rho = \nabla \cdot \mathbf{D}$ is exactly conserved in a discrete sense, and electrostatic solutions of the form $\mathbf{E} = -\nabla\phi$ indeed remain stationary in time (see Bondeson, Rylander, and Ingelström, 2005). In this chapter,

we show that these desirable properties are direct consequences of the variational and discrete differential structure of the Yee scheme, which mirrors the geometry of Maxwell's equations. Moreover, we will show how to construct other variational methods that, as a result, share these same numerical properties, while at the same time applying to more general domains.

3.1.1 Variational Integrators and Symmetry. Structure-preserving integrators have been used primarily for the simulation of classical mechanical systems, where features such as symplecticity, conservation of momentum, and conservation of energy are essential. (For a survey of various methods and applications, see Hairer et al., 2006.) Among these, *variational integrators* are developed by discretizing the Lagrangian variational principle of a system, and then requiring that numerical trajectories satisfy a discrete version of Hamilton's stationary-action principle. These methods are automatically symplectic, and they exactly preserve discrete momenta associated to symmetries of the Lagrangian: for instance, systems with translational invariance will conserve a discrete linear momentum, those with rotational invariance will conserve a discrete angular momentum, etc. In addition, variational integrators can be seen to display good long-time energy behavior, without artificial numerical damping (see Marsden and West, 2001, for a comprehensive overview of key results).

This variational approach was extended to discretizing general multisymplectic field theories, with an application to nonlinear wave equations, in Marsden et al. (1998, 2001), which developed the multisymplectic approach for continuum mechanics. Building on this work, Lew et al. (2003) introduced *asynchronous variational integrators* (AVIs), with which it becomes possible to choose a different time step size for each element of the spatial mesh, while still preserving the same variational and geometric structure as uniform-time-stepping schemes. These methods were implemented and shown to be not only practical, but in many cases superior to existing methods for problems such as nonlinear elastodynamics. Some further developments are given in Lew, Marsden, Ortiz, and West (2004).

While there have been attempts to apply the existing AVI theory to computational electromagnetics, these efforts encountered a fundamental obstacle. The key symmetry of Maxwell's equations is not rotational or translational symmetry,

as in mechanics, but a *differential gauge symmetry*. Without taking additional care to preserve this gauge structure, even variational integrators cannot be expected to capture the geometry of Maxwell's equations. As will be explained, we overcome this obstacle by combining variational methods with Discrete Exterior Calculus (DEC). This differential/gauge structure also turns out to be important for the numerical performance of the method, and is one of the hallmarks of the Yee scheme.

3.1.2 Preserving Discrete Differential Structure. As an illustration of this, consider the basic relation $\mathbf{B} = \nabla \times \mathbf{A}$, where \mathbf{B} is the magnetic flux and \mathbf{A} is the magnetic vector potential. Because of the vector calculus identities $\nabla \cdot \nabla \times = 0$ and $\nabla \times \nabla = 0$, this equation has two immediate and important consequences. First, \mathbf{B} is automatically divergence-free. Second, any transformation $\mathbf{A} \mapsto \mathbf{A} + \nabla f$ has no effect on \mathbf{B} ; this describes a gauge symmetry, for which the associated conserved momentum is $\nabla \times \mathbf{D} - \rho$ (which must equal zero by Gauss' law). A similar argument also explains the invariance of electrostatic solutions, since $\mathbf{E} = -\nabla\phi$ is curl-free and invariant under constant shifts in the scalar potential ϕ . Therefore, a proper variational integrator for electromagnetism should also preserve a discrete analog of these differential identities.

This can be done by viewing the objects of electromagnetism not as vector fields, but as *differential forms* in 4-D spacetime, as is typically done in the literature on classical field theory. Using the framework of DEC to discretize these differential forms, as previously introduced in Section 1.3.3, the resulting variational integrators automatically respect discrete differential identities such as $d^2 = 0$ (which contains the previous div-curl-grad relations) and Stokes' theorem. Consequently, they also respect the gauge symmetry of Maxwell's equations, and therefore preserve the associated discrete momentum.

3.1.3 Geometry Has Practical Consequences. The Yee scheme, as we will show, is a method of precisely this type, which explains many of its observed numerical qualities. For instance, one of its notable features is that the electric field \mathbf{E} and magnetic field \mathbf{H} do not live at the same discrete space or time locations, but at separate nodes on a staggered lattice. The reason why this particular setup leads

to improved numerics is not obvious: if we view \mathbf{E} and \mathbf{H} simply as vector fields in 3-space—the exact same type of mathematical object—why shouldn’t they live at the same points? Indeed, many finite element method (FEM) approaches do exactly this, resulting in a “nodal” discretization. However, from the perspective of differential forms in spacetime, it becomes clear that the staggered-grid approach is more faithful to the structure of Maxwell’s equations: as we will see, \mathbf{E} and \mathbf{H} come from objects that are dual to one another (the spacetime forms F and $G = *F$), and hence they naturally live on two staggered, dual meshes.

The argument for this approach is not merely a matter of theoretical interest: the geometry of Maxwell’s equations has important practical implications for numerical performance. For instance, the vector-field-based nodal discretization, used in FEM, results in spurious artifacts due to its failure to respect the underlying geometric structure. The Yee scheme, on the other hand, produces resonance spectra in agreement with theory, without spurious modes (see Bondeson et al., 2005). Furthermore, it has been shown in Haber and Ascher (2001) that staggered-grid methods can be used to develop fast numerical methods for electromagnetism, even for problems in heterogeneous media with highly discontinuous material parameters such as conductivity and permeability.

By developing a structure-preserving, geometric discretization of Maxwell’s equations, not only can we better understand the Yee scheme and its characteristic advantages, but we can also construct more general methods that share its desirable properties. This family of methods includes the “Yee-like” scheme of Bossavit and Kettunen (2000), which presented the first extension of Yee’s scheme to unstructured grids (e.g., simplicial meshes rather than rectangular lattices). General methods like these are highly desirable: rectangular meshes are not always practical or appropriate to use in applications where domains with curved and oblique boundaries are needed (see, for instance Clemens and Weiland, 2002). By allowing general discretizations while still preserving geometry, one can combine the best attributes of the FEM and Yee schemes.

3.1.4 Contributions. Using DEC as a structure-preserving, geometric framework for general discrete meshes, we have obtained the following results:

1. The Yee scheme is actually a variational integrator: that is, it can be obtained by applying Hamilton's principle of stationary action to a discrete Lagrangian.
2. Consequently, the Yee scheme is *multisymplectic* and *preserves discrete momentum maps* (i.e., conserved quantities analogous to the continuous case of electromagnetism). In particular, the conserved electrical charge density is understood as a discrete momentum map of this integrator, while the preservation of electrostatic potential solutions corresponds to the identity $d^2 = 0$, where d is the discrete exterior derivative operator.
3. We also create a foundation for more general schemes, allowing *arbitrary discretizations of spacetime*, not just uniform time steps on a spatial mesh. One such scheme, introduced here, is a new asynchronous variational integrator (AVI) for Maxwell's equations, where each spatial element is assigned its own time step size and evolves "asynchronously" with its neighbors. This means that one can choose to take small steps where greater refinement is needed, while still using larger steps for other elements. Since refining one part of the mesh does not restrict the time steps taken elsewhere, an AVI can be computationally efficient and numerically stable with fewer total iterations. In addition to the AVI scheme, we also describe how completely covariant spacetime integrators for electromagnetism can be implemented, without even requiring a 3+1 split into space and time components.

3.1.5 Outline. We will begin by reviewing Maxwell's equations: first developing the differential forms expression from a Lagrangian variational principle, and next showing how this is equivalent to the familiar vector calculus formulation. We will then motivate the use of DEC for computational electromagnetics, explaining how electromagnetic quantities can be modeled using discrete differential forms and operators on a spacetime mesh. These DEC tools will then be used to set up the discrete Maxwell's equations, and to show that the resulting numerical algorithm yields the Yee and Bossavit–Kettunen schemes as special cases, as well as a new AVI method. Finally, we will demonstrate that the discrete Maxwell's equations can also be derived from a discrete variational principle, and will explore its other

discrete geometric properties, including multisymplecticity and momentum map preservation.

3.2 MAXWELL'S EQUATIONS

This section quickly reviews the differential forms approach to electromagnetism, in preparation for the associated discrete formulation given in the next section. For more details, the reader can refer to Bossavit (1998) and Gross and Kotiuga (2004).

3.2.1 From Vector Fields to Differential Forms. Maxwell's equations, without free sources of charge or current, are traditionally expressed in terms of four vector fields in 3-space: the electric field \mathbf{E} , magnetic field \mathbf{H} , electric flux density \mathbf{D} , and magnetic flux density \mathbf{B} . To translate these into the language of differential forms, we begin by replacing the electric field with a 1-form E and the magnetic flux density by a 2-form B . These have the coordinate expressions

$$\begin{aligned} E &= E_x \, dx + E_y \, dy + E_z \, dz \\ B &= B_x \, dy \wedge dz + B_y \, dz \wedge dx + B_z \, dx \wedge dy, \end{aligned}$$

where $\mathbf{E} = (E_x, E_y, E_z)$ and $\mathbf{B} = (B_x, B_y, B_z)$. The motivation for choosing E as a 1-form and B as a 2-form comes from the integral formulation of Faraday's law,

$$\oint_C \mathbf{E} \cdot d\mathbf{l} = -\frac{d}{dt} \int_S \mathbf{B} \cdot d\mathbf{A},$$

where \mathbf{E} is integrated over curves and \mathbf{B} is integrated over surfaces. Similarly, Ampère's law,

$$\oint_C \mathbf{H} \cdot d\mathbf{l} = \frac{d}{dt} \int_S \mathbf{D} \cdot d\mathbf{A},$$

integrates \mathbf{H} over curves and \mathbf{D} over surfaces, so we can likewise introduce a 1-form H and a 2-form D .

Now, \mathbf{E} and \mathbf{B} are related to \mathbf{D} and \mathbf{H} through the usual constitutive relations

$$\mathbf{D} = \epsilon \mathbf{E}, \quad \mathbf{B} = \mu \mathbf{H}.$$

As shown in Bossavit and Kettunen (2000), we can view ϵ and μ as corresponding to Hodge operators $*_\epsilon$ and $*_\mu$, which map the 1-form "fields" to 2-form "fluxes" in

space. Therefore, this is compatible with viewing E and H as 1-forms, and D and B as 2-forms.

Note that in a vacuum, with $\epsilon = \epsilon_0$ and $\mu = \mu_0$ constant, one can simply express the equations in terms of \mathbf{E} and \mathbf{B} , choosing appropriate geometrized units such that $\epsilon_0 = \mu_0 = c = 1$, and hence ignoring the distinction between \mathbf{E} and \mathbf{D} and between \mathbf{B} and \mathbf{H} . This is typically the most familiar form of Maxwell's equations, and the one that most students of electromagnetism first encounter. In this presentation, we will restrict ourselves to the vacuum case with geometrized units; for geometric clarity, however, we will always distinguish between the 1-forms E and H and the 2-forms D and B .

Finally, we can incorporate free sources of charge and current by introducing the *charge density 3-form* $\rho \, dx \wedge dy \wedge dz$, as well as the *current density 2-form* $J = J_x \, dy \wedge dz + J_y \, dz \wedge dx + J_z \, dx \wedge dy$. These are required to satisfy the continuity of charge condition $\partial_t \rho + dJ = 0$, which can be understood as a conservation law (in the finite volume sense).

3.2.2 The Faraday and Maxwell 2-Forms. In Lorentzian spacetime, we can now combine E and B into a single object, the Faraday 2-form

$$F = E \wedge dt + B.$$

There is a theoretical advantage to combining the electric field and magnetic flux into a single spacetime object: this way, electromagnetic phenomena can be described in a relativistically covariant way, without favoring a particular split of spacetime into space and time components. In fact, we can turn the previous construction around: take F to be the fundamental object, with E and B only emerging when we choose a particular coordinate frame. Taking the Hodge star of F , we also get a dual 2-form

$$G = *F = H \wedge dt - D,$$

called the Maxwell 2-form. The equation $G = *F$ describes the dual relationship between E and B on one hand, and D and H on the other, that is expressed in the constitutive relations.

3.2.3 The Source 3-Form. Likewise, the charge density ρ and current density J can be combined into a single spacetime object, the source 3-form

$$\mathcal{J} = J \wedge dt - \rho.$$

Having defined \mathcal{J} in this way, the continuity of charge condition simply requires that \mathcal{J} be closed, i.e., $d\mathcal{J} = 0$.

3.2.4 Electromagnetic Variational Principle. Let A be the electromagnetic potential 1-form, satisfying $F = dA$, over the spacetime manifold X . Then define the 4-form Lagrangian density

$$\mathcal{L} = -\frac{1}{2} dA \wedge *dA + A \wedge \mathcal{J},$$

and its associated action functional

$$S[A] = \int_X \mathcal{L}.$$

Now, take a variation α of A , where α vanishes on the boundary ∂X . Then the variation of the action functional along α is

$$\begin{aligned} \mathbf{d}S[A] \cdot \alpha &= \left. \frac{d}{d\varepsilon} \right|_{\varepsilon=0} S[A + \varepsilon\alpha] \\ &= \int_X (-d\alpha \wedge *dA + \alpha \wedge \mathcal{J}) \\ &= \int_X \alpha \wedge (-d*dA + \mathcal{J}), \end{aligned}$$

where in this last equality we have integrated by parts, using the fact that α vanishes on the boundary. Hamilton's principle of stationary action requires this variation to be equal to zero for arbitrary α , thus implying the electromagnetic Euler–Lagrange equation,

$$d*dA = \mathcal{J}. \tag{3.1}$$

3.2.5 Variational Derivation of Maxwell's Equations. Since $G = *F = *dA$, then clearly Equation 3.1 is equivalent to $dG = \mathcal{J}$. Furthermore, since $d^2 = 0$, it follows

that $dF = d^2A = 0$. Hence, Maxwell's equations with respect to the Maxwell and Faraday 2-forms can be written as

$$dF = 0 \quad (3.2)$$

$$dG = \mathcal{J}. \quad (3.3)$$

Suppose now we choose the standard coordinate system (x, y, z, t) on Minkowski space $X = \mathbb{R}^{3,1}$, and define E and B through the relation $F = E \wedge dt + B$. Then a straightforward calculation shows that Equation 3.2 is equivalent to

$$\nabla \times \mathbf{E} + \partial_t \mathbf{B} = 0 \quad (3.4)$$

$$\nabla \cdot \mathbf{B} = 0. \quad (3.5)$$

Likewise, if $G = *F = H \wedge dt - D$, then Equation 3.3 is equivalent to

$$\nabla \times \mathbf{H} - \partial_t \mathbf{D} = \mathbf{J} \quad (3.6)$$

$$\nabla \cdot \mathbf{D} = \rho. \quad (3.7)$$

Hence this Lagrangian, differential forms approach to Maxwell's equations is *strictly equivalent* to the more classical vector calculus formulation in smooth spacetime. However, in discrete spacetime, we will see that the differential forms version is *not* equivalent to an arbitrary vector field discretization, but rather implies a particular choice of discrete objects.

3.2.6 Generalized Hamilton–Pontryagin Principle for Maxwell's Equations. We can also derive Maxwell's equations, variationally, by using a similar approach to the generalized Hamilton–Pontryagin principle, which we introduced in Section 1.3.2 for scalar fields. To do this, we treat A and F as separate fields, while G acts as a Lagrange multiplier, weakly enforcing the constraint $F = dA$. Define the extended action to be

$$S[A, F, G] = \int_X \left[-\frac{1}{2} F \wedge *F + A \wedge \mathcal{J} + (F - dA) \wedge G \right].$$

Then, taking the variation of the action along some α, ϕ, γ (vanishing on ∂X), we have

$$\begin{aligned}\mathbf{d}S[A, F, G] \cdot (\alpha, \phi, \gamma) &= \int_X [-\phi \wedge *F + \alpha \wedge \mathcal{J} + (\phi - d\alpha) \wedge G + (F - dA) \wedge \gamma] \\ &= \int_X [\alpha \wedge (\mathcal{J} - dG) + \phi \wedge (G - *F) + (F - dA) \wedge \gamma].\end{aligned}$$

Therefore, setting this equal to zero, we get the equations

$$dG = \mathcal{J}, \quad G = *F, \quad F = dA.$$

This is precisely equivalent to Maxwell's equations, as derived above. However, this approach provides some additional insight into the geometric structure of electromagnetics: the gauge condition $F = dA$ and constitutive relations $G = *F$ are *explicitly included in the equations of motion*, as a direct result of the variational principle.

3.2.7 Reducing the Equations. When solving an initial value problem, it is not necessary to use all of Maxwell's equations to evolve the system forward in time. In fact, the curl equations 3.4 and 3.6 automatically conserve the quantities $\nabla \cdot \mathbf{B}$ and $\nabla \cdot \mathbf{D} - \rho$. Therefore, the divergence equations 3.5 and 3.7 can be viewed simply as constraints on initial conditions, while the curl equations completely describe the time evolution of the system.

There are a number of ways to see why we can justify eliminating the divergence equations. A straightforward way is to take the divergence of Equations 3.4 and 3.6. Since $\nabla \cdot \nabla \times = 0$, we are left with

$$\partial_t(\nabla \cdot \mathbf{B}) = 0, \quad \partial_t(\nabla \cdot \mathbf{D}) + \nabla \cdot \mathbf{J} = \partial_t(\nabla \cdot \mathbf{D} - \rho) = 0.$$

Therefore, if the divergence constraints are satisfied at the initial time, then they are satisfied for all time, since the divergence terms are constant.

Another approach is to notice that Maxwell's equations depend only on the exterior derivative dA of the electromagnetic potential, and not on the value of A itself. Therefore, the system has a *gauge symmetry*: any gauge transformation $A \mapsto A + df$ leaves dA , and hence Maxwell's equations, unchanged. Choosing a time coordinate, we can then partially fix the gauge so that the electric scalar

potential $\phi = A(\partial/\partial t) = 0$ (the so-called Weyl gauge), and so A has only spatial components. In fact, these three remaining components correspond to those of the usual vector potential \mathbf{A} . The reduced Euler–Lagrange equations in this gauge consist only of Equation 3.6, while the remaining gauge symmetry $\mathbf{A} \mapsto \mathbf{A} + \nabla f$ yields a momentum map that automatically preserves $\nabla \cdot \mathbf{D} - \rho$ in time. Equations 3.4 and 3.5 are automatically preserved by the identity $d^2 A = 0$; they are not actually part of the Euler–Lagrange equations. A more detailed exposition of these calculations will be given in Section 3.5.2.

3.3 DISCRETE FORMS IN COMPUTATIONAL ELECTROMAGNETICS

In Section 1.3.3, we gave a quick review of the fundamental objects and operations of Discrete Exterior Calculus (DEC), a structure-preserving calculus of discrete differential forms. By construction, DEC automatically preserves a number of important geometric structures, and hence it provides a fully discrete analog of the tools used in the previous section to express the differential forms version of Maxwell’s equations. In subsequent sections, we will use this framework to formulate Maxwell’s equations discretely, emulating the continuous version.

3.3.1 Rationale Behind DEC for Computational Electromagnetism. Modern computational electromagnetism started in the 1960s, when the finite element method (FEM), based on *nodal basis functions*, was used successfully to discretize the differential equations governing 2-D static problems formulated in terms of a scalar potential. Unfortunately, the initial success of the FEM approach appeared unable to carry over to 3-D problems without spurious numerical artifacts. With the introduction of *edge elements* in Nédélec (1980) came the realization that a better discretization of the geometric structure of Maxwell’s electromagnetic theory was key to overcoming this obstacle (see Gross and Kotiuga, 2004 for more historical details). Mathematical tools developed by Weyl and Whitney in the 1950s, in the context of algebraic topology, turned out to provide the necessary foundations on which robust numerical techniques for electromagnetism can be built, as detailed in Bossavit (1998).

3.3.2 Initial and Boundary Values with DEC. Particular care is required to properly enforce initial and boundary conditions on the discrete spacetime boundary ∂K . For example, in electromagnetism, we may wish to set initial conditions for E and B at time t_0 —but while B is defined on ∂K at t_0 , E is not. In fact, as we will see, E lives on edges that are extruded between the time slices t_0 and t_1 , so unless we modify our definitions, we can only initialize E at the half-step $t_{1/2}$. (This half-step issue also arises with the standard Yee scheme.) There are some applications where it may be acceptable to initialize E and B at separate times (for example, when the fields are initialized randomly and integrated for a long time to compute a resonance spectrum), but we wish to be able to handle the more general case. Although our previous exposition of DEC thus far applies anywhere away from a boundary, notions as simple as “dual cell” need to be defined carefully on or near ∂K .

For a primal mesh K , the dual mesh $*K$ is defined as *the Voronoi dual of K restricted to K* . This truncates the portion of the dual cells extending outside of K ; compare Figure 3.1 with the earlier Figure 1.1. This new definition results in the addition of a dual vertex at the circumcenter of each boundary $(n-1)$ -simplex, in addition to the interior n -simplices as previously defined. To complete the dual mesh $*K$, we add a dual edge between adjacent dual vertices on the boundary, as well as between dual boundary vertices and their neighboring interior dual vertices, and proceed similarly with higher-dimensional dual cells. For intuition, one can imagine the $(n-1)$ -dimensional boundary to be a vanishingly thin n -dimensional shell. That is, each boundary $(k-1)$ -simplex can be thought of as a prismatic k -cell that has been “squashed flat” along the boundary normal direction. This process is quite similar to the use of “ghost cells” at the boundary, as is commonly done for finite volume methods (see LeVeque, 2002). Note that these additional dual cells provide the boundary ∂K with its own dual mesh $*(\partial K)$. In fact, the boundary of the dual is now equal to the dual of the boundary, i.e., $\partial(*K) = *(\partial K)$. Returning to the example of initial conditions on E and B , we recall that E is defined on extruded faces normal to the time slice t_0 . Therefore, thanks to the proper restriction of the Voronoi diagram to the domain, we can now define E on *edges* in ∂K at time t_0 , where these edges can be understood as vanishingly thin faces (i.e., extruded between some $t_{-\varepsilon}$ and t_0 for $\varepsilon \rightarrow 0$). Notice finally that with this construction of

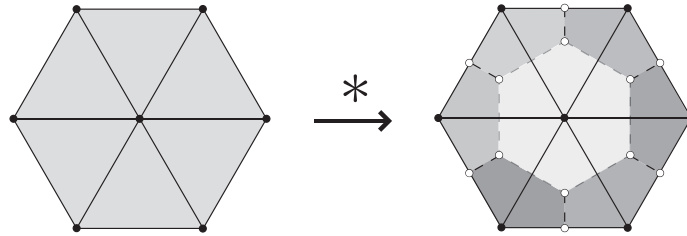


Figure 3.1: In this 2-D example, the dual mesh is properly defined near the boundary by adding dual vertices on the boundary edges. The restricted Voronoi cells of the primal boundary vertices (shaded at right) thus have boundaries containing both dual edges (dashed lines) *and* primal boundary half-edges.

$*K$, there is a dual relationship between Dirichlet conditions on the dual mesh and Neumann conditions on the primal mesh, e.g., between primal fields and dual fluxes, as expected.

3.3.3 Discrete Integration by Parts with Boundary Terms. With the dual mesh properly defined, dual forms can now be defined on the boundary. Therefore, the discrete duality between d and δ can be generalized to include nonvanishing boundary terms. If α is a primal $(k - 1)$ -form and β is a primal k -form, then

$$(d\alpha, \beta) = (\alpha, \delta\beta) + \langle \alpha \wedge * \beta, \partial K \rangle. \quad (3.8)$$

In the boundary integral, α is still a primal $(k - 1)$ -form on ∂K , while $*\beta$ is an $(n - k)$ -form taken on the boundary dual $(*(\partial K))$. Equation 3.8 is readily proved using the familiar method of discrete “summation by parts,” and thus agrees with the integration by parts formula for smooth differential forms.

3.3.4 A Spectrally Accurate Discrete Hodge Star. Throughout this chapter, we will exclusively use the “diagonal” approximation to the discrete Hodge star operator, although it is possible to construct higher-order Hodge stars. Because of the popularity of spectral methods in the computational electromagnetics community, we now show briefly how a spectral Hodge star may be constructed on a structured, periodic mesh.

Spectral Derivative at Primal Nodes. Suppose we have a 2π -periodic function f , which is discretized by sampling $f_j = f(x_j)$ at the N equally spaced points (where N is an even integer)

$$x_j = jh, \quad \text{for } j = -\frac{N}{2}, \dots, \frac{N}{2} - 1, \quad h = \frac{2\pi}{N}. \quad (3.9)$$

Spectral methods define a discrete derivative operator by using the property of the Fourier transform

$$\widehat{f'}_k = ik\widehat{f}_k.$$

Replacing this by the N -point discrete Fourier transform, we define the operator D_h to be

$$\widehat{D_h f}_k = ik\widehat{f}_k.$$

This provides an approximation to $f'(x_j)$ that is spectrally accurate and can be implemented efficiently using the Fast Fourier Transform.

Spectral Derivative at Dual Nodes. However, in DEC, it is essential that the derivatives be defined at the *half steps* $x_{j+1/2}$, which are the nodes of the dual mesh. The function f can easily be shifted to these points by multiplying in the frequency domain

$$\widehat{(f_{+1/2})}_k = e^{ikh/2}\widehat{f}_k,$$

so that the spectral derivative at half steps becomes

$$\widehat{(D_h f_{+1/2})}_k = ike^{ikh/2}\widehat{f}_k.$$

Modifying the Hodge Star instead of the Exterior Derivative. In DEC, the exterior derivative d is defined to satisfy a discrete Stokes' theorem, which in dimension 1 is

$$(df)_{j,j+1} = f_{j+1} - f_j,$$

corresponding to the fundamental theorem of calculus. This can be written in the frequency domain as

$$\widehat{df}_k = (e^{ikh} - 1)\widehat{f}_k.$$

Since d is purely a *topological* operator, maintaining this definition is essential to preserving differential structure. Therefore, to obtain a higher order of accuracy, we must focus instead on tuning the Hodge star, which is a *geometric* operator.

Spectral Discrete Hodge Star. We wish to construct an operator $*$ taking discrete 0-forms to 1-forms, such that

$$df = (D_h f_{+1/2}) dx = * (D_h f_{+1/2}),$$

i.e., so that DEC agrees with the spectral approximation to the derivative at half steps. If $\hat{*}$ corresponds to the Hodge in the frequency domain, then

$$(e^{ikh} - 1) \hat{f}_k = \hat{*}_k i k e^{ikh/2} \hat{f}_k.$$

Therefore

$$\hat{*}_k = \frac{e^{ikh} - 1}{ik e^{ikh/2}} = \frac{e^{ikh/2} - e^{-ikh/2}}{ik} = \frac{2 \sin(kh/2)}{k} = h \frac{\sin(kh/2)}{kh/2}.$$

To reduce this further, we use the fact $h = 2\pi/N$, and then

$$\hat{*}_k = h \frac{\sin(\pi k/N)}{\pi k/N} = h \text{sinc}(k/N).$$

Here the normalized sinc function is

$$\text{sinc}(x) = \frac{\sin(\pi x)}{\pi x},$$

where the singularity at $x = 0$ is removed so that $\text{sinc}(0) = 1$. Likewise, to go from 1-forms back to 0-forms, simply take the inverse

$$\widehat{(*^{-1})}_k = [h \text{sinc}(k/N)]^{-1}.$$

3.4 IMPLEMENTING MAXWELL'S EQUATIONS WITH DEC

In this section, we explain how to obtain numerical algorithms for solving Maxwell's equations with DEC. To do so, we will proceed in the following order. First, we will find a sensible way to define the discrete forms F , G , and \mathcal{J} on a spacetime mesh. Next, we will use the DEC version of the operators d and $*$ to obtain the discrete Maxwell's equations. While we haven't yet shown that these equations are variational in the discrete sense, we will show later in Section 3.5 that the Lagrangian derivation of the smooth Maxwell's equations also holds with the DEC operators, in precisely the same way. Finally, we will discuss how these equations can be used to define a numerical method for computational electromagnetics.

In particular, for a rectangular grid, we will show that our setup results in the traditional Yee scheme. For a general triangulation of space with equal time steps, the resulting scheme will be Bossavit and Kettunen's scheme. We will then develop an AVI method, where each spatial element can be assigned a different time step, and the time integration of Maxwell's equations can be performed on the elements asynchronously. Finally, we will comment on the equations for fully generalized spacetime meshes, e.g., an arbitrary meshing of $\mathbb{R}^{3,1}$ by 4-simplices.

Note that the idea of discretizing Maxwell's equations using spacetime cochains was mentioned in, e.g., Leok (2004), as well as in a paper by Wise (2006) taking the more abstract perspective of higher-level “ p -form” versions of electromagnetism and category theory.

3.4.1 Rectangular Grid. Suppose that we have a rectangular grid in $\mathbb{R}^{3,1}$, oriented along the axes (x, y, z, t) . To simplify this exposition (although it is not necessary), let us also suppose that the grid has uniform space and time steps $\Delta x, \Delta y, \Delta z, \Delta t$. Note that the DEC setup applies directly to a nonsimplicial rectangular mesh, since an n -rectangle does in fact have a circumcenter.

Setup. Since F is a 2-form, its values should live on 2-faces in this grid. Following the continuous expression of F

$$\begin{aligned} F = & E_x \, dx \wedge dt + E_y \, dy \wedge dt + E_z \, dz \wedge dt \\ & + B_x \, dy \wedge dz + B_y \, dz \wedge dx + B_z \, dx \wedge dy, \end{aligned}$$

and due to the tensor product nature of the regular grid, the exact assignment of each 2-face becomes simple: *the six components of F correspond precisely to the six types of 2-faces in a 4-D rectangular grid.* Simply assign the values $E_x \Delta x \Delta t$ to faces parallel to the xt -plane, $E_y \Delta y \Delta t$ to faces parallel to the yt -plane, and $E_z \Delta z \Delta t$ to faces parallel to the zt -plane. Likewise, assign $B_x \Delta y \Delta z$ to faces parallel to the yz -plane, $B_y \Delta z \Delta x$ to faces parallel to the xz -plane, and $B_z \Delta x \Delta y$ to faces parallel to the xy -plane. This is pictured in Figure 3.2.

Let us look at these values on the faces of a typical 4-rectangle $[x_k, x_{k+1}] \times [y_l, y_{l+1}] \times [z_m, z_{m+1}] \times [t_n, t_{n+1}]$. To simplify the notation, we can index each value of F by the midpoint of the 2-face on which it lives: for example, $F|_{k+\frac{1}{2}, l, m}^{n+\frac{1}{2}}$ is stored

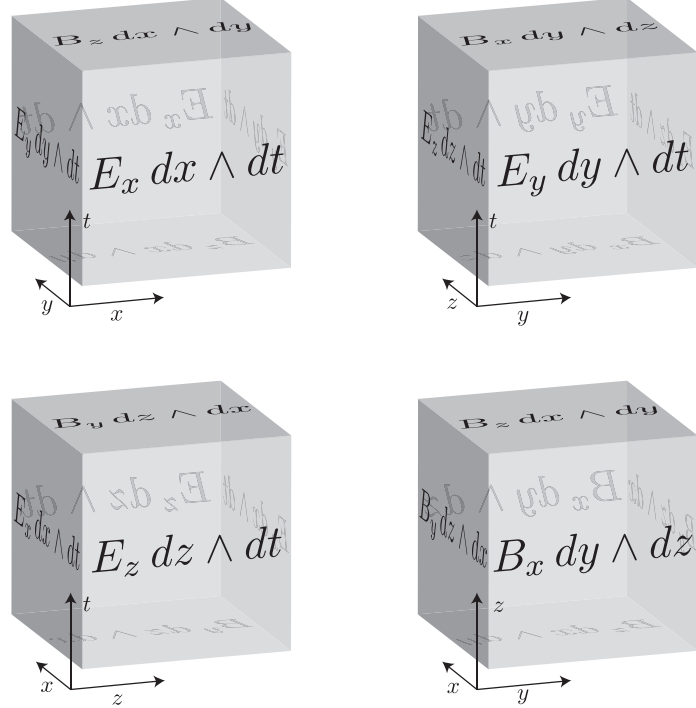


Figure 3.2: Values of F are stored on the primal 2-faces of a 4-D rectangular grid. Shown here are the three mixed space/time 3-cells, and the one purely spatial 3-cell (lower right).

on the face $[x_k, x_{k+1}] \times \{y_l\} \times \{z_m\} \times [t_n, t_{n+1}]$, parallel to the xt -plane. Hence, the following values are assigned to the corresponding faces:

$$xt\text{-face: } E_x|_{k+\frac{1}{2}, l, m}^{n+\frac{1}{2}} \Delta x \Delta t$$

$$yt\text{-face: } E_y|_{k, l+\frac{1}{2}, m}^{n+\frac{1}{2}} \Delta y \Delta t$$

$$zt\text{-face: } E_z|_{k, l, m+\frac{1}{2}}^{n+\frac{1}{2}} \Delta z \Delta t$$

$$yz\text{-face: } B_x|_{k, l+\frac{1}{2}, m+\frac{1}{2}}^n \Delta y \Delta z$$

$$xz\text{-face: } B_y|_{k+\frac{1}{2}, l, m+\frac{1}{2}}^n \Delta z \Delta x$$

$$xy\text{-face: } B_z|_{k+\frac{1}{2}, l+\frac{1}{2}, m}^n \Delta x \Delta y.$$

We see that a “staggered grid” arises from the fact that E and B naturally live on 2-faces, not at vertices or 4-faces.

Equations of Motion. The discrete equations of motion are, as in the continuous case,

$$dF = 0, \quad dG = \mathcal{J},$$

where now these equations are interpreted in the sense of DEC. Let us first look at the DEC interpretation of dF . Since dF is a discrete 3-form, it takes values on the 3-faces of each 4-rectangle. Its values are as follows:

$$\begin{aligned} \text{xyt-face:} & - \left(E_x|_{k+\frac{1}{2},l+1,m}^{n+\frac{1}{2}} - E_x|_{k+\frac{1}{2},l,m}^{n+\frac{1}{2}} \right) \Delta x \Delta t \\ & + \left(E_y|_{k+1,l+\frac{1}{2},m}^{n+\frac{1}{2}} - E_y|_{k,l+\frac{1}{2},m}^{n+\frac{1}{2}} \right) \Delta y \Delta t \\ & + \left(B_z|_{k+\frac{1}{2},l+\frac{1}{2},m}^{n+1} - B_z|_{k+\frac{1}{2},l+\frac{1}{2},m}^n \right) \Delta x \Delta y \\ \\ \text{xzt-face:} & - \left(E_x|_{k+\frac{1}{2},l,m+1}^{n+\frac{1}{2}} - E_x|_{k+\frac{1}{2},l,m}^{n+\frac{1}{2}} \right) \Delta x \Delta t \\ & + \left(E_z|_{k+1,l,m+\frac{1}{2}}^{n+\frac{1}{2}} - E_z|_{k,l,m+\frac{1}{2}}^{n+\frac{1}{2}} \right) \Delta z \Delta t \\ & - \left(B_y|_{k+\frac{1}{2},l,m+\frac{1}{2}}^{n+1} - B_y|_{k+\frac{1}{2},l,m+\frac{1}{2}}^n \right) \Delta x \Delta z \\ \\ \text{yzt-face:} & - \left(E_y|_{k,l+\frac{1}{2},m+1}^{n+\frac{1}{2}} - E_y|_{k,l+\frac{1}{2},m}^{n+\frac{1}{2}} \right) \Delta y \Delta t \\ & + \left(E_z|_{k,l+1,m+\frac{1}{2}}^{n+\frac{1}{2}} - E_z|_{k,l,m+\frac{1}{2}}^{n+\frac{1}{2}} \right) \Delta z \Delta t \\ & + \left(B_x|_{k,l+\frac{1}{2},m+\frac{1}{2}}^{n+1} - B_x|_{k,l+\frac{1}{2},m+\frac{1}{2}}^n \right) \Delta y \Delta z \\ \\ \text{xyz-face:} & \left(B_x|_{k+1,l+\frac{1}{2},m+\frac{1}{2}}^n - B_x|_{k,l+\frac{1}{2},m+\frac{1}{2}}^n \right) \Delta y \Delta z \\ & + \left(B_y|_{k+\frac{1}{2},l+1,m+\frac{1}{2}}^n - B_y|_{k+\frac{1}{2},l,m+\frac{1}{2}}^n \right) \Delta x \Delta z \\ & + \left(B_z|_{k+\frac{1}{2},l+\frac{1}{2},m+1}^n - B_z|_{k+\frac{1}{2},l+\frac{1}{2},m}^n \right) \Delta x \Delta y. \end{aligned}$$

Setting each of these equal to zero, we arrive at the following four equations:

$$\begin{aligned} \frac{B_x|_{k,l+\frac{1}{2},m+\frac{1}{2}}^{n+1} - B_x|_{k,l+\frac{1}{2},m+\frac{1}{2}}^n}{\Delta t} &= \\ \frac{E_y|_{k,l+\frac{1}{2},m+1}^{n+\frac{1}{2}} - E_y|_{k,l+\frac{1}{2},m}^{n+\frac{1}{2}}}{\Delta z} - \frac{E_z|_{k,l+1,m+\frac{1}{2}}^{n+\frac{1}{2}} - E_z|_{k,l,m+\frac{1}{2}}^{n+\frac{1}{2}}}{\Delta y} & \\ \\ \frac{B_y|_{k+\frac{1}{2},l,m+\frac{1}{2}}^{n+1} - B_y|_{k+\frac{1}{2},l,m+\frac{1}{2}}^n}{\Delta t} &= \\ \frac{E_z|_{k+1,l,m+\frac{1}{2}}^{n+\frac{1}{2}} - E_z|_{k,l,m+\frac{1}{2}}^{n+\frac{1}{2}}}{\Delta x} - \frac{E_x|_{k+\frac{1}{2},l,m+1}^{n+\frac{1}{2}} - E_x|_{k+\frac{1}{2},l,m}^{n+\frac{1}{2}}}{\Delta z} & \\ \\ \frac{B_z|_{k+\frac{1}{2},l+\frac{1}{2},m}^{n+1} - B_z|_{k+\frac{1}{2},l+\frac{1}{2},m}^n}{\Delta t} &= \\ \frac{E_x|_{k+\frac{1}{2},l+1,m}^{n+\frac{1}{2}} - E_x|_{k+\frac{1}{2},l,m}^{n+\frac{1}{2}}}{\Delta y} - \frac{E_y|_{k+1,l+\frac{1}{2},m}^{n+\frac{1}{2}} - E_y|_{k,l+\frac{1}{2},m}^{n+\frac{1}{2}}}{\Delta x} & \end{aligned}$$

and

$$\begin{aligned} \frac{B_x|_{k+1,l+\frac{1}{2},m+\frac{1}{2}}^n - B_x|_{k,l+\frac{1}{2},m+\frac{1}{2}}^n}{\Delta x} + \frac{B_y|_{k+\frac{1}{2},l+1,m+\frac{1}{2}}^n - B_y|_{k+\frac{1}{2},l,m+\frac{1}{2}}^n}{\Delta y} & \\ + \frac{B_z|_{k+\frac{1}{2},l+\frac{1}{2},m+1}^n - B_z|_{k+\frac{1}{2},l+\frac{1}{2},m}^n}{\Delta z} = 0. & \end{aligned} \tag{3.10}$$

These equations are the discrete version of the equations

$$\partial_t \mathbf{B} = -\nabla \times \mathbf{E}, \quad \nabla \cdot \mathbf{B} = 0.$$

Moreover, since E and B are differential forms, this can also be seen as a discretization of the *integral version* of Maxwell's equations as well! Because DEC satisfies a discrete Stokes' theorem, this automatically preserves the equivalence between the differential and integral formulations of electromagnetism.

Doing the same with the equation $dG = \mathcal{J}$, evaluating on dual 3-faces this time, we arrive at four more equations:

$$\begin{aligned} \frac{D_x|_{k+\frac{1}{2},l,m}^{n+\frac{1}{2}} - D_x|_{k+\frac{1}{2},l,m}^{n-\frac{1}{2}}}{\Delta t} &= \\ \frac{H_z|_{k+\frac{1}{2},l+\frac{1}{2},m}^n - H_z|_{k+\frac{1}{2},l-\frac{1}{2},m}^n}{\Delta y} - \frac{H_y|_{k+\frac{1}{2},l,m+\frac{1}{2}}^n - H_y|_{k+\frac{1}{2},l,m-\frac{1}{2}}^n}{\Delta z} &- J_x|_{k+\frac{1}{2},l,m}^n \\ \frac{D_y|_{k,l+\frac{1}{2},m}^{n+\frac{1}{2}} - D_y|_{k,l+\frac{1}{2},m}^{n-\frac{1}{2}}}{\Delta t} &= \\ \frac{H_x|_{k,l+\frac{1}{2},m+\frac{1}{2}}^n - H_x|_{k,l+\frac{1}{2},m-\frac{1}{2}}^n}{\Delta z} - \frac{H_z|_{k+\frac{1}{2},l+\frac{1}{2},m}^n - H_z|_{k-\frac{1}{2},l+\frac{1}{2},m}^n}{\Delta x} &- J_y|_{k,l+\frac{1}{2},m}^n \\ \frac{D_z|_{k,l,m+\frac{1}{2}}^{n+\frac{1}{2}} - D_z|_{k,l,m+\frac{1}{2}}^{n-\frac{1}{2}}}{\Delta t} &= \\ \frac{H_y|_{k+\frac{1}{2},l,m+\frac{1}{2}}^n - H_y|_{k-\frac{1}{2},l,m+\frac{1}{2}}^n}{\Delta x} - \frac{H_x|_{k,l+\frac{1}{2},m+\frac{1}{2}}^n - H_x|_{k,l-\frac{1}{2},m+\frac{1}{2}}^n}{\Delta y} &- J_z|_{k,l,m+\frac{1}{2}}^n \end{aligned}$$

and

$$\begin{aligned} \frac{D_x|_{k+\frac{1}{2},l,m}^{n+\frac{1}{2}} - D_x|_{k-\frac{1}{2},l,m}^{n+\frac{1}{2}}}{\Delta x} + \frac{D_y|_{k,l+\frac{1}{2},m}^{n+\frac{1}{2}} - D_y|_{k,l-\frac{1}{2},m}^{n+\frac{1}{2}}}{\Delta y} & \\ + \frac{D_z|_{k,l,m+\frac{1}{2}}^{n+\frac{1}{2}} - D_z|_{k,l,m-\frac{1}{2}}^{n+\frac{1}{2}}}{\Delta z} &= \rho|_{k,l,m}^{n+\frac{1}{2}}. \end{aligned} \tag{3.11}$$

This results from storing G on the dual grid, as shown in Figure 3.3. This set of equations is the discrete version of

$$\partial_t \mathbf{D} = \nabla \times \mathbf{H} - \mathbf{J}, \quad \nabla \cdot \mathbf{D} = \rho.$$

After eliminating the redundant divergence equations 3.10 and 3.11 (see Section 3.5.2 for details) and making the substitutions $\mathbf{D} = \epsilon \mathbf{E}$, $\mathbf{B} = \mu \mathbf{H}$, the remaining equations are precisely the Yee scheme, as formulated in Bondeson et al. (2005, pp. 67–68).

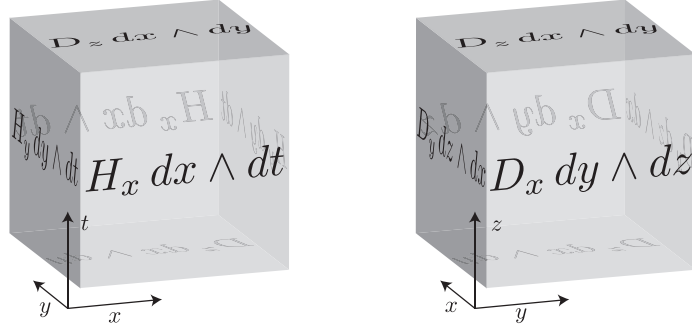


Figure 3.3: Values of $G = *F$ are stored on dual 2-faces in a rectangular grid. Shown here are a mixed space/time dual 3-cell (left), corresponding to a spacelike primal edge; and a purely spatial dual 3-cell (right), corresponding to a timelike primal edge. There are also two other mixed space/time cells, as in Figure 3.2, that are not shown here.

3.4.2 Unstructured Spatial Mesh with Uniform Time Steps. We now consider the case of an unstructured grid in space, but with uniform steps in time as advocated in, e.g., Bossavit and Kettunen (1999). Suppose that, instead of a rectangular grid for both space and time, we have an arbitrary space discretization on which we would like to take uniform time steps. (For example, we may be given a tetrahedral mesh of the spatial domain.) This mesh contains two distinct types of 2-faces. First, there are triangular faces that live entirely in the space mesh at a single position in time. Every edge of such a face is spacelike—that is, it has positive length—so the causality operator defined in Section 1.3.3 takes the value $\kappa = 1$. Second, there are rectangular faces that live between time steps. These faces consist of a single spacelike edge extruded by one time step. Because they have one timelike edge, these faces satisfy $\kappa = -1$. Again, the circumcentric-dual DEC framework applies directly to this type of mesh, since the prismatic extrusion of a 3-simplex still has a circumcenter.

Setup. Again, we can characterize the discrete values of F by looking at the continuous expression

$$F = E \wedge dt + B.$$

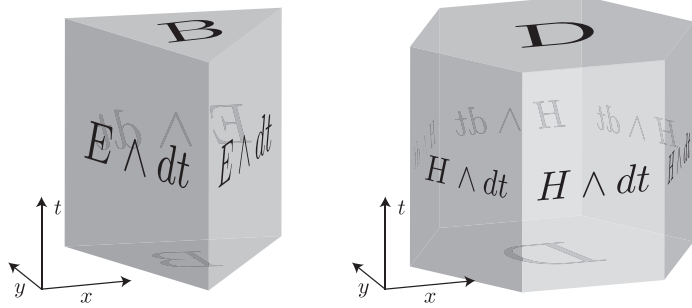


Figure 3.4: For an unstructured spatial mesh, F is stored on primal 2-faces (left), while $G = *F$ is stored on dual 2-faces (right). Shown here are the values on mixed space/time 3-cells. (The purely spatial 3-cells, which correspond to the divergence equations and do not contribute to the equations of motion, are not shown.)

Therefore, let us assign B to the purely spacelike faces and $E\Delta t$ to the mixed space/time faces. Looking at $G = *F$ shows that mixed dual faces should store $H\Delta t$ and spacelike dual faces should store D ; see Figure 3.4.

Equations of Motion. As in Bossavit (1998), we can store the values of each differential form over every spatial element in an array, using the method described in Section 1.3.3. This leads to the arrays B^n and H^n at whole time steps n , and $E^{n+1/2}$ and $D^{n+1/2}$ at half time steps. Let d_1 denote the edges-to-faces incidence matrix for the spatial domain. That is, d_1 is the matrix corresponding to the discrete exterior derivative, taken only in space, from primal 1-forms to primal 2-forms. Similarly, the transpose d_1^T corresponds to the exterior derivative from spatial dual 1-forms to dual 2-forms. Then the equation $dF = 0$, evaluated on all prismatic 3-faces, becomes

$$\frac{B^{n+1} - B^n}{\Delta t} = -d_1 E^{n+1/2}.$$

Likewise, the equation $dG = \mathcal{J}$, evaluated on all space/time 3-faces in the dual mesh, becomes

$$\frac{D^{n+1/2} - D^{n-1/2}}{\Delta t} = d_1^T H^n - J^n.$$

We can also evaluate $dF = 0$ and $dG = \mathcal{J}$ on spacelike 3-faces, e.g., tetrahedra; these simply yield the discrete versions of the divergence conditions for B and D , which can be eliminated.

Therefore, the DEC scheme for such a mesh is equivalent to Bossavit and Kettunen's Yee-like scheme; additionally, when the spatial mesh is taken to be rectangular, this integrator reduces to the standard Yee scheme. However, we now have solid foundations to extend this integrator to handle asynchronous updates for improved efficiency.

3.4.3 Unstructured Spatial Mesh with Asynchronous Time Steps. Instead of choosing the same time step size for every element of the spatial mesh, as in the previous two sections, it is often more efficient to assign each element its own, optimized time step, as done in Lew et al. (2003) for problems in elastodynamics. In this case, rather than the entire mesh evolving forward in time simultaneously, individual elements advance one-by-one, asynchronously—hence the name *asynchronous variational integrator* (AVI). As we will prove in Section 3.5, this asynchronous update process will maintain the variational nature of the integration scheme. Here, we again allow the spatial mesh to be unstructured.

Setup. After choosing a primal space mesh, assign each spatial 2-face (e.g., triangle) σ its own discrete time set

$$\Theta_\sigma = \left\{ t_\sigma^0 < \dots < t_\sigma^{N_\sigma} \right\}.$$

For example, one might assign each face a fixed time step size $\Delta t_\sigma = t_\sigma^{n+1} - t_\sigma^n$, taking equal time steps *within* each element, but with Δt varying *across* elements. We further require for simplicity of explanation that, except for the initial time, no two faces take the same time step: that is, $\Theta_\sigma \cap \Theta_{\sigma'} = \{t_0\}$ for $\sigma \neq \sigma'$.

In order to keep proper time at the edges e where multiple faces with different time sets meet, we let

$$\Theta_e = \bigcup_{\sigma \ni e} \Theta_\sigma = \left\{ t_e^0 \leq \dots \leq t_e^{N_e} \right\}.$$

Therefore the mixed space-time 2-faces, which correspond to the edge e extruded over a time step, are assigned the set of intermediate times

$$\Theta'_e = \left\{ t_e^{1/2} \leq \dots \leq t_e^{N_e-1/2} \right\},$$

where $t_e^{k+1/2} = (t_e^{k+1} + t_e^k)/2$. The values stored on a primal AVI mesh are shown in Figure 3.5.

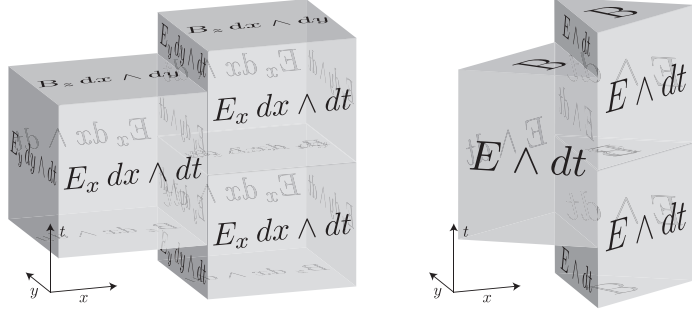


Figure 3.5: Shown here is part of an AVI mesh, for a rectangular spatial mesh (left) and for an unstructured spatial mesh (right). The different heights of the spacetime prisms reflect the fact that elements can take different time steps from one another. Moreover, these time steps can be asynchronous, as seen in the mismatch between the horizontal faces.

Since $\Theta_e \supset \Theta_\sigma$ when $e \subset \sigma$, each spatial edge e takes more time steps than any one of its incident faces σ ; as a result, it is not possible in general to construct a circumcentric dual on the entire spacetime AVI mesh, since the mesh is not prismatic and hence the circumcenter may not exist. Instead, we find the circumcentric dual to the *spatial* mesh, and assign same time steps to the primal and dual elements

$$\Theta_{*\sigma} = \Theta_\sigma, \quad \Theta_{*e} = \Theta_e.$$

This results in well-defined primal and dual cells for each 2-element in spacetime, and hence a Hodge star for this order. (A Hodge star on forms of different order is not needed to formulate Maxwell's equations.)

Equations of Motion. The equation $dF = 0$, evaluated on a mixed space/time 3-cell, becomes

$$\frac{B_\sigma^{n+1} - B_\sigma^n}{t_\sigma^{n+1} - t_\sigma^n} = -d_1 \sum \{E_e^{m+1/2} : t_\sigma^n < t_e^{m+1/2} < t_\sigma^{n+1}\}. \quad (3.12)$$

Similarly, the equation $dG = \mathcal{J}$ becomes

$$\frac{D_e^{m+1/2} - D_e^{m-1/2}}{t_e^{m+1/2} - t_e^{m-1/2}} = d_1^T \left(H_\sigma^n \mathbb{1}_{\{t_\sigma^n = t_e^m\}} \right) - J_e^m, \quad (3.13)$$

where $\mathbb{1}_{\{t_\sigma^n = t_e^m\}}$ equals 1 when face σ has $t_\sigma^n = t_e^m$ for some n , and 0 otherwise. (That is, the indicator function “picks out” the incident face that lives at the same time step as this edge.)

Solving an initial value problem can then be summarized by the following update loop:

1. Pick the minimum time t_σ^{n+1} where B_σ^{n+1} has not yet been computed.
2. Advance B_σ^{n+1} according to Equation 3.12.
3. Update $H_\sigma^{n+1} = *_{\mu}^{-1} B_\sigma^{n+1}$.
4. Advance $D_e^{m+3/2}$ on neighboring edges $e \subset \sigma$ according to Equation 3.13.
5. Update $E_e^{m+3/2} = *_{\varepsilon}^{-1} D_e^{m+3/2}$.

Iterative Time Stepping Scheme. As detailed in Lew et al. (2003) for elastodynamics, the explicit AVI update scheme can be implemented by selecting mesh elements from a priority queue, sorted by time, and iterating forward. However, as written above, the scheme is not strictly iterative, since Equation 3.13 depends on past values of E . This can be easily fixed by rewriting the AVI scheme to advance in the variables A and E instead, where the potential A effectively stores the cumulative contribution of E to the value of B on neighboring faces. Compared to the AVI for elasticity, A plays the role of the positions \mathbf{x} , while E plays the role of the (negative) velocities $\dot{\mathbf{x}}$. The algorithm is given as pseudocode in Figure 3.6, for the case where current $J = 0$. Note that if all elements take uniform time steps, the AVI reduces to the Bossavit–Kettunen scheme.

Numerical Experiments. We first present a simple numerical example demonstrating the good energy behavior of our asynchronous integrator. The AVI was used to integrate in time over a 2-D rectangular cavity with perfectly electrically conducting (PEC) boundaries, so that E vanishes at the boundary of the domain. E was given random values at the initial time, so as to excite all frequency modes, and integrated for 8 seconds. Each spatial element was given a time step equal to 1/10 of the stability-limiting time step determined by the CFL condition.

```

// INITIALIZE FIELDS AND PRIORITY QUEUE
for each spatial edge  $e$  do
     $A_e \leftarrow A_e^0$ ,  $E_e \leftarrow E_e^{1/2}$ ,  $\tau_e \leftarrow t_0$  // Store initial field values and times
    for each spatial face  $\sigma$  do
         $\tau_\sigma \leftarrow t_0$ 
        Compute the next update time  $t_\sigma^1$ 
        Q.push( $t_\sigma^1, \sigma$ ) // Push element onto queue with its next update time

// ITERATE FORWARD IN TIME UNTIL THE PRIORITY QUEUE IS EMPTY
repeat
     $(t, \sigma) \leftarrow Q.pop()$  // Pop next element  $\sigma$  and time  $t$  from queue
    for each edge  $e$  of element  $\sigma$  do
         $A_e \leftarrow A_e - E_e(t - \tau_e)$  // Update neighboring values of  $A$  at time  $t$ 
    if  $t < \text{final-time}$  then
         $B_\sigma \leftarrow d_1 A_e$ 
         $H_\sigma \leftarrow *_\mu B_\sigma$ 
         $D_e \leftarrow *_\epsilon E_e$ 
         $D_e \leftarrow D_e + d_1(e, \sigma) H_\sigma(t - \tau_\sigma)$ 
         $E_e \leftarrow *_\epsilon D_e$ 
         $\tau_\sigma \leftarrow t$  // Update element's time
        Compute the next update time  $t_\sigma^{\text{next}}$ 
        Q.push( $t_\sigma^{\text{next}}, \sigma$ ) // Schedule  $\sigma$  for next update
    until (Q.isEmpty())

```

Figure 3.6: Pseudocode for our Asynchronous Variational Integrator, implemented using a priority queue data structure for storing and selecting the elements to be updated.

This simulation was done for two different spatial discretizations. The first is a uniform discretization so that each element has identical time step size, which coincides exactly with the Yee scheme. The second discretization randomly partitioned the x - and y -axes, so that each element has completely unique spatial dimensions and time step size, and so the update rule is truly asynchronous. The energy plot for the uniform Yee discretization is shown in Figure 3.7, while the energy for the random discretization is shown in Figure 3.8. Even for a completely random, irregular mesh, our asynchronous integrator displays near-energy preservation qualities. Such numerical behavior stems from the variational nature of our integrator, which will be detailed in Section 3.5.

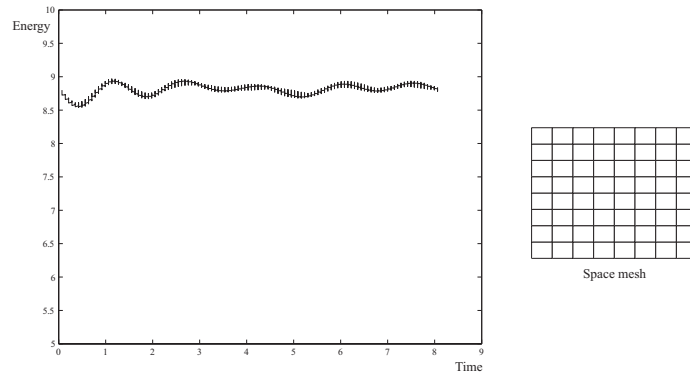


Figure 3.7: Energy vs. time for the AVI with uniform space and time discretization. This is the special case where the AVI reproduces the Yee scheme—which is well known to have good energy conservation properties, as seen here. (The vertical “tick marks” on the plot show where the elements become synchronized, since they take uniform time steps.)

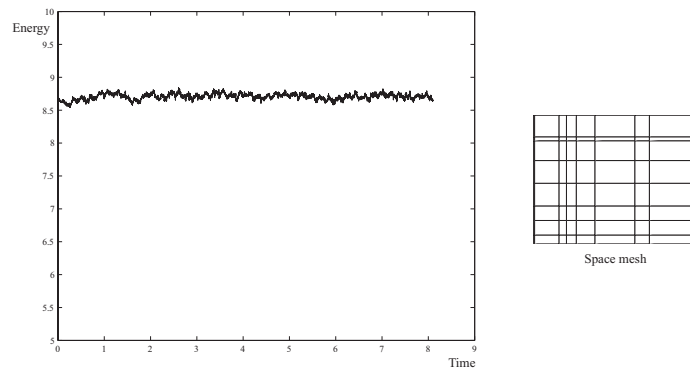


Figure 3.8: Energy vs. time for the AVI with random spatial discretization and fully asynchronous time steps. Despite the lack of regularity in the mesh and time steps, the AVI maintains the good energy behavior displayed by the Yee scheme.

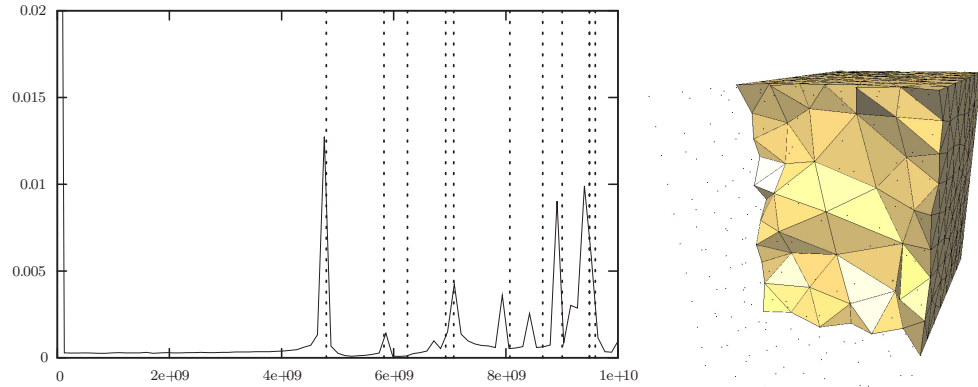


Figure 3.9: To produce the power spectrum shown at left, the electric field E was initialized with random data (to excite all frequencies) and integrated forward in time, measuring the field strength at a particular sample point for every time step, and then performing a discrete Fourier transform. The locations of the amplitude “spikes” are in close agreement with the analytic resonant frequencies, shown by the dashed vertical lines. The spatial mesh, shown at right, was refined closer to the boundary, and coarser in the interior, allowing the AVI to produce this result with fewer total steps than uniform-time-stepping would require.

In addition, we tested the performance of the AVI method with regard to computing the resonant frequencies of a 3-D rectangular cavity, but using an *unstructured* tetrahedral spatial mesh. While the resonant frequencies are relatively simple to compute analytically, nodal finite element methods are well known to produce spurious modes for this type of simulation. By contrast, as shown in Figure 3.9, the AVI simulation produces a resonance spectrum in close agreement with theory. Furthermore, by refining the mesh close to the spatial boundary, while using a coarser discretization in the interior, we were able to achieve these results with less computational effort than a uniformly fine mesh would require.

3.4.4 Fully Unstructured Spacetime Mesh. Finally, we look at the most general possible case: an arbitrary discretization of spacetime, such as a simplicial 4-complex. Such a mesh is completely relativistically covariant, so that F cannot be objectively separated into the components E and B without a coordinate frame. In

most engineering applications, relativistic effects are insignificant, so a 3+1 mesh (as in the previous subsections) is almost always adequate, and avoids the additional complications of spacetime mesh construction. Still, we expect that there are scientific applications where a covariant discretization of electromagnetism may be very useful. For example, many implementations of numerical general relativity (using Regge calculus for instance) are formulated on simplicial 4-complexes; one might wish to simulate the interaction of gravity with the electromagnetic field, or charged matter, on such a mesh.

Spacetime Mesh Construction. First, a quick caution on mesh construction: since the Lorentz metric is not positive definite, it is possible to create edges that have length 0, despite connecting two distinct points in $\mathbb{R}^{3,1}$ (so-called “null” or “lightlike” edges). Meshes containing such edges are degenerate—akin to a Euclidean mesh containing a triangle with two identical points. In particular, the DEC Hodge star is undefined for 0-volume elements (due to division by zero). Even without 0-volume elements, it is still possible for a spacetime mesh to violate causality, so extra care should be taken. Methods to construct causality-respecting spacetime meshes over a given spatial domain can be found in, e.g., Erickson, Guoy, Sullivan, and Üngör (2005) and Thite (2005).

When the mesh contains no inherent choice of a time direction, there is no canonical way to split F into E and B . Therefore, one must set up the problem by assigning values of F directly to 2-cells (or equivalently, assigning values of A to 1-cells). For initial boundary value problems, one might choose to have the initial and final time steps be prismatic, so that E and B can be used for initial and final values, while the internal discretization is general.

Equations of Motion. The equations $dF = 0$ and $dG = \mathcal{J}$ can be implemented directly in DEC. Since this mesh is generally unstructured, there is no simple algorithm as the ones we presented above. Instead, the equations on F results in a sparse linear system which, given proper boundary conditions, can be solved globally with direct or iterative solvers. However, it is clear from the previous three examples that the methods of Yee, Bossavit–Kettunen, and our AVI integrator are special cases where the global solution is particularly simple to compute via

synchronous or asynchronous time updates.

Mesh Construction and Energy Behavior. It is known that, while variational integrators in mechanics do not preserve energy exactly, they have excellent energy behavior, in that it tends to oscillate close to the exact value. This is only true, however, when the integrator takes time steps of uniform size; adaptive and other nonuniform stepping approaches can give poor results unless additional measures are taken to enforce good energy behavior. (See Hairer et al., 2006, Chapter VIII, for a good discussion of this problem for mechanics applications.)

Therefore, there is no reason to expect that *arbitrary* meshes of spacetime will yield energy results as good as the Yee, Bossavit–Kettunen, and AVI schemes. However, if one is taking a truly covariant approach to spacetime, “energy” is not even defined without specifying a time coordinate. Likewise, one would not necessarily expect good energy behavior from the other methods with respect to an arbitrary transformation of spatial coordinates. Which sort of mesh to choose is thus highly application dependent.

3.5 THEORETICAL RESULTS

In this section, we complete our exposition with a number of theoretical results about the discrete and continuous Maxwell’s equations. In particular, we show that the DEC formulation of electromagnetism derives from a discrete Lagrangian variational principle, and that this formulation is consequently multisymplectic. Furthermore, we explore the gauge symmetry of Maxwell’s equations, and detail how a particular choice of gauge eliminates the equation for $\nabla \cdot \mathbf{D} - \rho$ from the Euler–Lagrange equations, while preserving it automatically as a momentum map.

Theorem 3.5.1. *The discrete Maxwell’s equations are variational.*

Proof. The idea of this proof is to emulate the derivation of the continuous Maxwell’s equations from Section 3.2. Interpreting this in the sense of DEC, we will obtain the discrete Maxwell’s equations.

Given a discrete 1-form A and dual source 3-form \mathcal{J} , define the discrete Lagrangian 4-form

$$\mathcal{L}_d = -\frac{1}{2} dA \wedge *dA + A \wedge \mathcal{J},$$

with the corresponding discrete action principle

$$S_d[A] = \langle \mathcal{L}_d, K \rangle.$$

Then, taking a discrete 1-form variation α vanishing on the boundary, the corresponding variation of the action is

$$\mathbf{d}S_d[A] \cdot \alpha = \langle -d\alpha \wedge *dA + \alpha \wedge \mathcal{J}, K \rangle = \langle \alpha \wedge (-d*dA + \mathcal{J}), K \rangle.$$

(Here we use the bold \mathbf{d} to indicate that we are differentiating over the *smooth space of discrete forms* A , as opposed to differentiating over discrete spacetime, for which we use d .) Setting this equal to 0 for all variations α , the resulting discrete Euler–Lagrange equations are therefore $d*dA = \mathcal{J}$. Defining the discrete 2-forms $F = dA$ and $G = *F$, this implies $dF = 0$ and $dG = \mathcal{J}$, the discrete Maxwell’s equations. \square

3.5.1 Multisymplecticity. The concept of *multisymplecticity* for Lagrangian field theories was developed in Marsden et al. (1998), where it was shown to arise from the boundary terms for general variations of the action, i.e., those not restricted to vanish at the boundary. As originally presented, the Cartan form $\theta_{\mathcal{L}}$ is an $(n+1)$ -form, where the n -dimensional boundary integral is then obtained by contracting $\theta_{\mathcal{L}}$ with a variation. The multisymplectic $(n+2)$ -form $\omega_{\mathcal{L}}$ is then given by $\omega_{\mathcal{L}} = -\mathbf{d}\theta_{\mathcal{L}}$. Contracting $\omega_{\mathcal{L}}$ with two arbitrary variations gives an n -form that vanishes when integrated over the boundary, a result called the *multisymplectic form formula*, which results from the identity $\mathbf{d}^2 = 0$. In the special case of mechanics, where $n=0$, the boundary consists of the initial and final time points; hence, this implies the usual result that the symplectic 2-form ω_L is preserved by the time flow.

Alternatively, as communicated to us by Patrick (2004), one can view the Cartan form $\theta_{\mathcal{L}}$ as an n -form-valued 1-form, and the multisymplectic form $\omega_{\mathcal{L}}$ as an n -form-valued 2-form. Therefore, one simply evaluates these forms on tangent variations to obtain a boundary integral, rather than taking contractions. These two formulations are equivalent on smooth spaces. However, we will adopt Patrick’s

latter definition, since it is more easily adapted to problems on discrete meshes: $\theta_{\mathcal{L}}$ and $\omega_{\mathcal{L}}$ remain smooth 1- and 2-forms, respectively, but their n -form values are now taken to be discrete. See Figure 3.10 for an illustration of the discrete multisymplectic form formula.

Theorem 3.5.2. *The discrete Maxwell's equations are multisymplectic.*

Proof. Let $K \subset \mathcal{K}$ be an arbitrary subcomplex, and consider the discrete action functional S_d restricted to K . Suppose now that we take a discrete variation α , *without* requiring it to vanish on the boundary ∂K . Then variations of the action contain an additional boundary term

$$\mathbf{d}S_d[A] \cdot \alpha = \langle \alpha \wedge (-\mathbf{d}^* \mathbf{d}A + \mathcal{J}), K \rangle + \langle \alpha \wedge *dA, \partial K \rangle.$$

Restricting to the space of potentials A that satisfy the discrete Euler–Lagrange equations, the first term vanishes, leaving only

$$\mathbf{d}S_d(A) \cdot \alpha = \langle \alpha \wedge *dA, \partial K \rangle. \quad (3.14)$$

Then we can define the *Cartan form* $\theta_{\mathcal{L}_d}$ by

$$\theta_{\mathcal{L}_d} \cdot \alpha = \alpha \wedge *dA.$$

Since $\theta_{\mathcal{L}_d}$ takes a tangent vector α and produces a discrete 3-form on the boundary of the subcomplex, it is a *smooth 1-form taking discrete 3-form values*. Now, since the *space of discrete forms* is itself actually continuous, we can take the exterior derivative in the smooth sense on both sides of Equation 3.14. Evaluating along another first variation β (again restricted to the space of Euler–Lagrange solutions), we then get

$$\mathbf{d}^2 S_d[A] \cdot \alpha \cdot \beta = \langle \mathbf{d}\theta \cdot \alpha \cdot \beta, \partial K \rangle.$$

Finally, defining the multisymplectic form $\omega_{\mathcal{L}_d} = -\mathbf{d}\theta_{\mathcal{L}_d}$, and using the fact that $\mathbf{d}^2 S_d = 0$, we get the relation

$$\langle \omega_{\mathcal{L}_d} \cdot \alpha \cdot \beta, \partial K \rangle = 0 \quad (3.15)$$

for all variations α, β ; Equation 3.15 is a discrete version of the multisymplectic form formula. Since this holds for any subcomplex K , it follows that these schemes are multisymplectic. \square

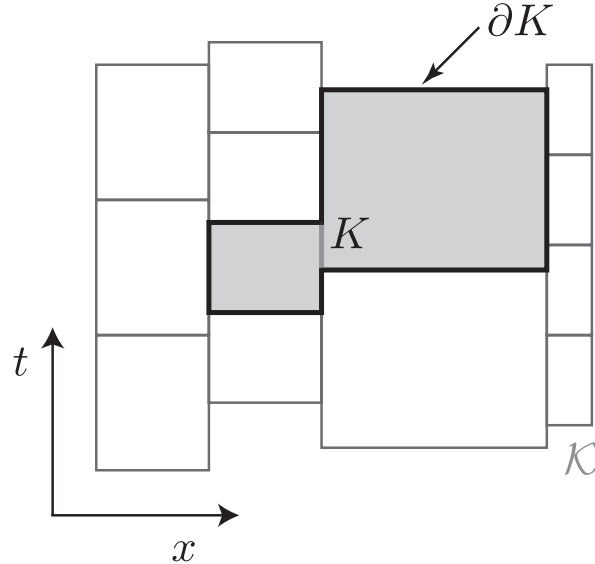


Figure 3.10: To illustrate the discrete multisymplectic form formula 3.15, we have here a 2-D asynchronous-time mesh \mathcal{K} , where the shaded region is an arbitrary subcomplex $K \subset \mathcal{K}$. Given any two variations α, β of the field, and the multisymplectic form $\omega_{\mathcal{L}_d}$, the formula states that $\omega_{\mathcal{L}_d} \cdot \alpha \cdot \beta$ vanishes when integrated over the boundary ∂K (shown in bold).

3.5.2 Gauge Symmetry Reduction and Covariant Momentum Maps. We now explore the symmetry of Maxwell's equations under gauge transformations. This symmetry allows us to reduce the equations by eliminating the time component of A (for some chosen time coordinate), effectively fixing the electric scalar potential to zero. Because this is an incomplete gauge, there is a remaining gauge symmetry, and hence a conserved momentum map. This conserved quantity turns out to be the charge density $\rho = \nabla \cdot \mathbf{D}$, which justifies its elimination from the Euler–Lagrange equations. These calculations are done with differential forms and exterior calculus, hence they apply equally to the smooth and discrete cases of electromagnetism.

3.5.3 Choosing a Gauge. Because Maxwell's equations only depend on dA , they are invariant under gauge transformations of the form $A \mapsto A + df$, where f is any scalar function on spacetime. If we fix a time coordinate, we can now choose the

Weyl gauge, so that the time component $A_t = 0$. Therefore, we can assume that

$$A = A_x \, dx + A_y \, dy + A_z \, dz.$$

In fact, A_x, A_y, A_z are precisely the components of the familiar vector potential \mathbf{A} , i.e., $A = \mathbf{A}^\flat$.

3.5.4 Reducing the Equations. Having fixed the gauge and chosen a time coordinate, we can now define two new “partial exterior derivative” operators, d_t (time) and d_s (space), where $d = d_t + d_s$. Since A contains no dt terms, $d_s A$ is a 2-form containing only the space terms of dA , while $d_t A$ contains the terms involving both space and time. That is,

$$d_t A = E \wedge dt, \quad d_s A = B.$$

Restricted to this subspace of potentials, the Lagrangian density then becomes

$$\begin{aligned} \mathcal{L} &= -\frac{1}{2} (d_t A + d_s A) \wedge * (d_t A + d_s A) + A \wedge \mathcal{J} \\ &= -\frac{1}{2} (d_t A \wedge * d_t A + d_s A \wedge * d_s A) + A \wedge J \wedge dt. \end{aligned}$$

Next, varying the action along a restricted variation α that vanishes on ∂X ,

$$\begin{aligned} \mathbf{d}S[A] \cdot \alpha &= \int_X (d_t \alpha \wedge d - d_s \alpha \wedge H \wedge dt + \alpha \wedge J \wedge dt) \\ &= \int_X \alpha \wedge (d_t D - d_s H \wedge dt + J \wedge dt). \end{aligned} \tag{3.16}$$

Setting this equal to zero by Hamilton’s principle, one immediately gets Ampère’s law as the sole Euler-Lagrange equation. The divergence constraint $d_s D = \rho$, corresponding to Gauss’ law, has been eliminated via the restriction to the Weyl gauge.

Noether’s Theorem Implies Automatic Preservation of Gauss’ Law. Let us restrict A to be an Euler-Lagrange solution in the Weyl gauge, but remove the previous requirement that variations α be fixed at the initial time t_0 and final time t_f . Then, varying the action along this new α , the Euler–Lagrange term disappears, but we now pick up an additional boundary term due to integration by parts

$$\mathbf{d}S[A] \cdot \alpha = \int_{\Sigma} \alpha \wedge D \Big|_{t_0}^{t_f},$$

where Σ denotes a Cauchy surface of X , corresponding to the spatial domain. If we vary along a gauge transformation $\alpha = d_s f$, then this becomes

$$\mathbf{d}S[A] \cdot d_s f = \int_{\Sigma} d_s f \wedge D \Big|_{t_0}^{t_f} = - \int_{\Sigma} f \wedge d_s D \Big|_{t_0}^{t_f}.$$

Alternatively, plugging $\alpha = d_s f$ into Equation 3.16, we get

$$\mathbf{d}S[A] \cdot d_s f = \int_X d_s f \wedge J \wedge dt = - \int_X f \wedge d_s J \wedge dt = - \int_X f \wedge d_t \rho = - \int_{\Sigma} f \wedge \rho \Big|_{t_0}^{t_f}.$$

Since these two expressions are equal, and f is an arbitrary function, it follows that

$$(d_s D - \rho) \Big|_{t_0}^{t_f} = 0.$$

This indicates that $d_s D - \rho$ is a conserved quantity, a momentum map, so if Gauss' law holds at the initial time, then it holds for all subsequent times as well.

3.5.5 Boundary Conditions and Variational Structure. It should be noted that the variational structure and symmetry of Maxwell's equations may be affected by the boundary conditions that one chooses to impose. There are many boundary conditions that one can specify independent of the initial values, such as the PEC condition used in the numerical example in Section 3.4.3. However, one can imagine more complicated boundary conditions where the boundary interacts nontrivially with the interior of the domain—such as dissipative or forced boundary conditions, where energy/momentum is removed from or added to the system. In these cases, one will obviously *not* conclude that the charge density $\nabla \cdot \mathbf{D}$ is conserved, but more generally that the *change* in charge is related to the flux through the spatial boundary. This is because, in the momentum map derivation above, the values of f on the initial time slice causally affects its values on the spatial boundary at intermediate times, not just on the final time slice. Thus, the spatial part of ∂X cannot be neglected for arbitrary boundary conditions.

3.6 CONCLUSION

The continued success of the Yee scheme for many applications of computational electromagnetism, for over four decades, illustrates the value of structure-preserving numerical integrators for Maxwell's equations. Recent advances by,

among others, Bossavit and Kettunen, and Gross and Kotiuga, have demonstrated the important role of compatible spatial discretization using differential forms, allowing for Yee-like schemes that apply on generalized spatial meshes. In this paper, we have extended this approach by considering discrete forms on *space-time*, encapsulating both space and time discretization, and have derived a general family of geometric numerical integrators for Maxwell's equations. Furthermore, since we have derived these integrators from a discrete variational principle, the resulting methods are provably multisymplectic and momentum-map-preserving, and they experimentally show correct global energy behavior. Besides proving the variational nature of well-known techniques such as the Yee and Bossavit–Kettunen schemes, we have also introduced a new asynchronous integrator, so that time step sizes can be taken nonuniformly over the spatial domain for increased efficiency, while still maintaining the desirable variational and energy behavior of the other methods.

Future Work. One promising avenue for future work involves increasing the order of accuracy of these methods by deriving higher-order discrete Hodge star operators. While this would involve redefining the Hodge star matrix to be non-diagonal, the discrete Maxwell's equations would remain formally the same, and hence there would be no change in the variational or multisymplectic properties proven here. It would be interesting to explore whether using a spectrally accurate Hodge star, such as the one developed in Section 3.3.4, might make the performance of these geometric schemes competitive for applications where non-variational spectral codes are currently favored.

Additionally, the recent work of Kale and Lew (2007) has shown that AVIs can be implemented as parallel algorithms for solid mechanics simulations. This uses the fact that, due to the asynchronous update procedure, an element does not need information from every one of its neighbors at every time step, which lessens the need for communication among parallel nodes. The resulting parallel AVIs, or PAVIs, can therefore take advantage of parallel computing architecture for improved efficiency. It is reasonable to expect that the same might be done in the case of our electromagnetic AVI.

While we have experimentally observed the fact that variational integrators

exhibit near-energy conservation, little is known about this behavior from a theoretical standpoint. In the case of ODEs in mechanics, backwards error analysis has shown that these methods exactly integrate a nearby smooth Hamiltonian system, although not much known about how this relates to the discrete variational principle on the Lagrangian side. Some initial work has been done in Oliver, West, and Wulff (2004) to understand, also by a backward error analysis approach, why discrete multisymplectic methods also display good energy behavior.

Finally, variational methods using discrete spacetime forms may be developed for field theories other than electromagnetism. Promising candidates include numerical general relativity and fluid dynamics, although the latter is complicated by the difficulty in finding a proper discretization of the infinite-dimensional diffeomorphism group. If discrete Lagrangian densities are developed for these theories, it should be straightforward to combine them with the electromagnetic Lagrangian, resulting in numerical methods to simulate, e.g., gravity coupled with an electromagnetic field, or the dynamics of a charged or magnetic fluid.

Chapter Four

Future Directions: Foundations for Discrete Gauge Theory and General Relativity

4.1 FIBER BUNDLES AND GAUGE THEORY

Fiber bundles are an important component of the modern, geometric approach to covariant field theory, especially gauge theory. To motivate their introduction, suppose we wish to describe a field over a space X , where the field takes values in some other space Y . We will refer to X as the *base space* and Y as the *fiber space* (the reasons for this nomenclature will soon become clear). Naïvely, one might describe such a field as a function $X \rightarrow Y$, or equivalently as a graph in the product space $X \times Y$.

However, not all fields can be described in this way. Consider the example of a vector field over an n -dimensional manifold X . The tangent space is $T_x X \cong \mathbb{R}^n$ for each point $x \in X$, so *locally* a vector field corresponds to a function $V_x \rightarrow \mathbb{R}^n$, where $V_x \ni x$ is some local coordinate neighborhood. Generally, though, one *cannot* extend this to a global function $X \rightarrow \mathbb{R}^n$, and hence a vector field is more than just an \mathbb{R}^n -valued function on X . Fundamentally, this is because the tangent bundle TX is not simply the product $X \times \mathbb{R}^n$. Rather, it is a bundle of the individual tangent spaces $T_x X \cong \mathbb{R}^n$, which may be connected to one another in nontrivial ways.

Informally, a fiber bundle with base X and fiber Y is a space that locally (though not necessarily globally) resembles the product space $X \times Y$. At each point $x \in X$, there is attached a copy of the fiber $Y_x \cong Y$, and moreover in a local neighborhood $V_x \ni x$, the collection of fibers over V_x is homeomorphic to $V_x \times Y$. This generalizes the concept of vector bundles (including the tangent bundles discussed above), which correspond to the special cases where Y is a vector space. We now formalize

this concept, loosely following the treatment of Steenrod (1951).

Definition 4.1.1. A *fiber bundle* with base X and fiber Y consists of a *bundle space* B , along with a *projection map* $\pi: B \rightarrow X$. In addition, there must exist a *local trivialization* for the bundle, consisting of an open covering of X by local neighborhoods V_j , along with homeomorphisms $\phi_j: V_j \times Y \rightarrow \pi^{-1}(V_j)$, which provide local coordinates for B . This local trivialization must satisfy the following conditions:

1. $(\pi \circ \phi_j)(x, y) = x$ for all $x \in V_j, y \in Y$ (i.e., the projection map corresponds, in local coordinates, to projection on the first factor),
2. if we define $\phi_{j,x}: Y \rightarrow \pi^{-1}(x)$ by $\phi_{j,x}(y) = \phi_j(x, y)$, then for any $x \in V_i \cap V_j$, the coordinate transition function $\phi_{j,x}^{-1} \circ \phi_{i,x}: Y \rightarrow Y$ corresponds to the action of a group element $\gamma_{ji}(x) \in G$, where G is a Lie group acting effectively on the left of Y called the *structure group* of the bundle. Moreover, the map $\gamma_{ji}: V_i \cap V_j \rightarrow G$, taking $x \mapsto \gamma_{ji}(x)$, is continuous.

For each $x \in X$, we call $Y_x = \pi^{-1}(x)$ the *fiber over x* .

A prototypical illustration of a fiber bundle satisfying this definition is shown in Figure 4.1.

In fact, given an open covering of the base, most of the geometric structure of a fiber bundle can be deduced from the coordinate transition maps γ_{ji} , without even specifying the individual coordinate functions ϕ_j . As long as the transition maps satisfy $\gamma_{kj}\gamma_{ji} = \gamma_{ki}$ whenever $V_i \cap V_j \cap V_k$ is nonempty, then one can construct an associated fiber bundle for *any* fiber Y with a left G -action by gluing together the local coordinate patches (see Steenrod, 1951, §3). For this reason, we can often safely assume that we are working with a *principal bundle*, in which the fiber $Y = G$ is equal to the structure group, and G acts on itself by left translation. For brevity, we will often refer to a principal bundle with structure group G as a *principal G -bundle*, or simply a *G -bundle*.

This bundle structure gives us a more powerful and covariant way to describe certain fields. Rather than functions $f: X \rightarrow Y$, which may only be defined locally, we can speak of these fields as *sections* of a fiber bundle with base X and fiber Y .

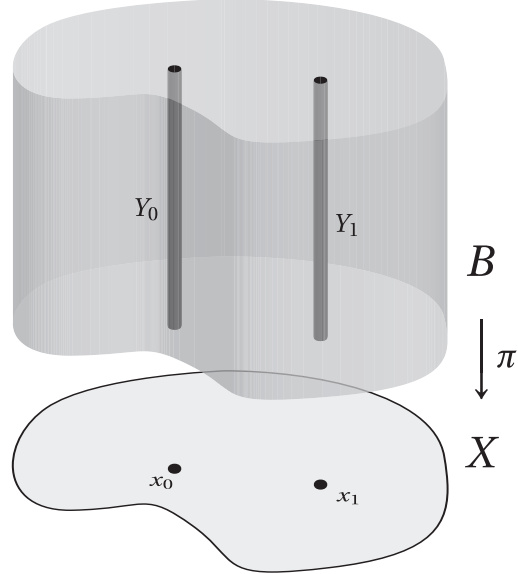


Figure 4.1: Here we see an illustrative diagram of a fiber bundle over a 2-D base \$X\$, with 1-D fiber \$Y\$. The projection map \$\pi\$ takes the 3-D bundle space \$B\$ down to the base. The fibers above the points \$x_0, x_1 \in X\$ are given by \$Y_0 = \pi^{-1}(x_0)\$ and \$Y_1 = \pi^{-1}(x_1)\$, respectively. Note that there are many different ways to identify the fibers \$Y_0\$ and \$Y_1\$; picking a particular homeomorphism between the two corresponds to a connection on the bundle.

Definition 4.1.2. A *section of a fiber bundle* is a function \$f: X \rightarrow B\$ such that \$\pi \circ f: X \rightarrow X\$ is the identity map. That is, for each \$x \in X\$, we have \$f(x) \in Y_x\$.

Gauge theory, however, is not directly concerned with sections of a bundle. Rather, it is concerned with *gauge fields*, which describe the manner in which different fibers are connected to one another. Maxwell's equations provide one of the simplest examples of such a gauge theory. The electromagnetic potential 1-form \$A \in \Omega^1(X)\$ can be thought of as the principal connection of a U(1)-bundle over spacetime, while the Faraday 2-form \$F\$ is the curvature of this principal connection. Locally, the principal connection of a \$G\$-bundle is a \$\mathfrak{g}\$-valued 1-form, where \$\mathfrak{g}\$ is the Lie algebra of \$G\$. Since \$\mathfrak{u}(1) \cong \mathbb{R}\$ is the Lie algebra for the case of Maxwell's equations,

we have thus far been able to ignore this principal bundle structure and simply see A and F as real-valued differential forms on the base. In large part, one can safely get away with this because $U(1)$ is an abelian group, and so $u(1) \cong \mathbb{R}$ has a trivial Lie bracket structure.

However, this is not the case for Lie groups in general, and in fact, most “interesting” gauge theories—such as Yang–Mills theory—have nonabelian gauge groups. In such cases, the previously introduced method of discretization by chains and cochains breaks down: we cannot simply add together the values of the connection 1-form for different edges along a path, since the order of composition matters. To incorporate the idea of “composable” transformations, which depend on the order in which a path is traversed, we need the mathematical framework of groupoids, which will be the subject of the next section.

4.2 LIE GROUPOIDS AND BUNDLE CONNECTIONS

Given a principal G -bundle, which we will denote $\pi: P \rightarrow P/G \cong X$, one can relate the structure of a principal connection to the study of certain *Lie groupoids* on X . In particular, there are two groupoids—called the *gauge groupoid* and the *monodromy groupoid*—that are particularly relevant to gauge theory, and which will be the theoretical underpinning of the subsequent discretization methods. It should be noted that there is a direct correspondence between this groupoid approach to connections, and the more traditional presentation of “infinitesimal connections” taking Lie algebra values, via the correspondence between a Lie groupoid and its associated Lie algebroid (see Mackenzie, 2005, Chapters 5–6).

4.2.1 Basic Definitions. Before delving into the particular groupoids relevant to gauge theory, we recall the definition of (Lie) groupoids.

Definition 4.2.1. A *groupoid* \mathcal{G} over a set of objects X , written $\mathcal{G} \rightrightarrows X$, consists of the following structures:

1. a pair of maps $\alpha: \mathcal{G} \rightarrow X$ and $\beta: \mathcal{G} \rightarrow X$, called the *source* and the *target*;

2. an associative binary operation $(h, g) \mapsto hg$ defined from $\mathcal{G}_2 \rightarrow \mathcal{G}$, where $\mathcal{G}_2 = \{(h, g) \in \mathcal{G} \times \mathcal{G} \mid \alpha(h) = \beta(g)\}$ is called the set of *composable pairs*, such that $\alpha(hg) = \alpha(g)$ and $\beta(hg) = \beta(h)$;
3. an identity map $1: X \rightarrow \mathcal{G}$, taking $x \mapsto 1_x$, having $\alpha(1_x) = \beta(1_x) = x$, and satisfying $g1_{\alpha(g)} = 1_{\beta(g)}g = g$ for all $g \in \mathcal{G}$;
4. an inverse map $\mathcal{G} \rightarrow \mathcal{G}$, taking $g \mapsto g^{-1}$, with $\alpha(g^{-1}) = \beta(g)$ and $\beta(g^{-1}) = \alpha(g)$, which satisfies $g^{-1}g = 1_{\alpha(g)}$ and $gg^{-1} = 1_{\beta(g)}$.

In the language of category theory, this can be put more succinctly: a groupoid is a (small) category in which every morphism is an isomorphism. For $x_0, x_1 \in X$, let $\text{Hom}(x_0, x_1) \subset \mathcal{G}$ denote the set of groupoid elements with source x_0 and target x_1 , that is, $\text{Hom}(x_0, x_1) = \alpha^{-1}(x_0) \cap \beta^{-1}(x_1)$.

The groupoid $\mathcal{G} \rightrightarrows X$ is said to be a *Lie groupoid* if in addition, \mathcal{G} and X are smooth manifolds, the maps defined above are smooth, and in particular α and β are surjective submersions.

Example 4.2.2 (groups as groupoids). As an important (albeit somewhat trivial) example, any group G can be considered as a groupoid over a single object. This is because any two elements $g, h \in G$ are composable, and so every element has the same source and target objects. In particular, a Lie group is a Lie groupoid over a single object.

Example 4.2.3 (pair groupoid). Given a smooth manifold X , the *pair groupoid* $X \times X \rightrightarrows X$ is a Lie groupoid, and one which plays a fundamental role in the theory of discrete Lagrangian mechanics (see Weinstein, 1996). The source and target maps for the pair groupoid are $\alpha: (x_1, x_0) \mapsto x_0$ and $\beta: (x_1, x_0) \mapsto x_1$, respectively; composition is given by $((x_2, x_1), (x_1, x_0)) \mapsto (x_2, x_0)$; the identity map is $x \mapsto (x, x)$; and the inverse map is $(x_1, x_0) \mapsto (x_0, x_1)$.

Example 4.2.4 (fundamental groupoid). If X is a smooth manifold, then the *fundamental groupoid* $\Pi(X) \rightrightarrows X$ is the Lie groupoid whose elements are homotopy classes of paths in X . That is, $\text{Hom}(x_0, x_1)$ is the homotopy class of paths from x_0 to x_1 , and in particular, $\text{Hom}(x, x) \cong \pi_1(X, x)$ is the fundamental group of X based at $x \in X$. In this groupoid, composition is defined by path concatenation, the

identity map $x \mapsto 1_x$ is given by the constant path at x , and inversion reverses the direction of a path.

Note that $\Pi(X) \cong X \times X$ if and only if X is simply connected, since a simply connected manifold has exactly one homotopy class of paths between any two points. Therefore, the fundamental groupoid can be seen as a more general version of the pair groupoid for nonsimply connected manifolds.

Example 4.2.5 (gauge groupoid). Suppose we have a principal bundle $P \rightarrow P/G \cong X$. The gauge groupoid describes the space of transformations from one fiber to another, i.e., G -equivariant diffeomorphisms between fibers. To introduce the formal definition, we will primarily follow the treatment of Mackenzie (2005). Consider the space $P \times P$ containing pairs of bundle elements $(y_1, y_0) \in Y_1 \times Y_0$, where as before $Y_0 = \pi^{-1}(x_0)$ and $Y_1 = \pi^{-1}(x_1)$ for some $x_0, x_1 \in X$. Since there is a left action $G \times P \rightarrow P$, we can also define a left action $G \times (P \times P) \rightarrow P \times P$ by applying the former action diagonally, i.e., $g(y_1, y_0) = (gy_1, gy_0)$. Then the *gauge groupoid* $(P \times P)/G \rightrightarrows X$ is the Lie groupoid of G -orbits $\{g(y_1, y_0) \mid g \in G\}$ in $P \times P$, where the groupoid operations are a straightforward extension of those previously given for the pair groupoid.

Example 4.2.6 (monodromy groupoid). Just as the fundamental groupoid $\Pi(X)$ was seen to be a generalized version of the pair groupoid $X \times X$, for nonsimply connected X , likewise the *monodromy groupoid* $\Pi(P)/G$ is a generalized version of the gauge groupoid $(P \times P)/G$ for nonsimply connected bundles.

4.2.2 Discrete Bundles and Path Connections. Mackenzie (2005) defines the idea of a *path connection* as lifting paths from the base to the groupoid. This provides a link between the language of groupoids described above, and the more familiar notion of a connection as providing “parallel transport” along a path. In gauge theory, one is generally concerned with path connections in either the gauge groupoid or the corresponding monodromy groupoid.

To discretize this idea of a path connection, let us suppose that we have an n -dimensional simplicial complex K , which triangulates some base manifold X . For any two neighboring n -simplices $\sigma_i, \sigma_j \in K_n$, with $\sigma_i \cap \sigma_j \neq \emptyset$, we assign a transition map $\gamma_{ji} \in G$. (Alternatively $\gamma_{ji} \in \tilde{G}$, where \tilde{G} is the universal cover of

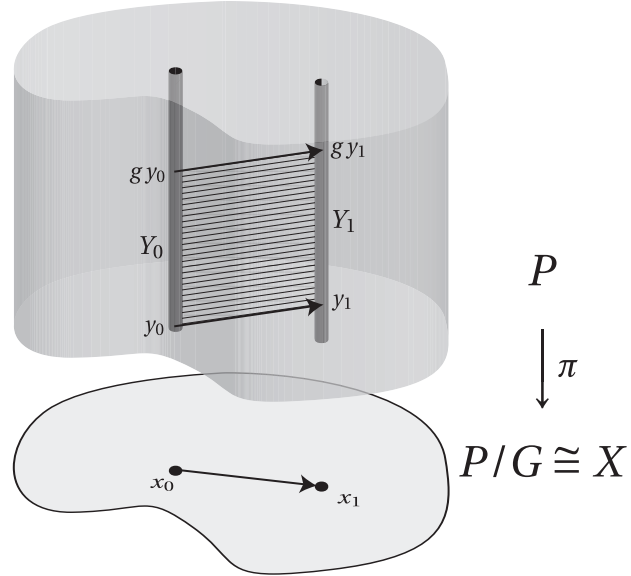


Figure 4.2: The gauge groupoid $(P \times P)/G$ consists of G -equivariant transformations between fibers of the principal bundle P . Here, we see an element of the gauge groupoid defined by identifying a representative pair of elements $y_0 \in Y_0$ and $y_1 \in Y_1$, and using their G -orbits to extend this to a bijection between Y_0 and Y_1 .

G.) That is, a *discrete connection* assigns a group element γ_{ji} to each directed edge $j \leftarrow i$ in the dual mesh. This can be extended to compute the *holonomy* of the connection over a discrete path or loop, by composing the group elements assigned to each edge in the path. (Reversing the direction of an edge causes its corresponding group element to be inverted.) This is consistent with the definitions used in certain approaches to discrete gauge theory (Oeckl, 2005).

In groupoid language, this corresponds to the following. Given a simplicial complex K , construct the directed graph whose vertices and edges are those of the dual mesh $*K$ (i.e., the adjacency graph for n -simplices). Now, there is a free functor (usually written $\text{Free} : \mathbf{Graph} \rightarrow \mathbf{Gpd}$) from the category of directed graphs to the category of groupoids. The *discrete path groupoid* $\mathcal{P}(K)$ is the free groupoid generated by this directed graph, i.e., whose elements are reduced sequences of composable directed edges. A discrete gauge connection is then a groupoid

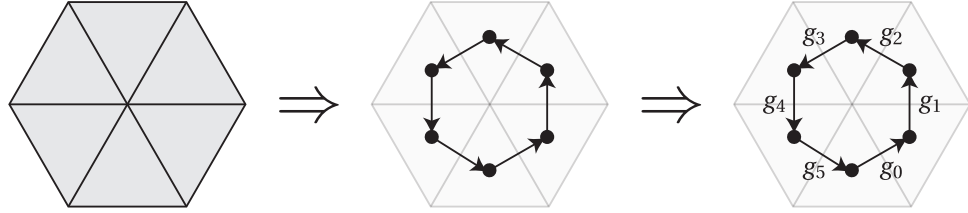


Figure 4.3: Starting with a primal mesh (left), we construct the discrete path groupoid, which is the free groupoid generated by the directed graph underlying the dual mesh (center). A discrete connection labels each directed edge with a group element, either belonging to the gauge group or to its universal cover (right); this generates a groupoid morphism from the discrete path groupoid to the gauge group, which can be considered as a groupoid over a single object.

morphism $\mathcal{P}(K) \rightarrow G$, where the group G is considered as a groupoid over a single object, while a discrete monodromy connection is a groupoid morphism $\mathcal{P}(K) \rightarrow \tilde{G}$, where again, \tilde{G} is the universal cover of G . These definitions are illustrated in Figure 4.3.

4.3 DISCRETE RIEMANNIAN GEOMETRY WITH FRAME BUNDLES

4.3.1 Angle Deficit as Discrete Gaussian Curvature. Consider a simplicial complex where all simplices are Euclidean, so that curvature only occurs only at *cone singularities* where simplices meet. According to a common approach, the curvature around an $(n - 2)$ -simplex σ^i is given by the corresponding *angle deficit* ε_i , shown in Figure 4.4. This can be stored as a *curvature 2-form* on the dual cell $*\sigma^i$. When $n = 2$, this corresponds to Gaussian curvature κ , which satisfies

$$\sum_i \varepsilon_i = \int \kappa dA = 2\pi\chi,$$

a result linking geometry and topology known as the Gauss–Bonnet theorem. We now show that the definition of “discrete curvature as angle deficit” preserves a discrete analog of the Gauss–Bonnet theorem.

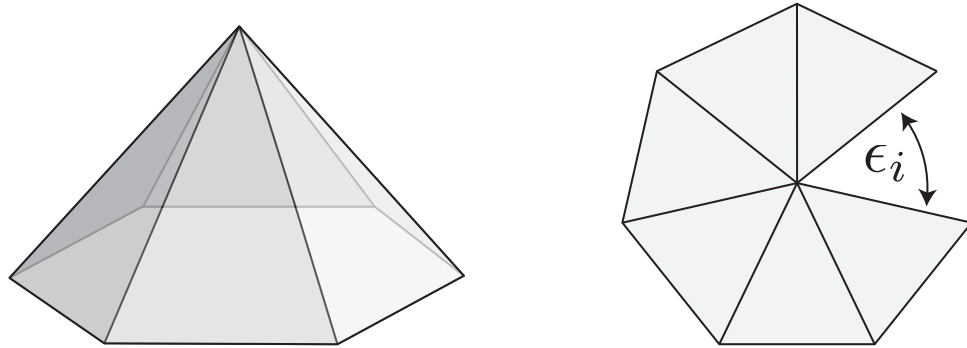


Figure 4.4: For a 2-D mesh composed of Euclidean triangles, curvature appears as a *cone singularity* where several triangles meet at a common vertex (left). This corresponds to an *angle deficit*: the angles around the vertex fail to add to 2π , as they would for a flat mesh. This deficit can be seen explicitly by cutting along an edge and laying the triangles flat (right).

Proposition 4.3.1 (Discrete Gauss–Bonnet). *If K is a triangulated 2-manifold without boundary, then the angle deficits ε_i sum to $\sum_i \varepsilon_i = 2\pi\chi$, where χ is the Euler characteristic of K .*

Proof. Let us start with the well-known formula $\chi = |K_0| - |K_1| + |K_2|$. The sum of the angle deficits is

$$\sum_i \varepsilon_i = \sum_i (2\pi - \theta_i) = 2\pi |K_0| - \sum_i \theta_i,$$

where θ_i is the angle sum around vertex i . Now, since each triangle has angle sum π , the total angle sum for K is $\sum_i \theta_i = \pi |K_2|$, and hence $\sum_i \varepsilon_i = 2\pi (|K_0| - \frac{1}{2} |K_2|)$. Finally, note that each triangle has three edges, and each edge is incident on two triangles, so $3|K_2| = 2|K_1|$, or equivalently $\frac{1}{2} |K_2| = |K_1| - |K_2|$. Therefore,

$$\sum_i \varepsilon_i = 2\pi \left(|K_0| - \frac{1}{2} |K_2| \right) = 2\pi (|K_0| - |K_1| + |K_2|) = 2\pi\chi,$$

which completes the proof. \square

4.3.2 Parallel Transport of Orthonormal Frames. There is an alternative way to understand why discrete curvature can be defined, reasonably, as the angle deficit

around an $(n - 2)$ -simplex. We can do this by discretizing the *Cartan formalism* for Riemannian geometry, which relates affine connections and Riemannian curvature to the principal connection and curvature forms on an orthonormal frame bundle.

Suppose that each n -simplex has its own local coordinate frame. This can be specified by an \mathbb{R}^n -valued 1-form e , called the *solder form*, which maps each directed edge in the simplex to its corresponding vector in the local coordinate frame. This lets us pull back a fixed metric on \mathbb{R}^n (e.g., the Euclidean metric) to a metric on each simplex. For example, the length of an edge is just the length of its corresponding vector in \mathbb{R}^n , that is, $|\sigma^i| = |e(\sigma^i)|$.

When two simplices are neighbors, we require their metrics to agree on the intersection. Therefore, the transition map between the two frames is given by a *rotation* in $\text{SO}(n)$. Labeling the corresponding dual edge by this rotation defines a connection 1-form A . The holonomy of this connection around the boundary of a dual face is the curvature 2-form $F = dA$. This curvature is precisely a *rotation through the angle deficit* ε_i , as illustrated in Figure 4.5. (This general setup was also used in Frauendiener, 2006, although here we will take a different approach to the equations of general relativity.)

Remark. Note that, if we use the gauge group $G = \text{SO}(n)$, we can only define curvature modulo 2π . One cannot distinguish, for example, between an angle deficit of π and $-\pi$, since they each correspond to the same $\text{SO}(n)$ group element, and only differ in their “winding number,” corresponding to different homotopy classes. To distinguish between these elements, we need to use the *universal cover*, which for $n > 2$ is given by the spin group $\tilde{G} = \text{Spin}(n)$.

4.3.3 General Relativity and Regge Calculus. Given the forms e and F defined above, we can now attempt to discretize the *Palatini action* of general relativity. In 3-D, this action can be written

$$S_{\pm} \int \text{tr}(e \wedge F) = \sum_i \langle e^i, F_i \rangle = \sum_i |\sigma^i| \varepsilon_i,$$

where the trace and the pairing $\langle \cdot, \cdot \rangle$ correspond to the Killing form on the Lie algebra $\mathfrak{so}(3) \cong \mathbb{R}^3$. Note that, since F_i is simply a rotation about the vector e^i in \mathbb{R}^3 , the vectors corresponding to e^i and F_i are parallel. Hence, $\langle e^i, F_i \rangle$ is simply the

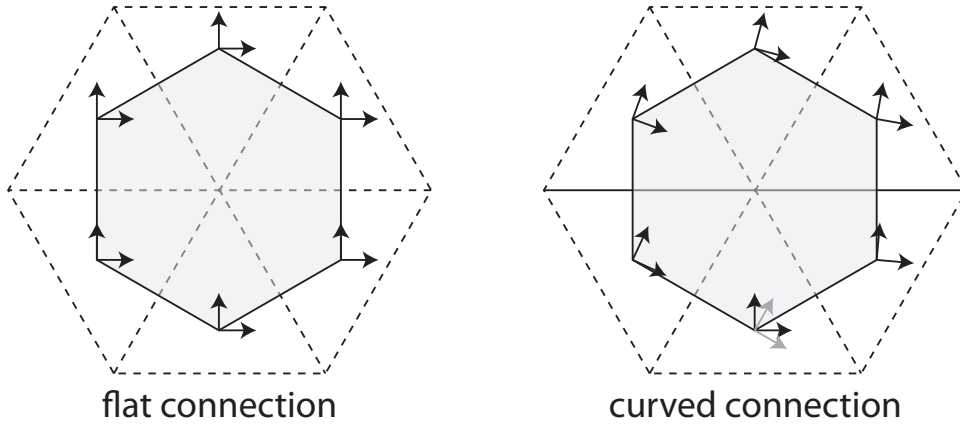


Figure 4.5: As another way to measure curvature on a discrete surface, we can parallel-translate an orthonormal frame around the vertex, i.e., along the boundary of its dual face, and measure the resulting rotation of the frame. For a flat connection, the frame undergoes no net rotation as it is transported (left). For a curved connection, however, the frame is rotated with respect to its initial configuration (right). The angle of this rotation precisely equals the angle deficit around the vertex.

product of their magnitudes $|\sigma^i| \varepsilon_i$. In 4-D, we define a bivector-valued discrete 2-form $B = e \wedge e$, so $S = \int B \wedge F = \sum_i 2|\sigma^i| \varepsilon_i$. (See Baez, 2000, and Miller, 1997 for a discussion related to this general approach.)

This agrees precisely with the discrete action of *Regge calculus* (Regge, 1961), which is an approach to discretizing general relativity based on the concept of curvature as angle deficit at a cone singularity. If, instead of using the special orthogonal group, we use its universal cover—the spin group—we in fact arrive at some proposed lattice quantum gravity models, which label edges and faces by spin symbols. In particular, for $\tilde{G} = \text{Spin}(3) = \text{SU}(2)$, we have the Ponzano–Regge model; for $\tilde{G} = \text{Spin}(4) = \text{SU}(2) \times \text{SU}(2)$, we get the Barrett–Crane model (Barrett and Crane, 1998); and for $\tilde{G} = \text{Spin}(3, 1) = \text{SL}(2, \mathbb{C})$, we get a discrete version of the Plebański action. (For further discussion of discrete models of gravity, both classical and quantum, refer to the survey by Regge and Williams, 2000.)

Bibliography

- Abraham, R., J. E. Marsden, and T. Ratiu (1988), *Manifolds, tensor analysis, and applications*, volume 75 of *Applied Mathematical Sciences*. Springer-Verlag, New York, second edition.
- Arnold, D. N., R. S. Falk, and R. Winther (2006), Finite element exterior calculus, homological techniques, and applications. *Acta Numer.*, **15**, 1–155.
- Ascher, U. M., and S. Reich (1999a), The midpoint scheme and variants for Hamiltonian systems: advantages and pitfalls. *SIAM J. Sci. Comput.*, **21**(3), 1045–1065 (electronic).
- Ascher, U. M., and S. Reich (1999b), On some difficulties in integrating highly oscillatory Hamiltonian systems. In *Computational molecular dynamics: challenges, methods, ideas (Berlin, 1997)*, volume 4 of *Lecture Notes in Computational Science and Engineering*, pages 281–296. Springer, Berlin.
- Ascher, U. M., S. J. Ruuth, and R. J. Spiteri (1997), Implicit-explicit Runge-Kutta methods for time-dependent partial differential equations. *Appl. Numer. Math.*, **25**(2-3), 151–167. Special issue on time integration.
- Auchmann, B., and S. Kurz (2006), A geometrically defined discrete Hodge operator on simplicial cells. *IEEE Trans. Magn.*, **42**(4), 643–646.
- Baez, J. C. (2000), An introduction to spin foam models of BF theory and quantum gravity. In *Geometry and quantum physics (Schladming, 1999)*, volume 543 of *Lecture Notes in Physics*, pages 25–93. Springer, Berlin. arXiv:gr-qc/9905087.
- Barrett, J. W., and L. Crane (1998), Relativistic spin networks and quantum gravity. *J. Math. Phys.*, **39**(6), 3296–3302. arXiv:gr-qc/9709028.

- Biesiadecki, J. J., and R. D. Skeel (1993), Dangers of multiple time step methods. *J. Comput. Phys.*, **109**(2), 318–328.
- Bondeson, A., T. Rylander, and P. Ingelström (2005), *Computational electromagnetics*, volume 51 of *Texts in Applied Mathematics*. Springer, New York.
- Bossavit, A. (1998), *Computational electromagnetism*. Electromagnetism, Academic Press Inc., San Diego, CA. Variational formulations, complementarity, edge elements.
- Bossavit, A., and L. Kettunen (1999), Yee-like schemes on a tetrahedral mesh, with diagonal lumping. *Int. J. Numer. Modell.*, **12**(1–2), 129–142.
- Bossavit, A., and L. Kettunen (2000), Yee-like schemes on staggered cellular grids: A synthesis between FIT and FEM approaches. *IEEE Trans. Magn.*, **36**(4), 861–867.
- Bott, R., and L. W. Tu (1982), *Differential forms in algebraic topology*, volume 82 of *Graduate Texts in Mathematics*. Springer-Verlag, New York.
- Boxerman, E., and U. Ascher (2004), Decomposing cloth. In *SCA '04: Proceedings of the 2004 ACM SIGGRAPH/Eurographics Symposium on Computer Animation*, pages 153–161. Eurographics Association, Aire-la-Ville, Switzerland. doi:10.1145/1028523.1028543.
- Bridges, T. J. (2006), Canonical multi-symplectic structure on the total exterior algebra bundle. *Proc. R. Soc. Lond. Ser. A Math. Phys. Eng. Sci.*, **462**(2069), 1531–1551.
- Clemens, M., and T. Weiland (2002), Magnetic field simulation using conformal FIT formulations. *IEEE Trans. Magn.*, **38**(2), 389–392.
- Crouzeix, M. (1980), Une méthode multipas implicite-explicite pour l'approximation des équations d'évolution paraboliques. *Numer. Math.*, **35**(3), 257–276.
- Desbrun, M., A. N. Hirani, and J. E. Marsden (2003), Discrete exterior calculus for variational problems in computer vision and graphics. In *Proceedings of the 42nd*

- IEEE Conference on Decision and Control (CDC)*, volume 5, pages 4902–4907. IEEE Press, Washington, DC.
- Desbrun, M., E. Kanso, and Y. Tong (2005), Discrete differential forms for computational modeling. In *SIGGRAPH '05: ACM SIGGRAPH 2005 Courses*, chapter 8. ACM Press, New York. doi:10.1145/1198555.1198666.
- Elcott, S., and P. Schröder (2005), Building your own DEC at home. In *SIGGRAPH '05: ACM SIGGRAPH 2005 Courses*. ACM Press, New York. doi:10.1145/1198555.1198667.
- Erickson, J., D. Guoy, J. Sullivan, and A. Üngör (2005), Building spacetime meshes over arbitrary spatial domains. *Engineering with Computers*, **20**(4), 342–353.
- Etzmuß, O., B. Eberhardt, and M. Hauth (2000), Implicit-explicit schemes for fast animation with particle systems. In *Proceedings of the 11th Eurographics Workshop on Computer Animation and Simulation (EGCAS)*, pages 137–151. Interlaken, Switzerland.
- Farr, W. M., and E. Bertschinger (2007), Variational integrators for the gravitational N -body problem. *Astrophys. J.*, **663**(2), 1420–1433. arXiv:astro-ph/0611416.
- Fermi, E., J. Pasta, and S. Ulam (1955), Studies of nonlinear problems. Report LA-1940. Los Alamos National Laboratory, Los Alamos, NM.
- Fong, W., E. Darve, and A. Lew (2007), Stability of asynchronous variational integrators. In *PADS '07: Proceedings of the 21st International Workshop on Principles of Advanced and Distributed Simulation*, pages 38–44. IEEE Computer Society Press, Washington, DC. doi:10.1109/PADS.2007.29.
- Frauendiener, J. (2006), Discrete differential forms in general relativity. *Classical Quantum Gravity*, **23**(16), S369–S385.
- Galgani, L., A. Giorgilli, A. Martinoli, and S. Vanzini (1992), On the problem of energy equipartition for large systems of the Fermi-Pasta-Ulam type: analytical and numerical estimates. *Phys. D*, **59**(4), 334–348.

- Gotay, M. J., and J. E. Marsden (2008), Momentum maps and classical fields. Draft version, to appear.
- Gross, P. W., and P. R. Kotiuga (2004), *Electromagnetic theory and computation: a topological approach*, volume 48 of *Mathematical Sciences Research Institute Publications*. Cambridge University Press, Cambridge.
- Haber, E., and U. M. Ascher (2001), Fast finite volume simulation of 3D electromagnetic problems with highly discontinuous coefficients. *SIAM J. Sci. Comput.*, **22**(6), 1943–1961.
- Hairer, E., C. Lubich, and G. Wanner (2003), Geometric numerical integration illustrated by the Störmer-Verlet method. *Acta Numer.*, **12**, 399–450.
- Hairer, E., C. Lubich, and G. Wanner (2006), *Geometric numerical integration*, volume 31 of *Springer Series in Computational Mathematics*. Springer-Verlag, Berlin, second edition. Structure-preserving algorithms for ordinary differential equations.
- Harrison, J. (2005), Ravello lecture notes on geometric calculus—Part I. Preprint. [arXiv:math-ph/0501001](https://arxiv.org/abs/math-ph/0501001).
- Hirani, A. N. (2003), *Discrete exterior calculus*. Ph.D. thesis, California Institute of Technology. Available from: <http://resolver.caltech.edu/CaltechETD:etd-05202003-095403>.
- Izaguirre, J. A., Q. Ma, T. Matthey, J. Willcock, T. Slabach, B. Moore, and G. Viamontes (2002), Overcoming instabilities in Verlet-I/r-RESPA with the mollified impulse method. In T. Schlick and H. H. Gan, editors, *Computational Methods for Macromolecules: Challenges and Applications—Proceedings of the 3rd International Workshop on Algorithms for Macromolecular Modeling*, volume 24 of *Lecture Notes in Computational Science and Engineering (LNCSE)*, pages 146–174. Springer, Berlin.
- Kale, K. G., and A. J. Lew (2007), Parallel asynchronous variational integrators. *Internat. J. Numer. Methods Engrg.*, **70**(3), 291–321.

- Leimkuhler, B. J., S. Reich, and R. D. Skeel (1996), Integration methods for molecular dynamics. In *Mathematical approaches to biomolecular structure and dynamics (Minneapolis, MN, 1994)*, volume 82 of *IMA Vol. Math. Appl.*, pages 161–185. Springer, New York.
- Leok, M. (2004), *Foundations of computational geometric mechanics*. Ph.D. thesis, California Institute of Technology. Available from: <http://resolver.caltech.edu/CaltechETD:etd-03022004-000251>.
- LeVeque, R. J. (2002), *Finite volume methods for hyperbolic problems*. Cambridge Texts in Applied Mathematics, Cambridge University Press, Cambridge.
- Lew, A., J. E. Marsden, M. Ortiz, and M. West (2003), Asynchronous variational integrators. *Arch. Ration. Mech. Anal.*, **167**(2), 85–146.
- Lew, A., J. E. Marsden, M. Ortiz, and M. West (2004), Variational time integrators. *Internat. J. Numer. Methods Engrg.*, **60**(1), 153–212.
- Mackenzie, K. C. H. (2005), *General theory of Lie groupoids and Lie algebroids*, volume 213 of *London Mathematical Society Lecture Note Series*. Cambridge University Press, Cambridge.
- Marsden, J. E., G. W. Patrick, and S. Shkoller (1998), Multisymplectic geometry, variational integrators, and nonlinear PDEs. *Comm. Math. Phys.*, **199**(2), 351–395.
- Marsden, J. E., S. Pekarsky, S. Shkoller, and M. West (2001), Variational methods, multisymplectic geometry and continuum mechanics. *J. Geom. Phys.*, **38**(3-4), 253–284.
- Marsden, J. E., and T. S. Ratiu (1999), *Introduction to mechanics and symmetry*, volume 17 of *Texts in Applied Mathematics*. Springer-Verlag, New York, second edition. A basic exposition of classical mechanical systems.
- Marsden, J. E., and M. West (2001), Discrete mechanics and variational integrators. *Acta Numer.*, **10**, 357–514.
- McLachlan, R. I., and D. R. J. O’Neale (2007), Comparison of integrators for the Fermi-Pasta-Ulam problem. Preprint NI07052-HOP. Isaac Newton Institute for

- Mathematical Sciences, Cambridge, UK. Available from: <http://www.newton.ac.uk/preprints/NI07052.pdf>.
- McLachlan, R. I., and G. R. W. Quispel (2002), Splitting methods. *Acta Numer.*, **11**, 341–434.
- Miller, W. A. (1997), The Hilbert action in Regge calculus. *Classical Quantum Gravity*, **14**(12), L199–L204.
- Moser, J., and A. P. Veselov (1991), Discrete versions of some classical integrable systems and factorization of matrix polynomials. *Comm. Math. Phys.*, **139**(2), 217–243.
- Nédélec, J.-C. (1980), Mixed finite elements in \mathbb{R}^3 . *Numer. Math.*, **35**(3), 315–341.
- Oeckl, R. (2005), *Discrete gauge theory*. Imperial College Press, London. From lattices to TQFT.
- Oliver, M., M. West, and C. Wulff (2004), Approximate momentum conservation for spatial semidiscretizations of semilinear wave equations. *Numer. Math.*, **97**(3), 493–535.
- O'Rourke, J. (1998), *Computational geometry in C*. Cambridge University Press, Cambridge, second edition.
- Patrick, G. W. (2004), Geometric classical field theory. Personal communication.
- Regge, T. (1961), General relativity without coordinates. *Nuovo Cimento*, **19**(3), 558–571.
- Regge, T., and R. M. Williams (2000), Discrete structures in gravity. *J. Math. Phys.*, **41**(6), 3964–3984.
- Steenrod, N. (1951), *The Topology of Fibre Bundles*. Princeton Mathematical Series, vol. 14, Princeton University Press, Princeton, NJ.
- Suris, Y. B. (1990), Hamiltonian methods of Runge-Kutta type and their variational interpretation. *Mat. Model.*, **2**(4), 78–87.

- Tarhasaari, T., L. Kettunen, and A. Bossavit (1999), Some realizations of a discrete Hodge operator: a reinterpretation of finite element techniques. *IEEE Trans. Magn.*, **35**(3), 1494–1497.
- Thite, S. (2005), *Spacetime meshing for discontinuous Galerkin methods*. Ph.D. thesis, University of Illinois at Urbana-Champaign.
- Wang, K., Weiwei, Y. Tong, M. Desbrun, and P. Schröder (2006), Edge subdivision schemes and the construction of smooth vector fields. In *SIGGRAPH '06: ACM SIGGRAPH 2006 Papers*, pages 1041–1048. ACM Press, New York. doi:10.1145/1179352.1141991.
- Weibel, C. A. (1994), *An introduction to homological algebra*, volume 38 of *Cambridge Studies in Advanced Mathematics*. Cambridge University Press, Cambridge.
- Weinstein, A. (1996), Lagrangian mechanics and groupoids. In *Mechanics day (Waterloo, ON, 1992)*, volume 7 of *Fields Inst. Commun.*, pages 207–231. American Mathematical Society, Providence, RI.
- Whitney, H. (1957), *Geometric integration theory*. Princeton University Press, Princeton, NJ.
- Wise, D. K. (2006), p -form electromagnetism on discrete spacetimes. *Classical Quantum Gravity*, **23**(17), 5129–5176.
- Yee, K. S. (1966), Numerical solution of initial boundary value problems involving Maxwell's equations in isotropic media. *IEEE Trans. Ant. Prop.*, **14**(3), 302–307.
- Yoshimura, H., and J. E. Marsden (2006), Dirac structures in Lagrangian mechanics. II. Variational structures. *J. Geom. Phys.*, **57**(1), 209–250.
- Zhang, G., and T. Schlick (1993), LIN: a new algorithm to simulate the dynamics of biomolecules by combining implicit-integration and normal mode techniques. *J. Comput. Chem.*, **14**(10), 1212–1233. doi:10.1002/jcc.540141011.
- Zhang, M., and R. D. Skeel (1997), Cheap implicit symplectic integrators. *Appl. Numer. Math.*, **25**(2-3), 297–302. Special issue on time integration.